MANEUVERABILITY IN RESTRICTED WATERS:

STATE OF THE ART

Masataka Fujino

Department of Naval Architecture
and Marine Engineering
College of Engineering
The University of Michigan
Ann Arbor, Michigan 48109

ABSTRACT

An overview of restricted-water maneuvering with heavy emphasis
on the course stability of ships in canals is presented, starting with
the underlying linear equations and proceeding to the theoretical
prediction of the stability derivatives, arriving finally at a careful
comparison of theory with published experimental data. Features include
an illustration of the use of the hypercircle method in providing upper
and lower limits on the solution of the boundary-value problem, a
discussion of the role of negative feedback in course stability, and
an outline of the technique of plotting the limit cycle on phase-planes
to evaluate nonlinear equation constants as a part of a discussion of
simple nonlinear models of maneuvering motion.

CONTENTS

Contents (continued)

NOMENCLATURE

A	aspect ratio
a,b,c,d,e	constant coefficients of the characteristic equation (2.23) for the maneuvering motion in a canal (see (2.24))
a',b',c',d',e'	constant coefficients of the characteristic equation (3.21) for the controlled maneuvering motion in a canal (see (3.22))
a,b,c,d	characters to designate the size of a rectangular cylinder and a rectangular canal (in part 4)
B	breadth of a ship
B(s)	Laplace transform of drift angle $\beta(t)$
C*	stability discriminant of the maneuvering motion in deep water or in shallow water (see (2.27))
C_y	three-dimensional correction factor of sway added mass
C_{yH}	correction factor C_y for a finite water depth H
$C_{y\infty}$	correction factor C_y for infinitely deep water
C_{zz}	three-dimensional correction factor of yaw added mass moment of inertia
C_{zzH}	correction factor C_{zz} for a finite water depth H
$C_{zz\infty}$	correction factor C_{zz} for infinitely deep water
D_2,D_3,D_4,D_5,D_6	areas enclosed by limit cycles on the various kinds of phase-plane
D(s)	Laplace transform of rudder angle $\delta(t)$
F_H	Froude number based on the water depth H: $U/\sqrt{Hg}$
F_n	Froude number based on the ship's length L: $U/\sqrt{Lg}$
g	acceleration of gravity

Nomenclature (continued)

H	water depth
H(s)	Laplace transform of lateral position, $\eta(t)$, of a ship in a canal
I_i	i-th vector of homogeneous complementary vector space π^*: $I_i = (p_{i1}^*, p_{i2}^*)$
I_{zz}	yaw mass moment of inertia of a ship about the vertical axis through the center of gravity
J_k	k-th vector of homogeneous associated vector space Ω^*: $J_k = (q_{k1}^*, q_{k2}^*)$
J_{zz}	yaw added mass moment of inertia
K	stability index of a ship defined by (2.46)
k_1, k_2, k_3, k_4, k_5	autopilot gain constants (see (3.20))
k_F	factor to describe the shallow water effects on the sway added mass, lateral force, and turning moment (see (4.92))
$k_i(A)$	factor to describe the shallow water effects on the sway added mass (i=1), yaw added mass moment of inertia (i=2), lateral force (i=3), and turning moment (i=4) (see (4.93))
k_δ	factor to describe the shallow water effect on the rudder force
L	ship's length between perpendiculars
m	ship's mass
m_y	sway added mass of a ship
m_y^*	sway added mass of a two-dimensional cyclinder
m_{yH}	added mass m_y at a finite water depth H
$m_{y\infty}$	added mass m_y in infinitely deep water
m_{ij}	element of the added mass tensor
m(m'), n(n')	integers to denote the subscript k(ℓ) of $J_k(J_\ell)$-vector

N	turning (yaw) moment acting on a ship
$\overline{N}$	amplitude of a sinusoidal yaw moment
$N_{\dot{v}}$	derivative of yaw moment with respect to sway acceleration
N_v	derivative of yaw moment with respect to sway velocity
$N_{\dot{r}}$	derivative of yaw moment with respect to yaw angular acceleration ($\equiv -J_{zz}$)
N_r	derivative of yaw moment with respect to yaw angular velocity
$N_{\dot{\delta}}$	derivative of yaw moment with respect to rudder turning rate
N_δ	derivative of yaw moment with respect to rudder angle
N_η	derivative of yaw moment with respect to a ship's offset distance in a canal
$N_{\dot{\beta}}$	derivative of yaw moment with respect to drift angular velocity
N_β	derivative of yaw moment with respect to drift angle
$N_{\beta H}$	derivative N_β for a finite water depth H
$N_{\beta \infty}$	derivative N_β for infinitely deep water
$N_{\beta WH}$	derivative N_β in a canal with width W and depth H
$N_{\beta \infty H}$	derivative N_β in shallow water H ($= N_{\beta H}$)
N_{rH}	derivative N_r for a finite water depth H
$N_{r \infty}$	derivative N_r for infinitely deep water
P_1, P_2	two components of a vector belonging to the complementary vector space π (see (4.12), (4.13))

Nomenclature (continued)

P_1^*, P_2^* two components of a vector belonging to the homogeneous complementary vector space π^* (see (4.15), (4.16))

$\bar{P}$ a fixed-vector of π-space

q_1, q_2 two components of a vector belonging to the associated vector space Ω (see (4.14))

q_1^*, q_2^* two components of a vector belonging to the homogeneous associated vector space Ω^*

$\bar{q}$ a fixed-vector of Ω-space

r yaw angular velocity

$\bar{r}$ amplitude of a sinusoidal yaw rate

$R(s)$ Laplace transform of yaw velocity $r(t)$

r_1, r_2 two components of a common vector of π and Ω spaces: $R = (r_1, r_2)$

R_π arbitrary point (or vector) in π-space

R_Ω arbitrary point (or vector) in Ω-space

S_B body surface immersed in the fluid

$S(x)$ sectional area of a body at x

T ship's draft

T_1, T_2, T_3 stability indices of a ship defined by (2.46)

t time

U ship's speed (resultant speed)

$U(t)$ unit step function (see (2.47))

u longitudinal component of ship's speed

v lateral component of ship's speed

W canal breadth

Nomenclature (continued)

x	longitudinal axis of a ship
X	hydrodynamic force along x-axis
y	transverse axis of a ship
Y	hydrodynamic force along y-axis or sway force
$\bar{Y}$	amplitude of a sinusoidal sway force Y
$Y_{\dot{v}}$	derivative of sway force with respect to sway acceleration ($\equiv -m_y$)
Y_v	derivative of sway force with respect to sway velocity
$Y_{\dot{r}}$	derivative of sway force with respect to yaw angular acceleration
Y_r	derivative of sway force with respect to yaw velocity
$Y_{\dot{\delta}}$	derivative of sway force with respect to rudder turning rate
Y_{δ}	derivative of sway force with respect to rudder angle
Y_{η}	derivative of sway force with respect to a ship's offset distance in a canal
$Y_{\dot{\beta}}$	derivative of sway force with respect to drift angular velocity
Y_{β}	derivative of sway force with respect to drift angle
$Y_{\beta H}$	derivative Y_{β} for a finite water depth H
$Y_{\beta \infty}$	derivative Y_{β} for infinitely deep water
$Y_{\beta WH}$	derivative Y_{β} in a canal with width W and depth H
$Y_{\beta \infty H}$	derivative Y_{β} in shallow water H ($=Y_{\beta H}$)
Y_{rH}	derivative Y_r for a finite water depth H

Nomenclature (continued)

$Y_{r\infty}$	derivative Y_r for infinitely deep water
$\alpha_0, \alpha_1, \alpha_2, \alpha_3$	constants included in the transfer function (2.36)
α_2^*	constant included in the transfer function (2.42) (see (2.44))
β	drift angle of a ship
$\bar{\beta}$	amplitude of a sinusoidal drift angle
$\gamma(\xi)$	strength of vortex at ξ
$\gamma_0, \gamma_1, \gamma_2, \gamma_3, \gamma_4$	constants included in the transfer function (2.38) (see (2.40))
δ	rudder angle
δ_0	a constant rudder angle
ϵ_1, ϵ_2	phase lags of sinusoidal sway force and yaw moment
$\zeta_0, \zeta_1, \zeta_2, \zeta_3$	constants included in the transfer function (2.39) (see (2.41))
η	an axis of a coordinate system fixed in space (see Fig. 1)
η_G	lateral position of the center of gravity of a ship in a canal
$\bar{\eta}_G$	amplitude of a sinusoidal lateral position $\eta(t)$
η_0	initial offset distance of a ship from the centerline of a canal
η_p	port bank distance parameter defined by Norrbin [23]
ξ	an axis of coordinate system fixed in space (see Fig. 1) or the stagger of two ships
ρ	density of the fluid
ϕ	velocity potential function

Nomenclature (continued)

ϕ_i velocity potential due to an elementary motion with unit velocity: $i=1$, surge; $i=2$, sway; $i=6$, yaw

ψ directional angle of a ship or stream function

$\Psi(s)$ Laplace transform of directional angle

ψ_0 initial deviation of directional angle

ω frequency of the motion

Nomenclature (continued)

Definition of dimensionless variables

I'_{zz} : $\dfrac{I_{zz}}{(1/2)\rho L^5}$

N'_r : $\dfrac{N_r}{(1/2)\rho L^4 U}$

J'_{zz} : $\dfrac{J_{zz}}{(1/2)\rho L^5}$

$N_{\dot{\delta}}{}'$: $\dfrac{N_{\dot{\delta}}}{(1/2)\rho L^4 U}$

K' : $\dfrac{KL}{U}$

N'_{δ} : $\dfrac{N_{\delta}}{(1/2)\rho L^3 U^2}$

m' : $\dfrac{m}{(1/2)\rho L^3}$

N'_{η} : $\dfrac{N_{\eta}}{(1/2)\rho L^2 U^2}$

m'_y : $\dfrac{m_y}{(1/2)\rho L^3}$

$N_{\dot{\beta}}{}'$: $\dfrac{N_{\dot{\beta}}}{(1/2)\rho L^4 U}$

N' : $\dfrac{N}{(1/2)\rho L^3 U^2}$

N'_{β} : $\dfrac{N_{\beta}}{(1/2)\rho L^3 U^2}$

$N_{\dot{v}}{}'$: $\dfrac{N_{\dot{v}}}{(1/2)\rho L^4}$

r' : $r\dfrac{L}{U}$

N'_v : $\dfrac{N_v}{(1/2)\rho L^3 U}$

T'_1, T'_2, T'_3 : $\dfrac{T_i U}{L}$ (i=1,2,3)

$N_{\dot{r}}{}'$: $\dfrac{N_{\dot{r}}}{(1/2)\rho L^5}$

t' : $t\dfrac{U}{L}$

Nomenclature (continued)   Definition of dimensionless variables

$v' \quad : \quad \dfrac{v}{U}$

$\beta' \quad : \quad \beta$

$Y' \quad : \quad \dfrac{Y}{(1/2)\rho L^2 U^2}$

$\delta' \quad : \quad \delta$

$Y_{\dot{v}}' \quad : \quad \dfrac{Y_{\dot{v}}}{(1/2)\rho L^3}$

$\eta' \quad : \quad \dfrac{\eta}{L}$

$Y_v' \quad : \quad \dfrac{Y_v}{(1/2)\rho L^2 U}$

$\psi' \quad : \quad \psi$

$Y_{\dot{r}}' \quad : \quad \dfrac{Y_{\dot{r}}}{(1/2)\rho L^4}$

$\omega' \quad : \quad \omega \dfrac{L}{U}$

$Y_{\dot{\delta}}' \quad : \quad \dfrac{Y_{\dot{\delta}}}{(1/2)\rho L^3 U}$

$Y_{\delta}' \quad : \quad \dfrac{Y_{\delta}}{(1/2)\rho L^2 U^2}$

$Y_{\eta}' \quad : \quad \dfrac{Y_{\eta}}{(1/2)\rho L U^2}$

$Y_{\dot{\beta}}' \quad : \quad \dfrac{Y_{\dot{\beta}}}{(1/2)\rho L^3 U}$

$Y_{\beta}' \quad : \quad \dfrac{Y_{\beta}}{(1/2)\rho L^2 U^2}$

1. *INTRODUCTION*

In the last ten years, the size of ships has greatly increased: for example, the size of the world's largest oil-tanker went from 150,000 DWT nine years ago to 480,000 DWT two years ago. This increase in displacement has brought serious difficulty in handling ships in harbors, especially when they are approaching and leaving the pier, or passing through the narrow waterways. When navigating at slow speed through a busy area where many kinds of ships run in different directions at different speeds, a supertanker requires the help of many tugboats.

As the ship displacement increased, the draft increased simultaneously from 16.0 m of ships a decade ago to 28.20 m for the 480,000 DWT tanker. The increase of draft amounts to the relative decrease of the water depth of existing harbors and waterways, so that a vessel's maneuverability tends to be very much affected by the finite water depth.

In the early stages of ship hydrodynamic research in restricted water, more attention was paid to the increase of the ship resistance than to the effect on the ship maneuverability. It was known from experience that the ship maneuverability in restricted water was much different from that in deep water, but there seemed to be a certain confusion with respect to its description. The maneuverability of a ship includes two inconsistent characteristics: one is the course-keeping quality or course stability and the other is the turning ability. When the course stability of a ship becomes poorer because

of the restriction of the waterway, the turning ability of the ship always becomes better, and vice versa. It doesn't make sense to say that the maneuverability of a ship becomes either better or worse in restricted water.

Another aspect of ship motion in shallow water is a conspicuous change of ship's attitude, i.e., bodily sinkage and trim, well known among experienced ship operators. According to the recent analysis by Tuck [1],** the magnitudes of the bodily sinkage and trim of a ship are related to the ship's speed as follows: As the ship's speed varies, both the bodily sinkage and the trim vary according to the factor $F_H^2/\sqrt{1-F_H^2}$, where Froude number F_H is defined by $U/\sqrt{Hg}$. That is to say, if the ship's speed is under the critical speed $\sqrt{Hg}$, both the bodily sinkage and the trim by the stern increase as the ship's speed approaches the critical speed. The change of the draft and trim of a ship can have a noticeable effect on the ship's maneuverability. It is, however, customary that most merchant ships reduce speed in restricted water, to the extent that rudder effectiveness is not degraded, and in most cases, bodily sinkage and trim do not become so large that the maneuverability of a ship is seriously affected.

In this monograph, the author will try to explain the maneuverability of ships in restricted waters, but the discussion will be confined to the course stability of ships moving at constant speed instead of to the turning ability at constant speed, since the course

---

**The number in brackets designates a reference listed at the end of this monograph.

stability can be described by linear equations of motion. Hence, in part 2, the linear maneuvering equations of motion will be introduced and the necessary and sufficient conditions for stability will be indicated. Furthermore, an essential difference between the response to the rudder deflection in either shallow or deep water, and the response in a canal, will be elucidated.

Based on the experimental data of the stability derivatives, the course stability in shallow water and in a canal will be discussed in part 3, and the improvement of the course stability in a canal by the adoption of automatic steering will be considered. Theoretical contributions have been made with regard to the restricted water effect on the stability derivatives. Although the quantitative accuracy of the theoretical predictions doesn't seem to be very good, the theory will become more important in the future because it is very time-consuming and expensive always to rely on experiments for the stability derivatives in restricted water. Therefore, in part 4, we shall clarify the discrepancy between the experimental results and the current theoretical method of prediction. The author believes this may be helpful in improving the theoretical approach.

Up to and including part 4, all discussions are based on the linear maneuvering equations of motion. If, however, the maneuvering motion deviates considerably from a straight line path at constant speed, the motion cannot be accurately predicted by the linear equations. In particular, when we predict the motion of an unstable ship, it is important to take account of the nonlinearity of the

hydrodynamic force acting on the ship. Otherwise, any perturbation due to a small disturbance cannot remain finite, but diverges to infinity. Hence, in part 5, we shall consider the nonlinear mathematical model describing the maneuvering motion. The stress will be laid exclusively on the simplified nonlinear models because, from the practical point of view, we can determine the unknowns appearing in such equations through the use of the time-history of the motion recorded on board ship or on a model of the vessel. Finally, such external forces as the wind, waves, and water currents will not be taken into account; that is, we shall consider the maneuvering motion of ships only in calm seas.

2. LINEAR MANEUVERING EQUATIONS OF MOTION IN RESTRICTED WATERS AND COURSE STABILITY

2.1. Linear Maneuvering Equations of Motion

In order to describe the maneuvering motion of a ship in restricted waters, we use two kinds of coordinate systems, O-$\xi\eta$ and G-xy, the former fixed in space and the latter fixed with respect to a moving ship. Figure 1 shows a ship moving in an uniform canal, where the coordinate axis $O\xi$ coincides with the centerline of the canal. The transverse section of the canal is assumed to be symmetric with respect to the centerline of the canal. The direction of the arrows shown in the figure indicates the positive values of such angles as the drift angle β, rudder angle δ, and directional angle ψ. Since we will (1) restrict our consideration to the planar motion of a ship on the $\xi\eta$-plane or xy-plane and (2) assume that the rolling motion of a ship is small, it is sufficient to take into consideration only three components of the ship's linear and angular velocity: u, v, and r.

The maneuvering motion of a ship traveling in calm seas used to be described by a set of ordinary differential equations with constant hydrodynamic coefficients. This method has been followed by many people since it was introduced by Davidson and Shiff [2], and Motora [3]. On the other hand, as Brard pointed out [4], even if the free

surface is replaced by a rigid wall, the vortex shed from a moving ship has a kind of memory effect on the hydrodynamic force acting on the ship. In other words, the hydrodynamic force is dependent not only on the instantaneous state of the ship motion but also on the past history of the motion.
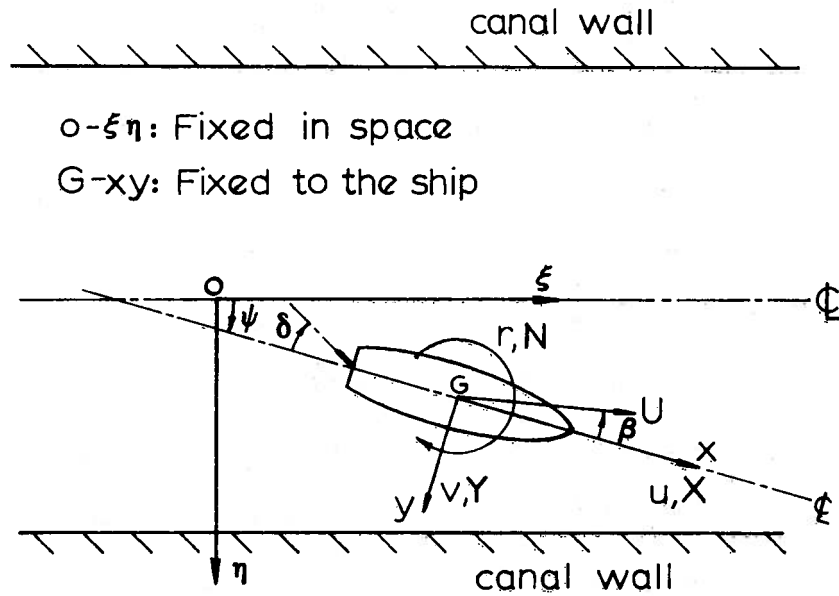

Figure 1. Coordinate system for describing the motion of a ship traveling in a canal.

In seakeeping, the hydrodynamic coefficients of the equations of motion are always considered as functions of the frequency of motion. From the mathematical point of view, it is, of course, strange that the ordinary differential equations have frequency-dependent coefficients. Several years ago, Cummins [5] gave a clue to solving this problem. He derived integro-differential equations as the governing equations of the seakeeping motion by paying attention to the frequency dependence of the hydrodynamic coefficients. Strictly speaking, the maneuvering motion also should be described by the integro-differential equations, or, what amounts to the same thing, the hydrodynamic coefficients of the maneuvering equations of motion should be considered as functions of the frequency of motion.

With this point in mind, the author compared two kinds of yaw response of a directionally stable ship to a stepwise deflection of the rudder; these were obtained (1) by taking account of the frequency dependence of the hydrodynamic coefficients, and (2) by neglecting the frequency dependence [6]. As a result, it was clear that the equations with the so-called slow-motion derivatives could produce a yaw response to the rudder deflection that was almost the same as that obtained from the integro-differential equations. Therefore, from a practical standpoint, the integro-differential equations which are the exact maneuvering equation of motion, can, with confidence, be replaced by a set of ordinary differential equations with constant stability derivatives, and this is done in the following discussion.

For the reference frame fixed to the moving ship, the ordinary differential equations of maneuvering motion are:

$$m \left(\frac{du}{dt} - rv\right) = X$$

$$m \left(\frac{dv}{dt} + ru\right) = Y \qquad (2.1)$$

$$I_{zz} \frac{dr}{dt} = N ,$$

where the right-hand terms X, Y, and N are the external forces and moment acting on a ship, which are assumed to be functions of the following variables: ship's acceleration, velocity, rudder angle, position in a canal, and attitude with respect to the centerline of a canal. The last two variables refer to the effect of the bank on the hydrodynamic force in a canal and are, of course, unnecessary when the ship motion takes place in deep water or in otherwise unrestricted shallow water.

Since the ship's lateral position in a canal, η, and the directional angle, ψ, serve to fix the position of the vessel in the canal, it is natural to assume that the hydrodynamic forces and moment acting on the ship in a canal are also functions of η and ψ [7]. That is, in symbolic form,

$$X = X (u, v, r, \delta, \dot{u}, \dot{v}, \dot{r}, \dot{\delta}, \eta, \psi)$$

$$Y = Y (u, v, r, \delta, \dot{u}, \dot{v}, \dot{r}, \dot{\delta}, \eta, \psi) \qquad (2.2)$$

$$N = N (u, v, r, \delta, \dot{u}, \dot{v}, \dot{r}, \dot{\delta}, \eta, \psi) .$$

In the equilibrium condition of motion, the ship travels in a straight

path on the centerline of a canal and at constant speed U. That is to say, all variables except for u are zero: $v=r=\delta=\dot{u}=\dot{v}=\dot{r}=\dot{\delta}=\eta=\psi=0$ and $u=U$.

In what follows, we assume that the perturbations from the equilibrium state are small. Describing a small perturbation with the symbol Δ, we have

$$
\left.
\begin{aligned}
u &= U + \Delta u \ , \qquad v = \Delta v \quad , \qquad r = \Delta r \ , \qquad \delta = \Delta\delta \\
\dot{u} &= \Delta\dot{u} \qquad , \qquad \dot{v} = \Delta\dot{v} \quad , \qquad \dot{r} = \Delta\dot{r} \ , \qquad \dot{\delta} = \Delta\dot{\delta} \\
\eta &= \Delta\eta \qquad , \qquad \psi = \Delta\psi \quad .
\end{aligned}
\right\} \qquad (2.3)
$$

Expanding the hydrodynamic forces and moment X, Y, and N with respect to the small perturbations of the variables and keeping the linear terms only, we obtain

$$
m\,\frac{d\Delta u}{dt} = X(U,0,0,0,0,0,0,0,0,0) + X_u\Delta u + X_v\Delta v + X_r\Delta r + X_\delta\Delta\delta
$$
$$
+ X_{\dot{u}}\Delta\dot{u} + X_{\dot{v}}\Delta\dot{v} + X_{\dot{r}}\Delta\dot{r} + X_{\dot{\delta}}\Delta\dot{\delta} + X_\eta\Delta\eta + X_\psi\Delta\psi \qquad (2.4)
$$

$$
m\left(\frac{d\Delta v}{dt} + Ur\right) = Y(U,0,0,0,0,0,0,0,0,0) + Y_u\Delta u + Y_v\Delta v + Y_r\Delta r + Y_\delta\Delta\delta
$$
$$
+ Y_{\dot{u}}\Delta\dot{u} + Y_{\dot{v}}\Delta\dot{v} + Y_{\dot{r}}\Delta\dot{r} + Y_{\dot{\delta}}\Delta\dot{\delta} + Y_\eta\Delta\eta + Y_\psi\Delta\psi \qquad (2.5)
$$

$$
I_{zz}\,\frac{d\Delta r}{dt} = N(U,0,0,0,0,0,0,0,0,0) + N_u\Delta u + N_v\Delta v + N_r\Delta r + N_\delta\Delta\delta
$$
$$
+ N_{\dot{u}}\Delta\dot{u} + N_{\dot{v}}\Delta\dot{v} + N_{\dot{r}}\Delta\dot{r} + N_{\dot{\delta}}\Delta\dot{\delta} + N_\eta\Delta\eta + N_\psi\Delta\psi \qquad , \qquad (2.6)
$$

where the coefficients X_u, X_v,......, Y_u, Y_v,......, N_u, N_v,......, N_ψ stand for the partial differential coefficients of X, Y, and N with respect to the subscript variables, which are evaluated at the equilibrium state (U,0,0,0,0,0,0,0,0,0). For example, the coefficient X_u is defined as the partial derivative $\partial X/\partial u$ at $u=U$, $v=r=...=\psi=0$.

The first term of the right-hand side of equation (2.4) means the total resistance of a ship traveling at a constant speed U, which is cancelled by the thrust of the ship's screw; hence, it will be omitted from now on. The first term $Y(U,0,0,\ldots,0)$ of equation (2.5) stands for a constant lateral force acting on a ship that travels on the centerline of a canal at a constant advance speed U. Therefore, if the ship's hull is symmetric with the vertical plane through the longitudinal axis Gx, this term must be negligibly small compared with the other terms.** This situation is also true for the first term of equation (2.6), i.e., $N(U,0,0,\ldots,0)$. Taking account of the symmetry of the ship's hull makes some of the stability derivatives of the above equations zero:

$$\left.\begin{array}{l} X_v = X_r = X_\delta = X_{\dot{v}} = X_{\dot{r}} = X_{\dot{\delta}} = X_\eta = X_\psi = 0 \\[2mm] Y_u = Y_{\dot{u}} = 0 \\[2mm] N_u = N_{\dot{u}} = 0 \qquad . \end{array}\right\} \qquad (2.7)$$

Furthermore, we assume that the hydrodynamic force and moment due to the ship's attitude in a canal, $Y_\psi \Delta\psi$ and $N_\psi \Delta\psi$, are negligibly small. In other words, the bank effect on the hydrodynamic force and moment acting on a ship can be expressed by only the lateral position of the

---

**Strictly speaking, this term has a finite value because of the asymmetry of the flow around the ship's hull, which is especially notable in a single-screw ship. In that case, we can reach equivalent linear expansions by assuming an oblique path of travel, i.e., u=U, $v=v_0$, r=0, $\delta=\delta_0$, $\dot{u}=\dot{v}=\dot{r}=\dot{\delta}=\eta=0$, $\psi=\psi_0$, as an equilibrium state of motion equivalent to the straight-line path of travel used to derive equations (2.4) to (2.6).

ship in the canal. Consequently, the linear equations (2.4) to (2.6) reduce to remarkably simple expressions:**

$$(m - X_{\dot{u}}) \frac{du}{dt} = X_u u \tag{2.8}$$

$$(m - Y_{\dot{v}}) \frac{dv}{dt} = Y_v v + (-mU + Y_r)r + Y_\delta \delta + Y_{\dot{r}} \dot{r} + Y_{\dot{\delta}} \dot{\delta} + Y_\eta \eta \tag{2.9}$$

$$(I_{zz} - N_{\dot{r}}) \frac{dr}{dt} = N_v v + N_r r + N_\delta \delta + N_{\dot{v}} \dot{v} + N_{\dot{\delta}} \dot{\delta} + N_\eta \eta \quad . \tag{2.10}$$

It is important to note that the longitudinal or surge equation is of closed form with respect to the longitudinal component of the velocity perturbation, and that the sway and yaw equations do not include the perturbation of surge velocity u. In other words, the surge motion doesn't couple with the sway and yaw motions, as far as the linear equations are concerned. Because of this, when we discuss the maneuvering motion accompanied by small velocity perturbations, it is sufficient to deal with equations (2.9) and (2.10). The set of those two equations is not complete, however, because there are three variables v, r, and η, and so we need one more relationship in order to completely define the maneuvering motion of a ship in a canal. For this purpose, auxiliary relationships will be introduced when we derive the necessary and sufficient conditions for the course stability in a canal.

In cases where it is unnecessary to take account of the bank effect on the hydrodynamic force, the last term in each of equations (2.9) and (2.10) can be omitted. That is, equations (2.9) and (2.10)

_____

**For simplicity, the symbol Δ is dropped.

without the last terms are a complete set describing the maneuvering
motion in deep water and in shallow water. The stability derivatives
of those equations vary according to the water depth.

Under the assumption of small perturbations, the drift angle β is
often used instead of the sway velocity v; we make the following
approximation:

$$v = - U \sin \beta \simeq - U \beta \qquad (2.11)$$

and then

$$\dot{v} \simeq - U \dot{\beta} \qquad . \qquad (2.12)$$

If we use the drift angle β instead of the sway velocity v, equations
(2.9) and (2.10) become:

$$-(m-Y_{\dot{\beta}}) U \frac{d\beta}{dt} = Y_\beta \beta + (-mU + Y_r)r + Y_\delta \delta + Y_{\dot{r}}\dot{r} + Y_{\dot{\delta}}\dot{\delta} + Y_\eta \eta \qquad (2.13)$$

$$(I_{zz}-N_{\dot{r}}) \frac{dr}{dt} = N_\beta \beta + N_r r + N_\delta \delta + N_{\dot{\beta}}\dot{\beta} + N_{\dot{\delta}}\dot{\delta} + N_\eta \eta \qquad . \qquad (2.14)$$

The stability derivative $-Y_{\dot{v}}$ or $-Y_{\dot{\beta}}$ is called the sway added mass, and
is often labeled m_y. The derivative $-N_{\dot{r}}$ is called the yaw added mass
moment of inertia and is replaced by J_{zz}. Denoting the non-dimensional
value by the prime ('), the dimensionless equations of motion are as
follows:

$$-(m'+m_y') \frac{d\beta'}{dt'} = Y_\beta' \beta' + (-m'+Y_r')r' + Y_\delta' \delta' + Y_{\dot{r}} \dot{r}' + Y_{\dot{\delta}} \dot{\delta}' + Y_\eta' \eta'$$

$$(2.15)$$

$$(I_{zz}' + J_{zz}') \frac{dr'}{dt'} = N_\beta' \beta' + N_r' r' + N_\delta' \delta' + N_{\dot{\beta}}' \dot{\beta}' + N_{\dot{\delta}}' \dot{\delta}' + N_\eta' \eta' \qquad .$$

$$(2.16)$$

2.2. *Conditions For Course Stability*

Now we consider the inherent course stability of a ship traveling in a canal. As mentioned in section 2.1, we need an auxiliary relationship connecting the dependent variables v, r, and η in order to make the linear equations (2.9) and (2.10) a complete set.

The time rate of change of a ship's offset distance from the centerline of a canal, $\dot{\eta}(t)$, is described as follows:

$$\frac{d\eta}{dt} = v \cos \psi + u \sin \psi$$
$$= U \sin (\psi - \beta) \qquad . \qquad (2.17)$$

Assuming that the angle $\psi - \beta$ is small, we obtain one auxiliary relationship:

$$\frac{d\eta}{dt} \simeq U (\psi - \beta) \qquad . \qquad (2.18)$$

The dimensionless counterpart of equation (2.18) is

$$\frac{d\eta'}{dt'} = \psi' - \beta' \qquad . \qquad (2.19)$$

We define

$$\frac{d\psi}{dt} = r \qquad , \qquad (2.20)$$

or

$$\frac{d\psi'}{dt'} = r' \qquad . \qquad (2.21)$$

The four equations (2.13), (2.14), (2.18), and (2.20) or their dimensionless counterparts, (2.15), (2.16), (2.19), and (2.21), describe completely the motion of a ship in a canal. Since all of these

equations are first-order linear ordinary differential equations with constant coefficients, the basic solutions have the form of an exponential function of time, namely, $\exp(\sigma t)$ or $\exp(\sigma' t')$. The factor σ of the exponential function is determined by solving the following equation, which is called the characteristic equation of a set of the linear ordinary differential equations:

$$
\begin{vmatrix}
-(m'+m_y')\sigma-Y_\beta' & -(-m'+Y_r')-Y_{\dot{r}}'\sigma' & -Y_\eta' & 0 \\
-N_{\dot{\beta}}'\sigma' & (I_{zz}'+J_{zz}')\sigma'-N_r' & -N_\eta' & 0 \\
1 & 0 & \sigma' & -1 \\
0 & -1 & 0 & \sigma'
\end{vmatrix} = 0
$$

(2.22)

or, in a simpler form,

$$a\sigma'^4 + b\sigma'^3 + c\sigma'^2 + d\sigma' + e = 0 \quad , \tag{2.23}$$

where the coefficients a, b, c, d, and e are real constants defined as follows:

$$
\left.
\begin{aligned}
a &= -(m'+m_y')\,(I_{zz}'+J_{zz}') - Y_{\dot{r}}'N_{\dot{\beta}}' \\
b &= (m'+m_y')\,N_r' - Y_\beta'\,(I_{zz}'+J_{zz}') - N_{\dot{\beta}}'\,(-m'+Y_r') - N_\beta'\,Y_{\dot{r}}' \\
c &= Y_\beta'\,N_r' - N_\beta'\,(-m'+Y_r') + Y_\eta'\,(I_{zz}'+J_{zz}') + N_\eta'\,Y_{\dot{r}}' \\
d &= (m'+m_y')\,N_\eta' - Y_\eta'\,N_r' - N_{\dot{\beta}}'\,Y_\eta' + N_\eta'\,(-m'+Y_r') \\
e &= Y_\beta'\,N_\eta' - Y_\eta'\,N_\beta'
\end{aligned}
\right\}
$$

(2.24)

The necessary and sufficient condition for course stability is that the real parts of the solution σ' of the algebraic equation (2.23) are all negative. From the Routh-Hurwitz criteria [8], this condition

is always satisfied when the following inequalities are satisfied:

$$\frac{b}{a} > 0 \ , \quad \frac{d}{a} > 0 \ , \quad \frac{e}{a} > 0 \ , \quad \frac{bcd-ad^2-b^2e}{a^3} > 0 \ . \qquad (2.25)$$

The four conditions of equation (2.25) are the necessary and sufficient conditions for course stability of a ship traveling in a canal. We can, however, reduce the number of the conditions by inspecting the magnitudes of the stability derivatives as well as their signs.

For instance, the coefficients a and b are always negative, because the virtual mass $m'+m_y'$ and the virtual mass moment of inertia $I_{zz}+J_{zz}$ are always positive and are considerably larger than the absolute values of the other acceleration derivatives, $Y_{\dot{r}}'$ and $N_{\dot{\beta}}'$; furthermore, the damping derivatives N_r' and Y_β' are always negative and positive respectively. Therefore, the first inequality of equation (2.25) is always satisfied. In addition, the coefficient e is also always negative, because the stability derivatives Y_η' and N_η' representing the bank effect are always positive and negative respectively. Physically, a ship traveling between two banks and parallel to them receives a suction force toward the nearer bank as the ship's bow is repelled by the bank. Therefore, the third inequality of equation (2.25) is also satisfied. Consequently, the second and fourth conditions, i.e., $d<0$ and $bcd-ad^2-b^2e<0$, are the conditions for course stability of a ship traveling in a canal.

In contrast, the condition for course stability of a ship moving in deep or shallow water, otherwise unrestricted, is quite simple. In this case, the maneuvering motion can be described completely by the

two equations (2.15) and (2.16). Therefore, the necessary and sufficient conditions for the course stability are

$$\frac{b}{a} > 0 \quad , \quad \frac{c^*}{a} > 0 \quad , \tag{2.26}$$

where c* is defined as follows:

$$c^* = Y_\beta' N_r' - N_\beta' \cdot (-m' + Y_r') \quad . \tag{2.27}$$

By the same reasoning through which we obtained the conditions of the course stability in a canal, the first inequality of equation (2.26) is always satisfied. Therefore, the condition for course stability of a ship traveling in deep or shallow water is that c* should be negative. In symbolic terms, the condition for the stability is

$$\frac{N_r'}{-m'+Y_r'} - \frac{N_\beta'}{Y_\beta'} > 0 \qquad \text{for } -m'+Y_r' < 0 \tag{2.28}$$

$$\frac{N_r'}{-m'+Y_r'} - \frac{N_\beta'}{Y_\beta'} < 0 \qquad \text{for } -m'+Y_r' > 0 \tag{2.29}$$

2.3. *Transfer Functions and the Stationary State of Motion Corresponding to a Constant Rudder Angle*

If we assume that all the initial values of the variables occurring in equations (2.15), (2.16), (2.19), and (2.21) are zero, Laplace transforms of those equations are as follows:

$$(\xi_1 s - \xi_2) \, B(s) = (\xi_5 s + \xi_3) R(s) + (\xi_6 s + \xi_4) D(s) + \xi_7 H(s) \tag{2.30}$$

$$(\eta_1 s - \eta_2) \, R(s) = (\eta_5 s + \eta_3) B(s) + (\eta_6 s + \eta_4) D(s) + \eta_7 H(s) \tag{2.31}$$

$$s H(s) = \Psi(s) - B(s) \tag{2.32}$$

$$s \Psi(s) = R(s) \tag{2.33}$$

where $B(s)$, $R(s)$, $D(s)$, $H(s)$, and $\Psi(s)$ are Laplace transforms of the

variables $\beta'(t')$, $r'(t')$, $\delta'(t')$, $\eta'(t')$, and $\psi'(t')$ respectively,

where $B(s)$, for example, is defined as

$$B(s) \equiv \mathcal{L}[\beta'(t')] = \int_0^\infty \beta'(t') e^{-st'} dt' \quad . \tag{2.34}$$

The stability derivatives of equations (2.15) and (2.16) are replaced

by the coefficients ξ_i and η_i for the sake of simplicity:

$$\xi_1 = -(m' + m_y')$$
$$\xi_2 = Y_\beta'$$
$$\xi_3 = -m' + Y_r'$$
$$\xi_4 = Y_\delta'$$
$$\xi_5 = Y_{\dot{r}}'$$
$$\xi_6 = Y_{\dot{\delta}}'$$
$$\xi_7 = Y_\eta'$$

$$\eta_1 = I_{zz}' + J_{zz}'$$
$$\eta_2 = N_r'$$
$$\eta_3 = N_\beta'$$
$$\eta_4 = N_\delta'$$
$$\eta_5 = N_{\dot{\beta}}'$$
$$\eta_6 = N_{\dot{\delta}}'$$
$$\eta_7 = N_\eta \quad . \tag{2.35}$$

Eliminating $B(s)$, $\Psi(s)$, and $H(s)$ from equations (2.30) through (2.33),

we obtain a transfer function which describes the ratio of yaw

response to the rudder deflection:

$$\frac{R(s)}{D(s)} = \frac{s (\alpha_0 s^3 + \alpha_1 s^2 + \alpha_2 s + \alpha_3)}{a s^4 + b s^3 + c s^2 + d s + e} \quad , \tag{2.36}$$

where the coefficients a, b, c, d, and e are exactly the same as those defined by equation (2.24), and the coefficients α_i are defined as follows:

$$\alpha_0 = \xi_6 \eta_5 + \xi_1 \eta_6$$

$$\alpha_1 = \xi_1 \eta_4 - \xi_2 \eta_6 + \xi_4 \eta_5 + \xi_6 \eta_3$$

$$\alpha_2 = -\xi_2 \eta_4 + \xi_4 \eta_3 - \xi_6 \eta_7 + \xi_7 \eta_6$$

$$\alpha_3 = -\xi_4 \eta_7 + \xi_7 \eta_4 \quad .$$

$$(2.37)$$

In a similar way, we obtain the other transfer functions:

$$\frac{B(s)}{D(s)} = \frac{\gamma_0 s^4 + \gamma_1 s^3 + \gamma_2 s^2 + \gamma_3 s + \gamma_4}{as^4 + bs^3 + cs^2 + ds + e} \tag{2.38}$$

$$\frac{H(s)}{D(s)} = \frac{\zeta_0 s^3 + \zeta_1 s^2 + \zeta_2 s + \zeta_3}{as^4 + bs^3 + cs^2 + ds + e} \quad , \tag{2.39}$$

where the coefficients γ_i and ζ_i are defined by

$$\gamma_0 = \xi_5 \eta_6 + \xi_6 \eta_1$$

$$\gamma_1 = \xi_3 \eta_6 + \xi_4 \eta_1 + \xi_5 \eta_4 - \xi_6 \eta_2$$

$$\gamma_2 = \xi_3 \eta_4 - \xi_4 \eta_2$$

$$\gamma_3 = -\xi_6 \eta_7 + \xi_7 \eta_6$$

$$\gamma_4 = -\xi_4 \eta_7 + \xi_7 \eta_4$$

$$(2.40)$$

and

$$\zeta_0 = -\xi_5 \eta_6 - \xi_6 \eta_1$$

$$\zeta_1 = \xi_1 \eta_6 - \xi_3 \eta_6 - \xi_4 \eta_1 - \xi_5 \eta_4 + \xi_6 \eta_2 + \xi_6 \eta_5$$

$$\zeta_2 = \xi_1 \eta_4 - \xi_2 \eta_6 - \xi_3 \eta_4 + \xi_4 \eta_2 + \xi_4 \eta_5 + \xi_6 \eta_3$$

$$\zeta_3 = -\xi_2 \eta_4 + \xi_4 \eta_3 \quad .$$

$$(2.41)$$

By comparison, the transfer functions describing the maneuvering motion in deep water and in shallow water are considerably simpler:

$$\frac{R(s)}{D(s)} = \frac{\alpha_0 s^2 + \alpha_1 s + \alpha_2 *}{a s^2 + b s + c *} \tag{2.42}$$

$$\frac{B(s)}{D(s)} = \frac{\gamma_0 s^2 + \gamma_1 s + \gamma_2}{a s^2 + b s + c *} \quad , \tag{2.43}$$

where the coefficient $\alpha_2 *$ is defined as α_2, with ξ_7 and η_7 being equal to zero; that is,

$$\alpha_2 * = -\xi_2 \eta_4 + \xi_4 \eta_3 \quad . \tag{2.44}$$

In particular, if we assume that both $Y_{\dot\delta}'$ and $N_{\dot\delta}'$ are zero, the well-known transfer function of the yaw velocity versus the rudder angle is derived from equation (2.42):

$$\frac{R(s)}{D(s)} = \frac{K(T_3 s + 1)}{(T_1 s + 1)(T_2 s + 1)} \quad , \tag{2.45}$$

where

$$T_1 T_2 = \frac{a}{c*} = \frac{-(m'+m_y')(I_{zz}'+J_{zz}') - Y_{\dot r}' N_{\dot \beta}'}{Y_\beta' N_r' - N_\beta'(-m'+Y_r')}$$

$$T_1 + T_2 = \frac{b}{c*} = \frac{(m'+m_y') N_r' - Y_\beta'(I_{zz}'+J_{zz}') - N_{\dot\beta}'(-m'+Y_r') - N_{\dot r}' Y_{\dot r}'}{Y_\beta' N_r' - N_\beta'(-m'+Y_r')}$$

$$K = \frac{\alpha_2 *}{c*} = \frac{-Y_\beta' \cdot N_\delta' + Y_\delta' N_\beta'}{Y_\beta' \cdot N_r' - N_\beta'(-m'+Y_r')}$$

$$T_3 = \frac{\alpha_1}{\alpha_2 *} = \frac{-(m'+m_y') N_\delta' + Y_\delta' N_{\dot\beta}'}{-Y_\beta' N_\delta' + Y_\delta' N_\beta'}$$

$$\left. \right\} \tag{2.46}$$

$$\cdot$$

-19-

It should be noted that the two transfer functions (2.42) and (2.43) for motion in deep or shallow water are of the same form, while the transfer functions (2.36) and (2.38) for motion in a canal are not. This dissimilarity in form produces a great difference between the stationary states of yaw and sway response to rudder deflection.

In either shallow water or deep water, the stationary state of the yaw response to a step deflection of the rudder, whose Laplace transform is written

$$\mathcal{L}[\delta_0' \ U(t')] = \frac{\delta_0'}{s} \quad , \quad (2.47)$$

is immediately determined from the final value theorem [9]:

$$\lim_{t' \to \infty} r'(t') = \lim_{s \to 0} sR(s) = \lim_{s \to 0} s \cdot \frac{\delta_0'}{s} \cdot \frac{\alpha_0 s^2 + \alpha_1 s + \alpha_2 *}{as^2 + bs + c*}$$

$$= \delta_0' \ \frac{\alpha_2 *}{c*} = K\delta_0' \quad . \quad (2.48)$$

Similarly, the stationary state of the sway response is

$$\lim_{t' \to \infty} \beta'(t') = \frac{\gamma_2}{c*} \ \delta_0' \quad . \quad (2.49)$$

Equation (2.48) says that the stationary state reached under a constant deflection of the rudder is a turning motion with a constant rate proportional to the rudder deflection. Schematically shown in Figure 2(a) is the above-mentioned stationary state for both a stable ship and an unstable ship. Of course, the stationary state of an unstable ship cannot be physically realized, because any quasi-equilibrium state is not stable.

For the case of a ship in a canal, the stationary state of the response to a step deflection of the rudder is not a stationary

turning, but a stationary drifting, because the stationary turning rate
is zero as shown here:

$$\lim_{t' \to \infty} r'(t') = \lim_{s \to 0} sR(s) = \lim_{s \to 0} s \cdot \frac{\delta_0}{s} \cdot \frac{s(\alpha_0 s + \alpha_1 s^2 + \alpha_2 s + \alpha_3)}{as^4 + bs^3 + cs^2 + ds + e} = 0 \quad . \tag{2.50}$$

The stationary values of the other variables are

$$\lim_{t' \to \infty} \beta'(t') = \delta_0 \frac{\gamma_4}{e} \tag{2.51}$$

$$\lim_{t' \to \infty} \psi'(t') = \lim_{s \to 0} s \cdot \frac{R(s)}{s} = \frac{\delta_0 \alpha_3}{e} = \frac{\delta_0 \gamma_4}{e} = \lim_{t' \to \infty} \beta'(t') \tag{2.52}$$

$$\lim_{t' \to \infty} \eta'(t') = \delta_0 \frac{\zeta_3}{e} \quad . \tag{2.53}$$

As the above equations indicate, the stationary state is a steady
drifting or steady oblique movement parallel to the centerline of a
canal but on a different straight line whose deviation from the
centerline is determined by equation (2.53). As the stationary turning
rate in shallow or deep water is proportional to the rudder angle, so
the stationary drift angle and the deviation of ship's path from the
centerline of a canal are proportional to the rudder angle.

For a positive rudder angle, namely, a port rudder, the stationary
values of the drift angle, directional angle, and the deviation from
the centerline are

$$\beta'(\infty) = \psi'(\infty) = \delta_0 \frac{\gamma_4}{e} > 0 \tag{2.54}$$

$$\eta'(\infty) = \delta_0 \frac{\zeta_3}{e} < 0 \quad , \tag{2.55}$$

because the coefficients e and γ_4 are always negative and the coefficient

-21-

ζ_3 is always positive**. Figure 2(b) shows a ship in a canal drifting with a positive rudder deflection δ_0. Whether or not the oblique travel is realizable depends on whether the state is one of stable equilibrium; if it is a state of unstable equilibrium, then it can not be physically realized.

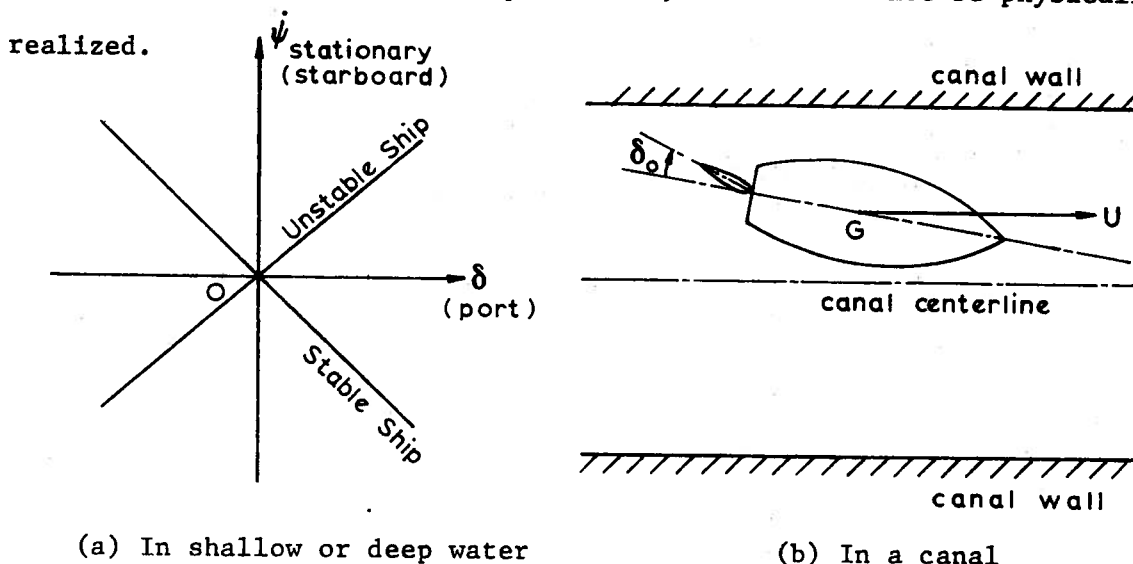(a) In shallow or deep water   (b) In a canal

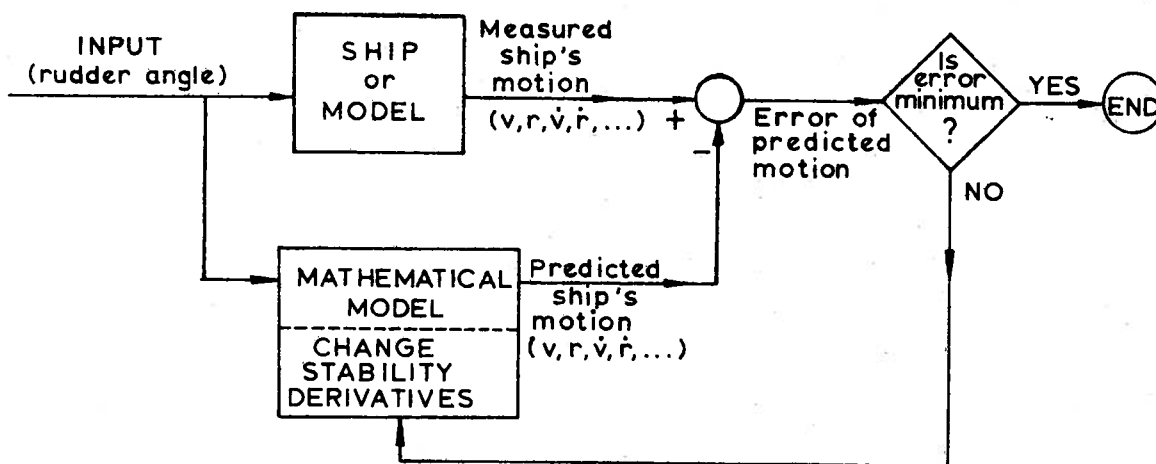Figure 2. Stationary state of ship's response to a constant deflection of rudder.

Figure 3. Principle of the method to determine the stability derivatives from the free-sailing model test.

**See the numerical examples of the stability derivatives given in part 3.

3. EXPERIMENTAL DETERMINATION OF THE STABILITY DERIVATIVES AND THE MANEUVERABILITY OF SHIPS IN RESTRICTED WATERS

When we want to discuss the maneuverability of a ship in restricted waters quantitatively, we have to know the numerical values of the stability derivatives. At the present stage of development of theoretical hydrodynamics, it appears to be difficult to predict the stability derivatives accurately by mathematical calculation. Therefore, if we need reasonably accurate values of the stability derivatives, we must rely on experimental measurements. However, as is well known, the experimental determination is not completely reliable, the most serious obstacle being the so-called scale effect on the hydrodynamic force or the stability derivatives.

Since the hydrodynamic force, which is important for investigating the maneuvering motion of a ship, is closely related to the viscid character of real fluid, the difference in Reynolds number between the model and the full-sized ship makes impossible the exact correspondance of the model-scale experimental results to the full-scale phenomena. This difference could be especially serious in the investigation of the restricted water effect, because the boundary layer around a model is relatively thicker than that of its full-scale counterpart. One can guess that the shallow water effect of the model could be exaggerated by the thicker boundary layer around the model. Unfortunately, we do not presently have an appropriate method by which the experimental

results can be corrected so as to correspond to the real ship; they must be used without correction.

3.1. *Experimental Determination of the Stability Derivatives*

Among the existing experimental methods to determine the stability derivatives, the captive model test is presently the most reliable. In principle, it is also possible to determine the stability derivatives from the free-sailing model test. Some data have been obtained by using a real model [10] and other work has been done using a computer simulation of the maneuvering motion [11]. The principle of such methods is schematically shown in Figure 3.

Since the input rudder deflection to a ship or a model is known, we can determine the difference between the measured ship's motion and the predicted ship's motion obtained by assuming numerical values of the stability derivatives in the mathematical model. Then the stability derivatives are adjusted so as to minimize the error of the predicted ship's motion.** A major defect of this method is that the accuracy of the stability derivatives determined by this method is seriously affected by the accuracy of the measured ship's motion. According to an example shown in [11], even slight noise involved in the measured ship motion diminishes the accuracy of the stability

---

**The detailed description of the method to minimize the error will be omitted here. See the original papers [10, 11].

-24-

derivatives determined this way. Therefore, as stated before, the captive model test is more suitable for determining the stability derivatives than is the free-sailing model test.

There exist two ways of conducting captive model tests. One way is to measure the stationary hydrodynamic force due to a stationary motion and the other is to measure the unsteady hydrodynamic force due to an unsteady motion. The rotating arm test (R.A.T.) belongs to the former category and the test by the planar motion mechanism (P.M.M.) belongs to the latter.

It is in general very difficult to determine such acceleration derivatives as $Y_{\dot{v}}$, $Y_{\dot{r}}$, $N_{\dot{v}}$, and $N_{\dot{r}}$ from the R.A.T. and furthermore, the R.A.T. requires a special kind of water basin. For these reasons, it is usually better to use the P.M.M.

The method to determine the stability derivatives using the P.M.M. will be described briefly.

(1) Pure Sway Motion

The longitudinal centerline of a model traveling with constant speed is kept parallel to the mean advancing direction of the model (that is, the direction of motion of the towing carriage), while the center of gravity of the model travels on a sinusoidal path. Hence, the yaw angular velocity and acceleration of the model are always zero. This motion can be realized by giving a sinusoidal oscillation denoted by equation (3.1) to a model traveling with speed U:

$$\eta_G = \bar{\eta}_G \cos (\omega t + \frac{\pi}{2}) \qquad . \qquad (3.1)$$

Then the sway velocity of the model is

$$v = \dot{\eta}_G = -\bar{\eta}_G \omega \sin (\omega t + \pi/2) \qquad . \qquad (3.2)$$

Therefore, the drift angle β of the model also varies in a sinusoidal way, if the sway velocity is small compared with the speed of advance U:

$$\beta = \tan^{-1} (\frac{-v}{U}) \simeq \frac{\bar{\eta}_G \omega}{U} \sin (\omega t + \pi/2)$$

$$\equiv \bar{\beta} \cos \omega t \qquad \text{where } \bar{\beta} = \frac{\bar{\eta}_G \omega}{U} \qquad . \qquad (3.3)$$

On the other hand, in order to force the model to move in pure sway, we need to apply to the model the force and moment as given:

$$Y(t) = \{ (m+m_y)U\bar{\beta}\omega + Y_\eta \bar{\eta}_G \} \sin \omega t - Y_\beta \bar{\beta} \cos \omega t \qquad (3.4)$$

$$N(t) = (N_{\dot{\beta}} \bar{\beta}\omega + N_\eta \bar{\eta}_G) \sin \omega t - N_\beta \bar{\beta} \cos \omega t \qquad . \qquad (3.5)$$

This force and moment can be described in another way:

$$Y(t) = \bar{Y} \cos (\omega t - \varepsilon_1) \qquad (3.6)$$

$$N(t) = \bar{N} \cos (\omega t - \varepsilon_2) \qquad , \qquad (3.7)$$

where $\bar{Y}$ and $\bar{N}$ are the amplitudes of the force and moment respectively, and ε_1 and ε_2 are the phase lags behind the sinusoidal drift angle. Equating equations (3.4) and (3.5) to equations (3.6) and (3.7) respectively, we obtain

$$\bar{Y} \cos \varepsilon_1 = -Y_\beta \bar{\beta} \qquad (3.8)$$

$$\bar{Y} \sin \varepsilon_1 = (m+m_y) U\bar{\beta}\omega + Y_\eta \bar{\eta}_G \qquad (3.9)$$

$$\bar{N} \cos \varepsilon_2 = -N_\beta \bar{\beta} \qquad (3.10)$$

$$\bar{N} \sin \varepsilon_2 = N_{\dot{\beta}} \bar{\beta}\omega + N_\eta \bar{\eta}_G \qquad . \qquad (3.11)$$

Therefore, we can determine the stability derivatives if we know the amplitudes $\overline{Y}$ and $\overline{N}$, and the phase lags ε_1 and ε_2, because $\overline{\beta}$, $\overline{\eta}_G$, ω, and U are known.

(ii) Pure Yawing Motion

The longitudinal centerline of a model is always tangential to a sinusoidal path of the C.G. of the model. Hence, the model's drift angle β and its time-derivative $\dot{\beta}$ are always zero. This motion can be realized by making the model's transverse position η_G and yaw angular velocity r satisfy the relationships

$$\eta_G = \overline{\eta}_G \cos (\omega t + \pi) \tag{3.12}$$

$$r = \overline{r} \cos \omega t \quad , \tag{3.13}$$

where $\overline{r}$ should be equal to $\overline{\eta}_G \omega^2/U$.

The force and moment that should be applied to the model to achieve pure yaw motion are

$$Y(t) = Y_{\dot{r}} \; \overline{r}\omega \sin \omega t - [(-mU + Y_r) \; \overline{r} - Y_\eta \; \overline{\eta}_G] \cos \omega t \tag{3.14}$$

$$N(t) = -(I_{zz}+J_{zz}) \; \overline{r}\omega \sin \omega t - (N_r \; \overline{r} - N_\eta \; \overline{\eta}_G) \cos \omega t \; . \tag{3.15}$$

Supposing that the force and moment are represented by equations (3.6) and (3.7)**, the desired stability derivatives can be determined as follows:

$$\overline{Y} \cos \varepsilon_1 = (mU - Y_r) \; \overline{r} + Y_\eta \; \overline{\eta}_G \tag{3.16}$$

$$\overline{Y} \sin \varepsilon_1 = Y_{\dot{r}} \; \overline{r}\omega \tag{3.17}$$

$$\overline{N} \cos \varepsilon_2 = -N_r \; \overline{r} + N_\eta \; \overline{\eta}_G \tag{3.18}$$

$$\overline{N} \sin \varepsilon_2 = -(I_{zz}+J_{zz}) \; \overline{r} \; \omega \quad . \tag{3.19}$$

**The phase angles ε_1 and ε_2 should be defined as the lag behind the sinusoidal yaw angular velocity.

It must be noted that the eight formulas (3.8) to (3.11) and (3.16) to (3.19) are not sufficient to determine the stability derivatives definitely, since ten unknowns are involved in those formulas, but there are some methods available for completing the determination. The experimental values of the stability derivatives, quoted from reference [15] in the next section, were determined thus: the derivatives Y_η and N_η denoting the bank effect were obtained from the straight-line towing of a model on different offset lines parallel to the centerline of a canal. Then the remaining eight derivatives were determined through the above eight equations (3.8) to (3.11) and (3.16) to (3.19). The derivatives describing the rudder effectiveness, Y_δ and N_δ, were obtained from the straight-line towing of a model along the centerline of a canal, with the rudder angle being varied.

3.2. *Available Data on the Stability Derivatives in Restricted Waters*

When we judge the course stability of a ship in shallow water or in deep water, it is sufficient to know the four damping derivatives Y_β, N_β, Y_r, and N_r. Alternatively, we can judge whether or not a ship possesses course stability from the results of spiral and reversed spiral tests. On the other hand, if we wish to judge the course stability of a ship in a canal, we have to know other stability derivatives, namely, the acceleration and bank effect derivatives besides the four damping derivatives. At present, existing data on the

stability derivatives in restricted waters are limited. Below is a list of the data.

    (i)   Available Data for the Shallow Water Effect on the Stability Derivatives.

Author	Kind of experiment (stability derivative)
Brard [12]	Oblique tow (Y_β, N_β)
Motora and Couch [13]	Oblique tow (Y_β, N_β), straight tow (Y_δ, N_δ)
	P.M.M. test (Y_r, N_r)
Nussbaum [14]	Oblique tow (Y_β, N_β)
Fujino [15]	P.M.M. (all linear derivatives)
van Berlekom and Goddard** [16]	P.M.M. (all linear derivatives)

    (ii)   Available Data for the Bank Effect on the Stability Derivatives

Author	Kind of experiment (stability derivative)
Brard [12]	Oblique tow (Y_β, N_β)
Schoenherr [17]	Straight tow (Y_η, N_η)
Moody [18]	Oblique tow (Y_β, N_β), straight tow (Y_η, N_η)
Nussbaum [14]	Oblique tow (Y_β, N_β), straight tow (Y_η, N_η)
Fujino [15]	P.M.M. (all linear derivatives)
Eda [19]	Oblique tow (Y_β, N_β)
	Straight tow (Y_δ, N_δ, Y_η, N_η)
Norrbin [20]	Straight tow (Y_η, N_η)

**The shallow water effects on the stability derivatives are described by additional terms which are functions of the bottom clearance.

As stated previously, all of the linear stability derivatives are necessary for judging the course stability in a canal, but publications other than reference [15] do not give the numerical values for the acceleration derivatives.

In the following sections, we shall discuss the course stability of a ship in restricted waters and then try to remove the instability in canals by adopting some kinds of simple autopilots. In order to help the reader understand the following discussion clearly, the experimental data of the stability derivatives already published in reference [15] will be again printed in this text.

The principal dimensions of the models used in the experiment are tabulated in Table 1. The experiments were executed in shallow water and in canals whose transverse sections were trapezoidal with both banks taking an angle of 45°. The experimental results of the stability derivatives are shown in Tables 2 and 3. From these tables, it is obvious that the main stability derivatives, namely, the added mass m_y, the added mass moment of inertia J_{zz}, and the damping coefficients Y_β, N_β, Y_r, and N_r are strongly dependent on the depth and width of the waterway; most importantly, decrease of the water depth brings a remarkable increase in the magnitude of the main stability derivatives.

Table 1. Principal dimensions of the models used at P.M.M. tests [15].

	Mariner type ship	Oil-tanker
Length between perpendiculars, mm	2500.0	2000.0
Breadth, mm	359.8	327.6
Draft fore, mm	106.5	110.3
aft, mm	125.5	110.3
mean, mm	116.0	110.3
Displacement, Kg	61.44	58.44
Block coefficient, C_b	0.589	0.805
Radius of gyration, k L	k=0.254	k=0.282
L.C.B. from midship	39.4mm behind	50.8mm front
Rudder area, mm^2	---	3390.9
Propeller diameter, mm	104.2	53.8
Pitch, mm	108.1	39.8
Expanded area ratio	0.565	0.619
Boss ratio	0.189	0.182
Rake angle	7°46'	7°01'
Blade thickness ratio	0.0451	0.0572
Number of blades	4	5
Direction of rotation	right	right
Scale	$^1/64.37$	$^1/145.0$

Table 2.A. Linear stability derivatives of a Mariner type ship in shallow water (All stability derivative values must be multiplied by 10^{-3})

(a) $F_n = 0.0905$ (7 knots, full-scale ship)

H/T	1.21	1.50	1.93	2.50	∞
$m'+m_y'$	32.4	23.5	19.7	18.2	15.6
Y_β'	86.9	29.8	18.7	15.0	14.6
$N_{\dot\beta}'$	-0.791	-0.411	0.039	0.088	0.071
N_β'	12.5	8.67	6.25	4.52	3.53
$-m'+Y_r'$	3.55	-2.64	-4.20	-4.26	-4.92
Y_r'	-3.45	-0.87	-0.51	-0.44	-0.21
N_r'	-6.32	-3.23	-2.62	-2.30	-2.28
$I_{zz}'+J_{zz}'$	1.32	1.20	1.10	1.04	1.03
Y_δ'	5.21	3.43	3.85	3.12	2.94
N_δ'	-1.48	-1.68	-1.59	-1.64	-1.49

Table 2.A.   (b) $F_n = 0.155$ (12 knots, full-scale ship)

H/T	1.50	1.93	2.50	∞
$m' + m_y'$	30.9	20.9	19.1	16.1
Y_β'	52.5	24.5	17.4	13.8
$\dot{N}_\beta'$	-1.39	0.241	0.147	0.061
N_β'	12.0	7.14	5.21	3.57
$-m' + Y_r'$	-5.47	-5.71	-4.43	-5.27
$\dot{Y}_r'$	-2.10	-1.56	-0.56	-0.21
N_r'	-3.17	-2.53	-2.22	-2.14
$I_{zz}' + J_{zz}'$	1.09	1.01	0.964	0.894
Y_δ'	3.70	3.11	2.89	2.90
N_δ'	-1.48	-1.38	-1.35	-1.31

Table 2.B. Linear stability derivatives of an oil-tanker in shallow water (all stability derivative values must be multiplied by 10^{-3})

(a) $F_n = 0.0675$ (7 knots, full-scale ship)

H/T	1.23	1.50	1.89	2.50	∞
$m'+m_y'$	55.7	40.9	34.2	30.3	26.2
Y_β'	77.4	38.3	25.9	21.8	20.0
N_β'	-0.591	-0.538	0.230	0.148	0.090
N_β'	26.9	15.8	11.4	7.78	5.03
$-m'+Y_r'$	-5.20	-9.30	-9.60	-10.38	-10.78
Y_r'	-1.181	-0.905	-0.618	-0.749	-0.437
N_r'	-5.60	-4.25	-3.55	-3.36	-3.15
$I_{zz}'+J_{zz}'$	2.68	2.23	2.03	1.91	1.79

Table 2.B.   (b) F_n = 0.103 (12 knots, full-scale ship)

H/T	1.30	1.50	1.89	2.50	∞
$m'+m_y'$	51.6	43.4	35.7	32.0	26.7
Y_β'	70.0	41.8	27.9	23.5	19.5
$N_{\dot\beta}'$	-0.715	0.249	0.374	0.350	-0.110
N_β'	25.9	17.4	12.3	8.86	5.49
$-m'+Y_r'$	-4.44	-8.77	-8.93	-9.94	-9.96
Y_r'	-1.76	-1.60	-1.58	-1.31	-0.793
N_r'	-4.70	-4.49	-3.79	-3.50	-3.40
$I_{zz}'+J_{zz}'$	2.86	2.60	2.11	1.88	1.76
Y_δ'	4.18	3.98	4.18	3.96	3.49
N_δ'	-1.66	-2.03	-1.80	-1.90	-1.85

Table 3. (a) Linear stability derivatives of a Mariner type ship in canals: $F_n=0.0905$ (7 knots, full-scale ship) (all stability derivative values must be multiplied by 10^{-3})

H/T	1.3			1.5			1.9		
W/B	5.56	4.17	2.78	5.56	4.17	2.78	5.56	4.17	2.78
$m' + m_y'$	26.3	30.9	35.7	23.8	25.0	25.8	19.8	20.2	21.2
Y_β'	57.0	73.7	96.7	30.1	35.6	41.6	20.3	21.8	23.2
$N_{\dot\beta}'$	-0.469	-0.555	-0.699	0.134	-0.012	0.015	0.041	-0.023	0.124
N_β'	12.5	14.2	18.4	8.50	9.86	12.08	5.88	6.67	7.23
$-m' + Y_r'$	2.17	4.37	7.78	-1.42	-0.362	2.21	-3.60	-3.54	-2.57
$Y_{\dot r}'$	-2.17	-2.62	-3.41	-1.34	-1.17	-1.47	-0.676	-0.722	-0.826
N_r'	-4.93	-5.47	-7.27	-3.62	-3.75	-4.43	-2.74	-2.90	-3.07
$I_{zz}' + J_{zz}'$	1.25	1.41	1.82	1.24	1.28	1.42	1.11	1.16	1.21
Y_δ'	4.45	4.63	4.78	3.68	3.92	4.37	3.60	3.67	3.59
N_δ'	-1.94	-1.93	-2.36	-1.78	-1.89	-2.06	-1.52	-1.66	-1.76
Y_η'	6.99	13.4	33.5	4.23	9.20	27.4	2.35	5.35	13.31
N_η'	-1.14	-3.24	-12.5	-0.689	-1.77	-5.01	-0.305	-0.846	-2.43

Table 3. (b) Linear stability derivatives of an oil-tanker in canals: $F_n = 0.0675$ (7 knots, full-scale ship) (all stability derivative values must be multiplied by 10^{-3})

| H/T	1.2			1.5			1.9		
W/B	6.11	4.58	3.05	6.11	4.58	3.05	6.11	4.58	3.05
$m' + m_y'$	61.1	61.9	69.3	41.0	41.6	42.6	34.1	35.5	35.7
Y_β'	78.4	94.7	142.6	42.2	46.6	49.6	29.2	29.6	29.5
$N_{\dot\beta}'$	-1.24	-0.924	-2.07	0.435	0.059	0.571	0.172	0.061	0.123
N_β'	29.8	33.8	48.4	17.3	18.7	20.4	11.8	12.6	12.9
$-m' + Y_r'$	1.94	7.66	17.83	-5.68	-4.68	1.08	-8.82	-7.48	-6.42
$Y_{\dot r}'$	-2.69	-3.16	-5.84	-0.767	-0.948	-1.53	-1.08	-0.930	-1.07
N_r'	-6.93	-7.11	-10.12	-4.35	-4.65	-5.78	-4.04	-4.12	-4.71
$I_{zz}' + J_{zz}'$	3.16	3.43	4.93	2.32	2.35	2.92	2.10	2.16	2.33
Y_η'	7.58	16.6	52.6	2.97	9.78	38.6	2.42	6.14	16.0
N_η'	-1.32	-2.83	-10.4	-0.467	-1.43	-4.12	-0.440	-1.02	-2.86
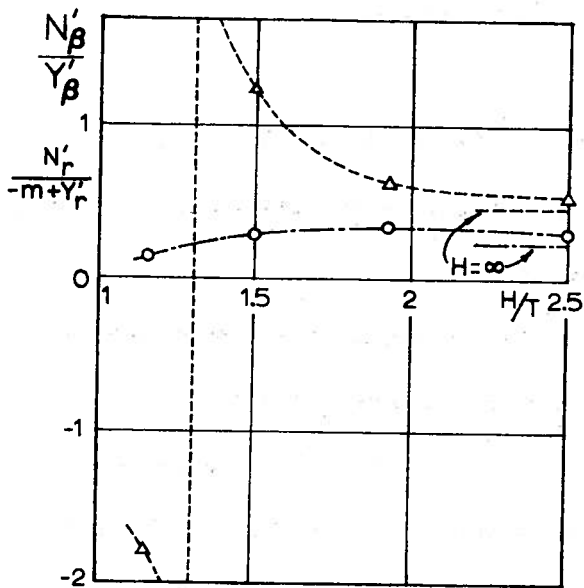
(a) $F_n = 0.0905$
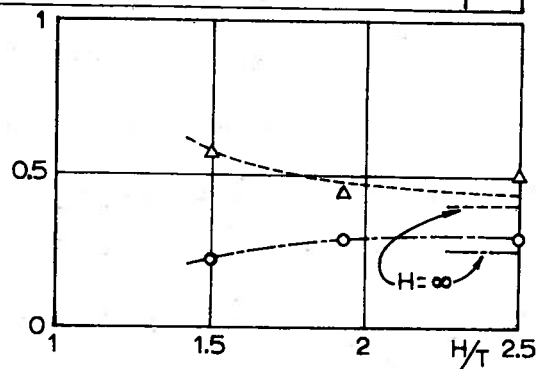
(b) $F_n = 0.155$

Figure 4. Variation of the two ratios, N_β'/Y_β' and $N_r'/(-m'+Y_r')$ of a Mariner type ship in the various water depths [15].
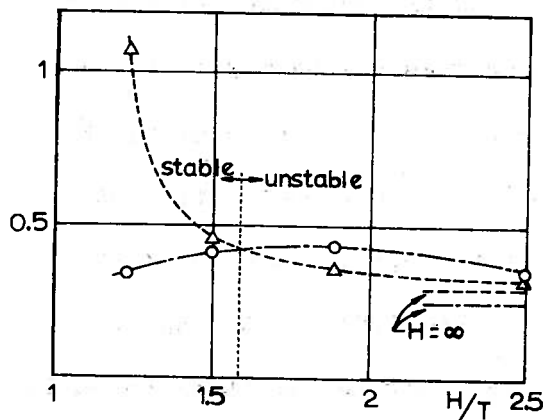
(a) $F_n = 0.0675$
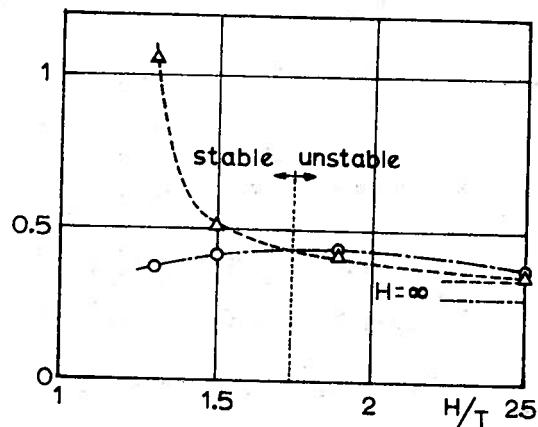
(b) $F_n = 0.103$

Figure 5. Variation of the ratios N_β'/Y_β' and $N_r'/(-m'+Y_r')$ of an oil-tanker in various water depths [15].

3.3. *Course Stability of Ships in Restricted Waters*

Using the experimental values shown in Tables 2 and 3, we shall examine the course stability of ships in shallow water and then in canals.

(i) Course Stability in Shallow Water

The course stability of a ship traveling in shallow water can be judged by the sign of the difference between two ratios, $N_r'/(-m'+Y_r')$ and N_β'/Y_β', as stated in section 2.2. Those two ratios, obtained from the numerical values of Tables 2 and 3, are shown in Figures 4 and 5. These figures show that the ratio $N_r'/(-m'+Y_r')$ increases monotonically with decrease in water depth, tending toward infinity at a critical water depth. In water shallower than this critical depth, the ratio $N_r'/(-m'+Y_r')$ changes its sign from positive to negative, and the absolute value of this ratio decreases as the water depth decreases (see Figure 4(a)).**

The ratio N_β'/Y_β' behaves differently: As the water depth decreases from infinity, the ratio N_β'/Y_β' increases until the water depth becomes less than a certain depth, where the ratio begins to decrease. In other words, the ratio N_β'/Y_β' has a convex form, if it is plotted against the water depth as shown in Figures 4 and 5. This convex character of the N_β'/Y_β' curve affects the course stability significantly.

**The same description can be found on page 233 of Brard's paper [12].

Although the oil-tanker is stable on its course in infinitely deep water, it becomes unstable in a certain range of water depth, which is, in terms of the ratio H/T, from about 1.5 to about 2.6. When the water depth becomes even shallower than this, the course stability is not only recovered but becomes more stable than in deep water.

In the case of a Mariner-type ship, the convex character of the N_β'/Y_β' curve still exists, but it doesn't bring instability, because the course stability in deep water is so strong that the N_β'/Y_β' value cannot exceed the $N_r'/(-m'+Y_r')$ value even at the water depth where the N_β'/Y_β' value has its own maximum value. However, the stability indices T_1' and T_2', which are calculated from equation (2.46) but not shown here, tell us that in almost the same range of water depth as the instability range in the case of the oil-tanker, the Mariner-type ship also becomes temporarily less stable as the water depth decreases (see reference [15].

The Mariner-type ship is very stable on its course in extremely shallow water. This means that the final turning rate of a ship obtained by keeping the rudder angle at a fixed angle is significantly smaller in extremely shallow water than in deep water, but the response of a ship to the deflection of the rudder is faster in extremely shallow water than in deep water.**

**It has been said that the ship becomes more sluggish in very shallow water. But, in the author's opinion, this description is not correct.

In order to investigate the ship's speed effect on the instability range of the water depth found in the case of the oil-tanker, additional experiments were performed in the speed range of 3 kts to 11 kts, full scale [21]. As a result, it was confirmed that the instability range of the water depth was almost constant despite speed variation.

(ii) Course Stability in Canals

As stated in Section 2.2, the course stability of a ship traveling in a canal can be decided by the signs of the coefficient d and the expression $bcd-ad^2-b^2e$; both d and $bcd-ad^2-b^2e$ should be negative for stability. After manipulation of the stability derivatives shown in Table 3, it was established that the second inequality, $bcd-ad^2-b^2e<0$, was not satisfied in every case, that is, in every combination of water depth and canal width; furthermore, the first inequality $d<0$ was not satisfied in some cases [15]. Consequently, both the Mariner-type ship and the oil-tanker proved to be unstable on their courses in canals.

With respect to the instability of ships in canals, one explanation proposed is that because of the hydrodynamic nature, that is, $Y_\eta>0$, $N_\eta<0$ and $N_\psi>0$**, no ship can possess fixed-controls positional stability on the centerline of a canal and, therefore, any ship operating on the canal centerline is in a position of unstable equilibrium. But this description is not precise because,

---

**In this monograph, the hydrodynamic force due to directional angle ψ is not taken into consideration.

even if the signs of the derivatives Y_η and N_η were reversed, it is still possible that the inequality d<0 might not be satisfied, as has been seen. The ship is still unstable on the centerline of a canal in cases where the coefficient d is positive.

It is consequently incorrect to say that the instability of ships in canals is due to the aforesaid sign-nature of the stability derivatives Y_η and N_η. Speaking more accurately, the instability in canals is really due to the increased complexity of the conditions to be satisfied for course stability. As explained in section 2.2., the characteristic equation in a canal that the eigenvalue must satisfy is the fourth-order algebraic equation (2.23), while that in deep water is of second-order. From the physical point of view, this complication is a consequence of the dependence of the hydrodynamic force on the ship's position, which doesn't occur in unrestricted water.

3.4. *Improvement of Course Stability by Means of Autopilots*

Although ships are unstable in canals, most of them can travel through a canal without risk, because the helmsman can correct the deviation of his ship from the desired course by adequately steering the control surface. As is known well, the instability of the open-loop characteristic of a system can be removed or reduced by

adding an appropriate feed-back loop to the system. This is one of the main reasons why automatic control with a negative feed-back loop is widely used; an example is the autopilot of a ship. The system consisting of the ship's dynamics plus a negative feed-back loop can be stable even if the open-loop ship's dynamics are unstable. The simplest physical realization of a negative feed-back loop is the manual steering executed by a helmsman on the bridge.

In this section, we shall try to correct the instability of a ship traveling on the centerline of a canal by adopting some kinds of simple autopilots. In the following discussion, we consider five controlled variables: directional angle or yaw angle ψ', yaw angular velocity r', yaw angular acceleration $\dot{r}'$, offset distance from the centerline η_G', and the rate of change of offset distance $\dot{\eta}_G'$. Furthermore, we shall restrict our consideration to proportional control, in which the gain constants are denoted by the coefficients k_i for the five controlled variables.

The rudder angle of the autopilot is expressed as follows:

$$\delta' = k_1 \psi' + k_2 r' + k_3 \dot{r}' + k_4 \eta_G' + k_5 \dot{\eta}_G' \quad . \tag{3.20}$$

Substituting this into equations (2.15) and (2.16), in which the terms including the rudder rate $\dot{\delta}'$ are omitted, we obtain the characteristic equation equivalent to equation (2.23) for the open loop:

$$a'\sigma^4 + b'\sigma^3 + c'\sigma^2 + d'\sigma + e' = 0 \quad , \tag{3.21}$$

where

$$a' = a + k_3 a_3$$

$$b' = b + k_2 b_2 + k_3 b_3 + k_5 b_5$$

$$c' = c + k_1 c_1 + k_2 c_2 + k_3 c_3 + k_4 c_4 + k_5 c_5 \qquad\qquad (3.22)$$

$$d' = d + k_1 d_1 + k_2 d_2 + k_4 d_4 + k_5 d_5$$

$$e' = e + k_1 e_1 + k_4 e_4 \qquad .$$

The coefficients a,b,c,d, and e of equation (3.22) are exactly the same as those defined by equation (2.24), and the subscripted coefficients a_3, b_2, ..., e_4 are defined as follows:

$$a_3 = b_2 = c_1 = -\xi_1 \eta_4 - \xi_4 \eta_5 = -\alpha_1$$

$$b_5 = c_4 = \xi_4 \eta_1 + \xi_5 \eta_4 = -\zeta_1$$

$$b_3 = c_2 = d_1 = d_5 = e_4 = \xi_2 \eta_4 - \xi_4 \eta_3 = -\alpha_2 \qquad\qquad (3.23)$$

$$c_5 = d_4 = -\xi_1 \eta_4 + \xi_3 \eta_4 - \xi_4 \eta_2 - \xi_4 \eta_5 = -\zeta_2$$

$$c_3 = d_2 = e_1 = \xi_4 \eta_7 - \xi_7 \eta_4 = -\alpha_3 = -\gamma_4 \qquad .$$

The necessary and sufficient conditions for the stability of a ship plus the autopilot defined by the equation (3.20) are as follows:

$$\frac{b'}{a'} > 0, \quad \frac{d'}{a'} > 0, \quad \frac{e'}{a'} > 0, \quad \frac{b'c'd' - a'd'^2 - b'^2 e'}{a'^3} > 0 \quad . \quad (3.24)$$

Therefore, if it is possible to choose the gain constants k_i to satisfy the four conditions simultaneously, we can remove the instability of a ship traveling in a canal.

Five kinds of autopilot will be examined separately, in order to clarify the characteristics of each autopilot and to consider the possibility of removing the instability by its use. The following

examination will be referred exclusively to the Mariner-type ship, because the rudder derivatives of the oil-tanker in canals are lacking.

(i) Directional Control

An autopilot using directional control means that the ship's rudder is automatically deflected to extinguish the deviation of ship's directional angle or heading angle from the desired course, which is the centerline of a canal in the following discussion. In this case, the gain constants k_i except for k_1 are zero. Accordingly,

$$a' = a, \quad b' = b, \quad c' = c + k_1 c_1, \quad d' = d + k_1 d_1, \quad e' = e + k_1 e_1 \quad . \tag{3.25}$$

Then the stability conditions, i.e., the inequalities (3.24), diminish to three inequalities, since the first condition of (3.24) is always

$$\left. \begin{aligned} &d' = d + k_1 d_1 < 0 \\ &e' = e + k_1 e_1 < 0 \\ &b'c'd' - a'd'^2 - b'^2 e' = (bc_1 d_1 - ad_1^2)k_1^2 + (bcd_1 + bc_1 d - 2add_1 - b^2 e_1)k_1 \\ &\qquad\qquad\qquad + bcd - ad^2 - b^2 e < 0 \quad . \end{aligned} \right\} \tag{3.26}$$

Using the stability derivatives, tabulated in Table 3, we solved these three inequalities, and the results are shown in Table 4. From this table, one can conclude that it is always possible to remove the instability of a ship traveling in a canal by adopting directional control with a reasonable gain constant.

It must, however, be noted that the value of the gain constant k_1 for removal of the instability is bounded not only from below

Table 4. The permissible range of gain constant k_1 necessary to remove the inherent instability of a Mariner type ship in canals: $F_n=0.0905$

H/T=1.30			
condition to be satisfied	W/B=5.56	W/B=4.17	W/B=2.78
$d'<0$ $e'<0$ $b'c'd'-a'd'^2-b'^2e'<0$	$0.031 < k_1$ $k_1<18.0$ $k_1<-19.2$, $0\ 532<k_1$	$-0.161 < k_1$ $k_1<39.4$ $k_1<-27.2$, $0.893<k_1$	$-0.869 < k_1$ $k_1<93.4$ $k_1<-34.0$, $1.94<k_1$
permissible range of k_1	$0.532<k_1<18.0$	$0.893 <k_1< 39.4$	$1.94 <k_1 <93.4$
H/T=1.50			
condition to be satisfied	W/B=5.56	W/B=4.17	W/B=2.78
$d'<0$ $e'<0$ $b'c'd'-a'd'^2-b'^2e'<0$	$-0.008< k_1$ $k_1<11.4$ $k_1<-5.41$, $0.667<k_1$	$-0.085< k_1$ $k_1<14.7$ $k_1<-7.34$, $1.12<k_1$	$-0.138< k_1$ $k_1<15.6$ $k_1<-12.2$, $2.32<k_1$
permissible range of k_1	$0.667<k_1 <11.4$	$1.12<k_1<14.7$	$2.32<k_1<15.6$
H/T=1.90			
condition to be satisfied	W/B=5.56	W/B=4.17	W/B=2.78
$d'<0$ $e'<0$ $b'c'd'-a'd'^2-b'^2e'<0$	$0.024<k_1$ $k_1<8.09$ $k_1<-3.32$, $0.610<k_1$	$0.024<k_1$ $k_1<9.40$ $k_1<-3.81$, $1.21<k_1$	$-0.089 <k_1$ $k_1<10.4$ $k_1<-5.09$, $2.08<k_1$
permissible range of k_1	$0.610<k_1<8.09$	$1.21 <k_1< 9.40$	$2.08 <k_1 < 10.4$

but also from above. This situation is somewhat different from that which we encounter when removing the instability in the open sea, because, apart from an upper limit which may technically exist, an upper limit on the gain constant k_1 of the directional control used to stabilize an unstable ship in open water does not mathmatically exist. The characteristic equation for the open-water case is of second-order, as the denominator of equation (2.42) or (2.43) indicates. When directional control is adopted to remove the instability in the open sea, the characteristic equation which the eigenvalue should satisfy changes into a third order equation:

$$a\sigma^3 + b\sigma^2 + (c^* + k_1 c_1)\sigma + k_1 d_1 = 0 \quad . \tag{3.27}$$

Consequently, the necessary and sufficient conditions for course stability are

$$\frac{b}{a} > 0, \quad \frac{c^* + k_1 c_1}{a} > 0, \quad \frac{k_1 d_1}{a} > 0, \quad \frac{(bc_1 - ad_1)k_1 + bc^*}{a^2} > 0 \quad . \tag{3.28}$$

Taking account of the fact that both c_1 and d_1 are negative while $bc_1 - ad_1$ is positive, it is easily understood that any inequality of (3.28) gives the lower limit of the gain constant k_1; thus k_1 should satisfy

$$k_1 > \max \left(0, \; -\frac{c^*}{c_1}, \; \frac{-bc^*}{bc_1 - ad_1} \right) = \frac{-bc^*}{bc_1 - ad_1} \quad , \tag{3.29}$$

or, in other words, the upper bound of the gain constant k_1 to remove the instability of a ship in deep water is infinite. It can be seen from Table 4 that the range of the gain constant k_1

necessary to remove the instability in canals is wider in a narrower canal rather than in a broader canal, but the lower bound of the gain is greater in a narrower canal than in a broader canal.

Similar, but slightly different results have been obtained by Eda, with respect to the desired value of the gain constant k_1 necessary to remove the instability [19]. From the eigenvalue analysis of the characteristic equation, he too has indicated that the gain of the directional control has not only a lower limit but also an upper limit (See Figure 6). According to his analysis, however, the permissible range of the gain k_1 get narrower as the canal width decreases. It must be kept in mind that the characteristic equation derived in reference [19] is higher by one order than equation (3.21), because Eda took into account a non-zero time constant of the rudder response to the ordered helm angle, while the time constant was assumed to be zero when we derived equation (3.21).

(ii) Yaw Rate Control and Yaw Acceleration Control

Equating the gain constants k_i except for k_2 and k_3 to zero, and repeating the same procedure as that used to obtain the permissible range of the gain k_1, we can determine the k_2 and k_3 values necessary to remove the instability of a ship traveling in a canal by adopting the yaw rate control and yaw acceleration control respectively. As a result of such an analysis, it was concluded that it was impossible to remove the instability in
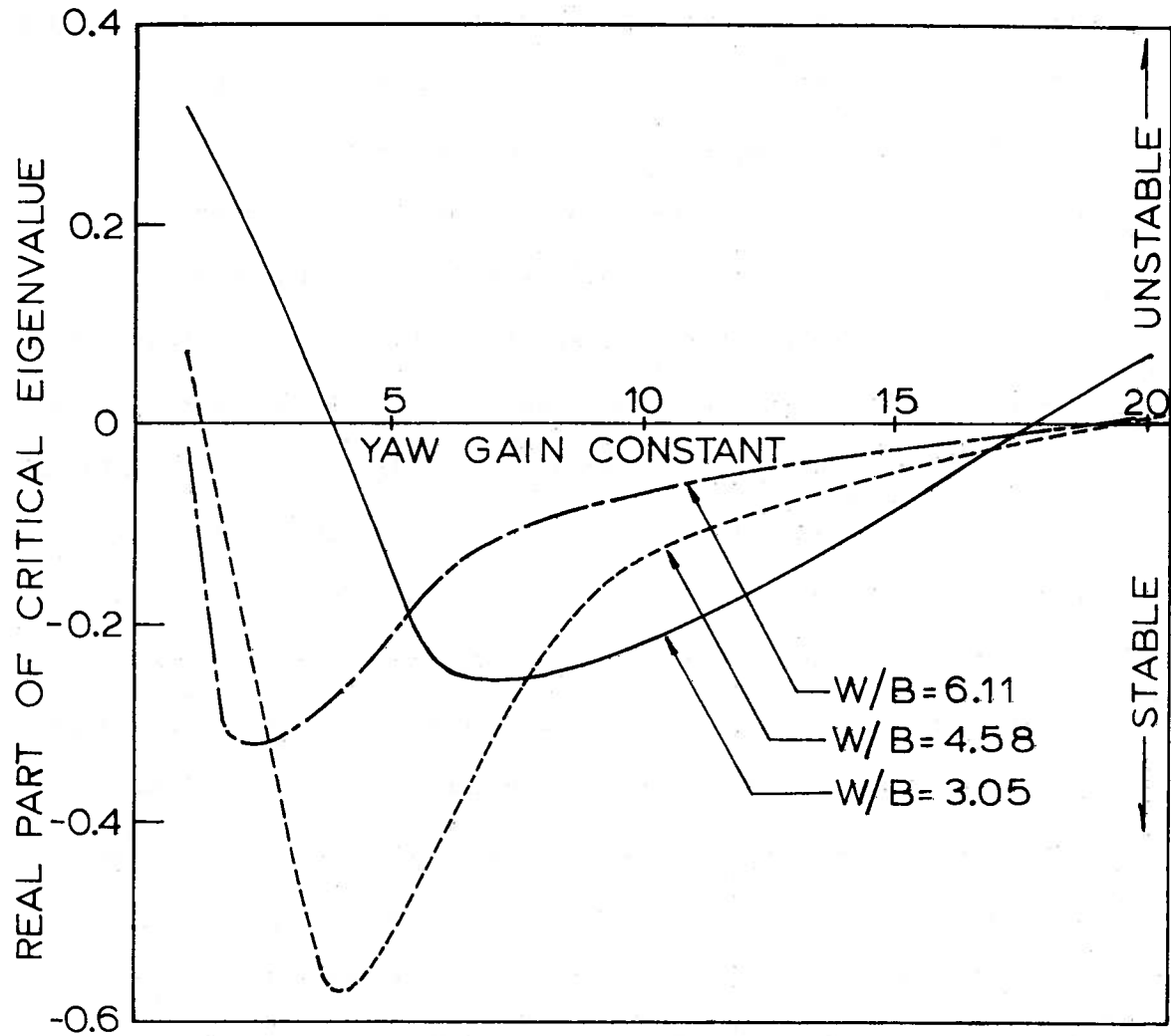
Figure 6. Yaw gain constant necessary to remove the inherent instability of a tanker traveling on the centerline of canals through the use of directional control; $F_n = 0.054$, $h/T = 1.20$ [19].

canals except through the use of yaw acceleration control in a few cases [22].

(iii) Offset Distance Control

"Offset distance control" means that the rudder is automatically steered to cancel the deviation of a ship's position from the centerline of a canal. After examination of the effectiveness of the offset distance control, it was obvious that this kind of autopilot could not remove the instability in a canal [22]. In fact, the feed-back of offset distance tends to degrade the stability of a ship. For example, Eda's eigenvalue analysis indicates that the real part of the "critical" eigenvalue is still positive despite adoption of offset distance control, and, further-more, it indicates that a high value of the gain k_4 results in a larger positive real part of the critical eigenvalue, that is, higher instability compared with the inherent instability. At first sight, this conclusion seems contrary to intuition. It has, nevertheless, been verified by computer prediction of the ship's trajectory in a canal [23]. In Figure 7 are shown the ship's trajectories computed for an initial offset: the solid line is obtained by including the feed-back of the ship's lateral deviation and the dotted line is obtained by eliminating the feed-back of the ship's position. This illustration indicates that the feed-back of the ship's lateral deviation from the desired path decreases the effectiveness of the autopilot.
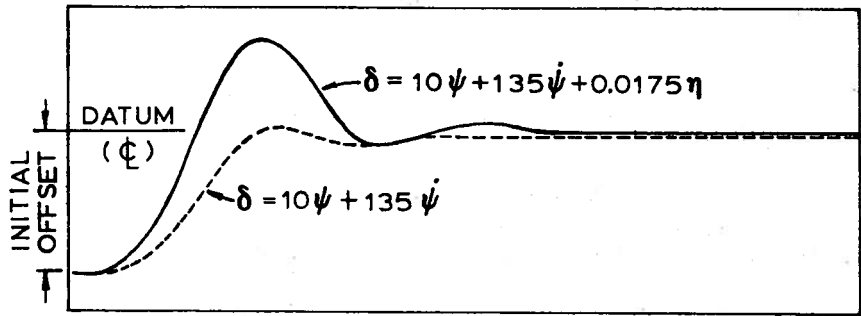
Figure 7. Computer prediction of the path of the center of gravity of a ship (C_b=0.806) traveling in a canal (^{H}/T=1.29, ^{W}/B=2.98) under the action of autopilots. Initial offset of the ship is 20 meters to starboard [23].
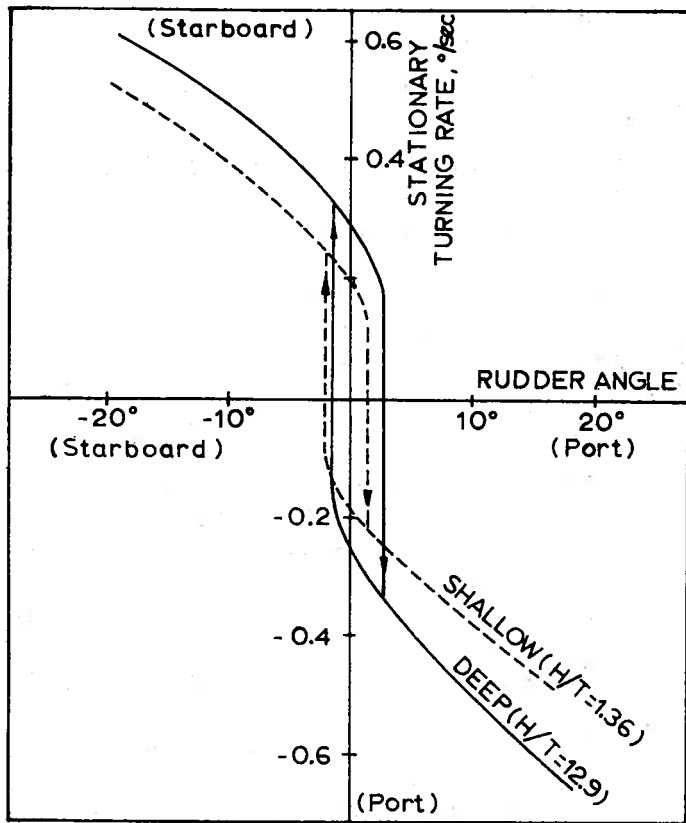

Figure 8. Comparison of the results of spiral tests of a Great Lakes ore-carrier in deep water and in shallow water [13].

(iv) Offset Rate Control

In this case, the necessary and sufficient conditions for stability are as follows:

$$b + k_5 b_5 < 0$$

$$d + k_5 d_5 < 0$$

$$b_5 c_5 d_5 k_5^3 + (bc_5 d_5 + b_5 cd_5 + b_5 c_5 d - ad_5^2 - b_5^2 e) k_5^2$$

$$+ (bcd_5 + bc_5 d + b_5 cd - 2add_5 - 2bb_5 e)k_5 + bcd - ad^2 - b^2 e < 0.$$

(3.30)

The permissible range of the gain constant k_5 necessary to remove the inherent instability in canals is shown in Table 5. Equation (2.18) or (2.19) tells us that the feed-back of the offset rate, $\dot{\eta}_G$, is partially equivalent to the feed-back of the directional angle, but not completely because the negative feed-back of the offset rate simultaneously brings the positive feed-back of the drift angle β', which increases the inherent instability. Therefore, as shown in Table 5, it is not always possible to remove the inherent instability by means of the offset rate control.

Summarizing the above discussion, it can be said that the inherent instability of a ship traveling in a canal can be removed easily by adopting a simple autopilot, namely, the directional control. The gain constant k_1 necessary to remove the instability is bounded not only from the lower side but also from the upper side; therefore, an excessively large value of the gain k_1 doesn't improve the inherent instability.

Now we shall examine the directional control in more detail. In

Table 5. The permissible range of gain constant k_5 necessary to remove the inherent instability of a Mariner type ship in canals: $F_n = 0.0905$

H/T = 1.30

condition to be satisfied	W/B = 5.56	W/B = 4.17	W/B = 2.78
$b'<0$	$k_5<17.7$	$k_5<20.1$	$k_5<21.9$
$d'<0$	$0.031<k_5$	$-0.161<k_5$	$-0.869<k_5$
$b'c'd'-a'd'^2-b'^2e'<0$	$k_5<-19.8,\ 0.547<k_5<8.74$	$k_5<-22.6,\ 0.910<k_5<10.1$	$k_5<-24.5,\ 1.93<k_5<10.9$
permissible range of k_5	$0.547<k_5<8.74$	$0.910<k_5<10.1$	$1.93<k_5<10.9$

H/T = 1.50

condition to be satisfied	W/B = 5.56	W/B = 4.17	W/B = 2.78
$b'<0$	$k_5<16.1$	$k_5<17.7$	$k_5<16.9$
$d'<0$	$-0.008<k_5$	$-0.085<k_5$	$-0.138<k_5$
$b'c'd'-a'd'^2-b'^2e'<0$	$k_5<-8.45,\ 0.756<k_5<6.92$	$k_5<-9.77,\ 1.37<k_5<7.32$	$k_5<-12.6,\ 3.09<k_5<6.69$
permissible range of k_5	$0.756<k_5<6.92$	$1.37<k_5<7.32$	$3.09<k_5<6.69$

H/T = 1.90

condition to be satisfied	W/B = 5.56	W/B = 4.17	W/B = 2.78
$b'<0$	$k_5<14.5$	$k_5<14.5$	$k_5<15.0$
$d'<0$	$0.024<k_5$	$0.024<k_5$	$-0.089<k_5$
$b'c'd'-a'd'^2-b'^2e'<0$	$k_5<-8.85,\ 0.842<k_5<3.39$	$k_5<-8.34$	$k_5<-7.74$
permissible range of k_5	$0.842<k_5<3.39$	nothing	nothing

order to clarify its characteristics, let us consider a ship's motion subsequent to some initial values given to the variables describing the motion. Assume initial values of directional angle and lateral position, denoted by ψ_0 and η_0 respectively. We are interested in the final state of the ship's motion brought about by the prescribed deviations.

If we assume that the initial values of $\eta'(t')$ and $\psi'(t')$ are η_0 and ψ_0 respectively, but that those of the other variables $\beta'(t)$ and $r'(t')$ are zero, then the Laplace transforms of equations (2.19) and (2.21), namely equations (2.32) and (2.33), should be replaced by equations (3.31) and (3.32) respectively:

$$sH(s) - \eta_0 = \Psi(s) - B(s) \tag{3.31}$$

$$s\Psi(s) - \psi_0 = R(s) \ . \tag{3.32}$$

Furthermore, the relationship of the rudder angle versus the deviation of directional angle, which describes the characteristic of the directional control, is expressed as follows:

$$D(s) = k_1 \Psi(s) \ . \tag{3.33}$$

From equations (2.30), (2.31), (3.31), (3.32) and (3.33), we obtain

$$\Psi(s) = \frac{\psi_0(as^3 + bs^2 + cs - \xi_7\eta_2 + \xi_3\eta_7) + \eta_0[(\xi_1\eta_7 + \xi_7\eta_5)s - e]}{as^4 + (b - k_1\alpha_0)s^3 + (c - k_1\alpha_1)s^2 + (d - k_1\alpha_2)s + e - k_1\alpha_3} \quad (3.34)$$

$$B(s) = \frac{\psi_0[k_1\gamma_0 s^3 + k_1\gamma_1 s^2 + (\xi_7\eta_1 + \xi_5\eta_7 + k_1\gamma_2)s + \xi_3\eta_7 - \xi_7\eta_2]}{as^4 + (b - k_1\alpha_0)s^3 + (c - k_1\alpha_1)s^2 + (d - k_1\alpha_2)s + e - k_1\alpha_3}$$

$$+ \frac{\eta_0[(\xi_5\eta_7 + \xi_7\eta_1)s^2 + (\xi_3\eta_7 - \xi_7\eta_2 - k_1\gamma_3)s - k_1\gamma_4]}{as^4 + (b - k_1\alpha_0)s^3 + (c - k_1\alpha_1)s^2 + (d - k_1\alpha_2)s + e - k_1\alpha_3} \quad (3.35)^{**}$$

However, if we assume that both derivatives $Y_{\dot\delta}'$ and $N_{\dot\delta}'$ are zero, then α_0, γ_0, and γ_3 become zero. From the final-value theorem, it is obvious that

$$\lim_{t'\to\infty} \psi'(t') = \lim_{s\to 0} s\Psi(s) = 0 \qquad (3.36)$$

$$\lim_{t'\to\infty} \beta'(t') = \lim_{s\to 0} sB(s) = 0 \qquad . \qquad (3.37)$$

These final values of $\psi'(t')$ and $\beta'(t')$ are in stable equilibrium; in other words, they are realizable if we choose k_1 from the permissible range stated earlier. In addition, the final value of the ship's lateral deviation $\eta'(t')$ also becomes zero:

$$\lim_{t'\to\infty} \eta'(t') = \lim_{s\to 0} sH(s) \qquad (3.38)$$

$$= \lim_{s\to 0} (\Psi(s) - B(s) + \eta_0') = 0 \qquad .$$

**The author has found that this equation as written in reference [22] is incorrect. The coefficient of $\eta_0 S^2$ in the numerator should be $\xi_5\eta_7 + \xi_7\eta_1 \equiv Y_{\dot r}'N_\eta' + Y_\eta'(I_{zz}' + J_{zz}')$, while in [22], it is written $-\xi_5\eta_7 + \xi_7\eta_1$. Consequently, Figure 55 in [22] should also be corrected.

This conclusion is attractive because directional control can eliminate not only the deviation of the directional angle but also the lateral deviation of a ship traveling in a canal. This fact is also shown in Figure 7. That is, the autopilot without feed-back of the lateral deviation, i.e., $\delta = 10\psi + 135\dot{\psi}$, can eliminate the initial offset of a ship.

3.5. *Turning Ability of Ships in Shallow Water*

As stated in the introduction, the course stability and the turning ability of a ship are two characteristics which are contradictory to one another. The description of the course stability with respect to the water-depth dependence also holds true for the turning ability, if the conclusions are reversed. That is, whenever the course stability becomes better, the turning ability becomes worse, and vice versa. For example, we can say that the turning ability in extremely shallow water is worse than in deep water. Accordingly, we shall mention some experimental results with respect to the shallow water effect on the turning ability of a ship, and infer the shallow water effect on the course stability from them.

As to full-scale experiments, there exist only a few spiral maneuvers [13], because it is very difficult to find a part of the sea of sufficiently uniform depth. In Figure 8 are shown the results of

the spiral test of a Great Lakes ore-carrier. This figure says that the turning ability in shallow water is worse than that in deep water.**
Other experimental results obtained with free-sailing models also indicate the same effect: The turning ability gets steadily worse as the water depth decreases [24]. In the same reference, the ship's speed effect on the turning ability in shallow water was examined in detail and is quoted here in Figure 9. From this figure, it is obvious that the speed effect is weak: The dimensionless turning rate, which is defined as the ratio of turning radius to ship's length, decreases slightly as the ship's speed increases.

On the other hand, there exists another experimental result which says that the turning ability does not always get monotonically worse with decreasing water depth [25]. As a result of spiral tests executed with some self-propelled models of large-sized oil-tankers, it was established that the stationary turning rate was larger at a certain range of water depth than in deep water. Roughly speaking, the water depth that brought about better turning ability is close to the water depth that reduced the course stability as described in a previous section.

_____

**It must be noted that the ship's draft is not exactly same in both cases. In deep water, the ship's fore and aft drafts were 23 feet and 23 feet 6 inches respectively, while they were 21 feet and 23 feet respectively in shallow water. In particular, the larger trim by stern in shallow water may exaggerate poor turning ability.
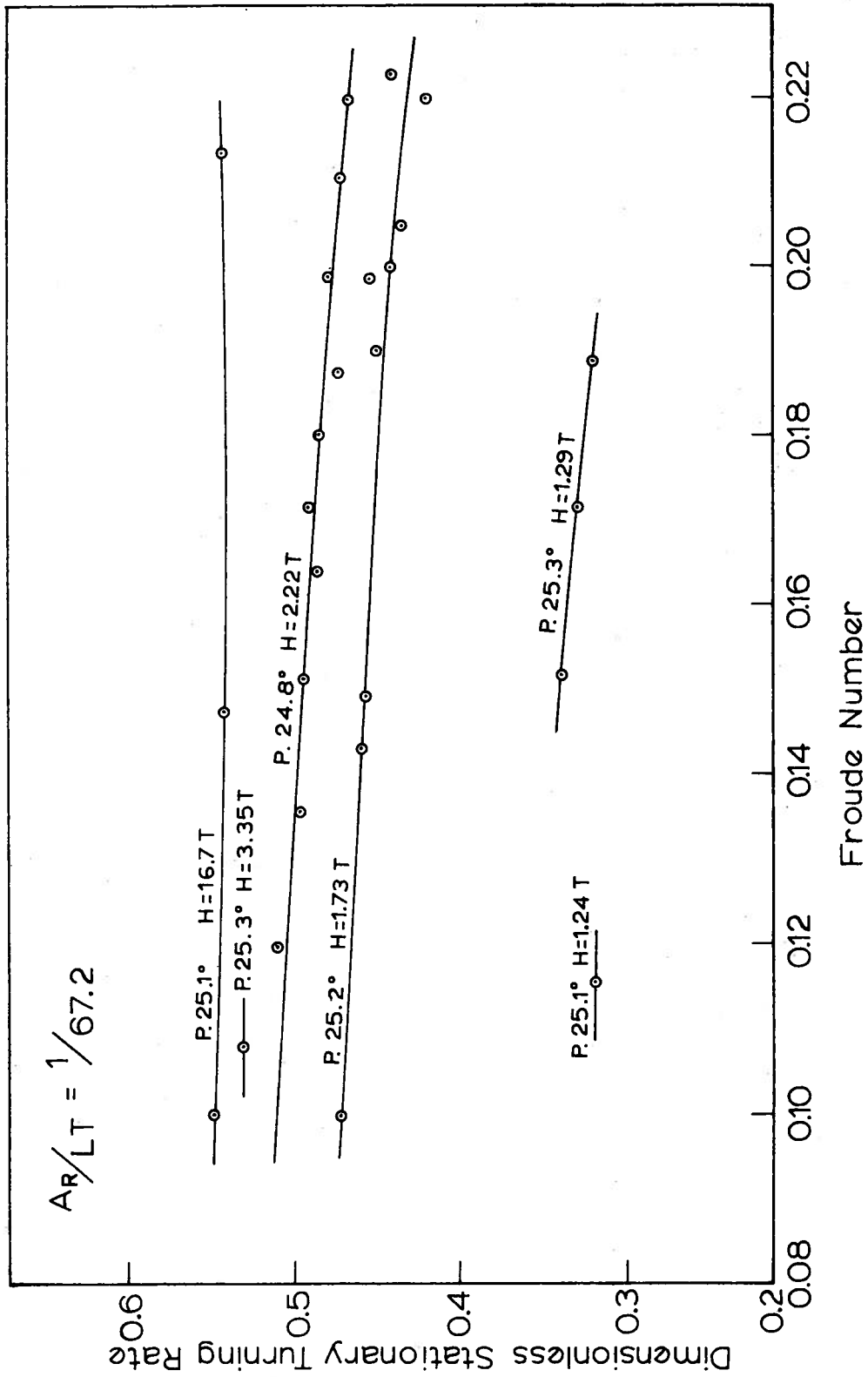
Figure 9. Speed effect on the turning ability of an oil-tanker ($C_b=0.81$) in shallow water [24]. (P: port rudder)

4. COMPARISON BETWEEN THE EXPERIMENTAL AND THEORETICAL VALUES OF THE STABILITY DERIVATIVES

In the previous chapter, the maneuverability of ships in restricted waters, particularly the course stability of ships in shallow water and in canals, was discussed only in terms of the experimental stability derivative values. However, extensive labor and time are needed to obtain all the stability derivatives from experiments, because the variable parameters in the experiments in restricted water are much more numerous than those in deep water. Besides the variable paramenters in deep water, we have to consider the variation of the water depth, canal width, lateral position of a ship in a canal, and so on. Therefore, it is desirable to estimate adequately the stability derivatives on the basis of the theoretical background rather than experimental work. In this chapter, some published theoretical works will be quoted and compared with the experimental results.

4.1. Sway Added Mass and Yaw Added Mass Moment of Inertia

The sway added mass (or the yaw added mass moment of inertia) is defined as the in-phase component of the hydrodynamic force (or moment) acting on a moving ship, with respect to the linear (or angular) acceleration of the ship. If the ship's speed and the frequency of motion are sufficiently small, the free surface can be replaced by a rigid wall. In this case, the sway hydrodynamic force Y and the yaw

moment N acting on a moving body that has three velocity components

(u, v, r) are described in terms of the added mass tensor as follows:

$$Y = -\dot{u}m_{12} - \dot{v}m_{22} - \dot{r}m_{26} - rum_{11} - rvm_{12} - r^2m_{16} \tag{4.1}$$

$$N = -\dot{u}m_{16} - \dot{v}m_{26} - \dot{r}m_{66} - (u^2-v^2)\,m_{12} - uv\,(m_{22} - m_{11}) - rum_{26} + rvm_{16} \quad, \tag{4.2}$$

where

$$m_{ij} = -\rho\iint\limits_{S_B}\phi_\gamma\,\frac{\partial\phi_i}{\partial n}\,dS \quad \text{(n:\ \ unit normal inwards the fluid)} \tag{4.3}$$

and ϕ_i (i=1,2,6) stands for the velocity potential due to each of the

elementary motions, and the subscript i = 1,2, and 6 means surge, sway,

and yaw motion respectively [26]. Assuming that the body (ship) has a

symmetrical center plane (xz plane), the equations (4.1) and (4.2)

reduce to

$$Y = -\dot{v}m_{22} - \dot{r}m_{26} - rum_{11} \tag{4.4}$$

$$N = -\dot{v}m_{26} - \dot{r}m_{66} - uv(m_{22} - m_{11}) - rum_{26} \quad . \tag{4.5}$$

Furthermore, if the ship is sufficiently slender, the longitudinal

added mass or the surge added mass m_{11} is very small compared with other

kinds of added mass.

Comparing each term of equations (4.4) and (4.5) with the

equivalent term of equations (2.9) and (2.10), we obtain

$$\left.\begin{aligned}
m_{22} &= -\,Y_{\dot{v}} \equiv m_y \\[4pt]
m_{26} &= -\,Y_{\dot{r}} = -\,N_{\dot{v}} \\[4pt]
m_{66} &= -\,N_{\dot{r}} \equiv J_{zz} \quad,
\end{aligned}\right\} \tag{4.6}$$

and the instability yaw moment (or Munk moment) $-uv(m_{22}-m_{11})$ and the term $-rum_{26}$ correspond to the terms $N_v v$ and $N_r r$ in equation (2.10). It should be noted that since the hydrodynamic force and moment in equations (4.4) and (4.5) have been obtained by neglecting the lifting-surface effect and the existance of the vortex sheet shed from the trailing edge of the body (ship), the hydrodynamic coefficients of equations (4.4) and (4.5) do not exactly correspond to the equivalent stability derivatives of equations (2.9) and (2.10). In particular, the damping force due to sway velocity, i.e., $Y_v v$ in the equation (2.9), can not be deduced from potential theory. Furthermore, the second relationship of equation (4.6), i.e., $Y_{\dot{r}} = N_{\dot{v}}$, is not always satisfied by the experimental results [27].

Assuming that the ship is sufficiently slender, we can calculate m_{22}, m_{26}, m_{66} from the strip theory synthesis as follows:

$$\left. \begin{array}{c} - Y_{\dot{v}} \\ - Y_{\dot{r}} = - N_{\dot{v}} \\ - N_{\dot{r}} \end{array} \right\} = \int_L m_y^*(x) \left\{ \begin{array}{c} 1 \\ x \\ x^2 \end{array} \right\} dx \quad , \quad (4.7)$$

where $m_y^*(x)$ is the sway added mass of a two-dimensional cylinder possessing the same transverse sectional form as that of the ship at section x. Consequently, using the slender-body assumption, it is essential for the theoretical estimation of the sway added mass and the yaw added mass moment of inertia of a three-dimensional body to obtain the sway added mass of two-dimensional bodies.

The sway added mass m_{22} defined

$$m_{22} = - \rho \iint\limits_{S_B} \phi_2 \frac{\partial \phi_2}{\partial n} \, dS \qquad\qquad (4.3')$$

is the kinetic energy of the fluid due to the motion caused by the transverse translation of the body. Using a form of Gauss's theorem, we get

$$m_{22} = \rho \iiint\limits_{V} (\text{grad } \phi_2)^2 dV \qquad , \qquad\qquad (4.8)$$

where the volume integral is taken throughout the whole fluid region surrounding the body.

4.1.1. *Sway Added Mass of Two-Dimensional Bodies in Canals*

In this section, the sway added mass of a two-dimensional body moving transversely in a canal will be obtained by calculating the kinetic energy of the fluid layer with unit thickness that is completely enclosed by the body surface, the canal walls, and the free surface (see Figure 10). The following numerical calculation will be restricted to the simple case where both the body and the canal have rectangular cross-sections. The method can be extended to include other geometrical forms of the body and the canal.

Assuming an ideal incompressible fluid, the fluid motion can be described by a velocity potential function which satisfies the Laplace

equation in the fluid domain:

$$\frac{\partial^2 \phi}{\partial y^2} + \frac{\partial^2 \phi}{\partial z^2} = 0 \qquad \text{in the fluid domain S} \quad , \qquad (4.9)$$

and furthermore satisfies the given boundary conditions:

$$\frac{\partial \phi}{\partial n} = g(s) \qquad \text{on a boundary } \Gamma_1 \qquad (4.10)$$

$$\phi = f(s) \qquad \text{on the remaining boundary } \Gamma_2 , \qquad (4.11)$$

where $g(s)$ and $f(s)$ are the known functions of distance s measured along the boundary and from a prescribed point on the boundary.

One of the orthodox solutions is to express the velocity potential function in terms of singularities distributed on the contour of the body, and then to integrate $\phi \partial \phi / \partial n$ along the whole body-contour in order to get the added mass.

On the other hand, it is possible to evaluate the kinetic energy of the fluid without determining the velocity potential function itself. According to this method, which is called the hypercircle method, we can determine the upper and lower bounds of the added mass [28, 29]. This is the great advantage of the method, since most of the numerical methods give only an approximate value and cannot provide information regarding the accuracy of the obtained value, that is, how close the given approximate value is to the exact value.

Determining the velocity potential function ϕ that satisfies the boundary conditions (4.10) and (4.11) is exactly equivalent to obtaining a common vector of the two vector spaces that are defined as

follows [30]:**

(I) Complementary vector space $\pi(p_1, p_2)$: This is a vector space in which any vector has two components p_1 and p_2 defined by the equations

$$\frac{\partial p_1}{\partial y} + \frac{\partial p_2}{\partial z} = 0 \qquad \text{in the fluid domain} \qquad (4.12)$$

$$p_1 \frac{\partial y}{\partial n} + p_2 \frac{\partial z}{\partial n} = g(s) \qquad \text{on the boundary } \Gamma_1 \quad . \qquad (4.13)$$

(II) Associated vector space $\Omega(q_1, q_2)$: This is a vector space in which any vector has two components q_1 and q_2 defined as the first partial derivatives of any function ϕ that satisfies the boundary condition $\phi = f(s)$ on Γ_2 ; that is,

$$q_1 = \frac{\partial \phi}{\partial y} , \qquad q_2 = \frac{\partial \phi}{\partial z} \qquad (4.14)$$

where $\phi = f(s)$ on the boundary Γ_2 .

From the definition of these two spaces, it is evident that the common vector $R = (r_1, r_2)$ of these two spaces, if obtained, is the exact solution of the boundary value problem at hand. This exact solution is, however, not easy to obtain, and so we shall be content with an approximate solution as follows: First, we introduce two homogeneous vector spaces of π and Ω spaces, by replacing the nonhomogeneous boundary conditions on Γ_1 and Γ_2 with the homogeneous conditions.

**The reader who want to study the hypercircle method in more detail should refer to this book.

(III) Homogeneous complementary vector space $\pi^*(p *, p *)$:

This is a subspace of the space π, in which any vector

has two components defined as follows:

$$\frac{\partial p_1^*}{\partial y} + \frac{\partial p_2^*}{\partial z} = 0 \quad \text{in the fluid domain S} \quad (4.15)$$

$$p_1^* \cdot \frac{\partial y}{\partial n} + p_2^* \frac{\partial z}{\partial n} = 0 \quad \text{on the boundary } \Gamma_1 \quad . \quad (4.16)$$

Hereafter, we shall denote a vector of this space as I_i,

a vector with a variable subscript i, i.e., $I_i = p_{i1}^*, p_{i2}^*)$.

(IV) Homogeneous associated vector space $\Omega^*(q_1*, q_2*)$:

Two components q_1^* and q_2^* of any vector in this space,

which will be denoted as J_k with the subscript k being

varied, are defined as

$$q_{k1}^* = \frac{\partial \phi_k^*}{\partial y} \quad , \qquad q_{k2}^* = \frac{\partial \phi_k^*}{\partial z} \quad , \qquad (4.17)$$

where ϕ_k^* is zero on the boundary Γ_2.

Then we shall define a p-vector of the π-space as the linear

combination of $\bar{p}$-vector and I_i-vectors:

$$p = \bar{p} + \sum_{i=1}^{N} a_i \cdot I_i \quad . \quad (4.18)$$

Similarly, a q-vector of the Ω-space is defined as the linear

combination of $\bar{q}$-vector and J_k-vectors:

$$q = \bar{q} + \sum_{k=1}^{M} b_k J_k \quad , \quad (4.19)$$

where $\bar{p}$ and $\bar{q}$ are arbitrary vectors of π-and Ω-space respectively, and

the real coefficients a_i and b_k are unknown at this stage.

We now introduce the scalar product (U, V) of two arbitrary vectors U and V:

$$U = (u_1, u_2) \qquad V = (v_1, v_2)$$

then

$$(U,V) = \iint_S (u_1 v_1 + u_2 v_2) dS \qquad , \qquad (4.20)$$

where the surface integral is taken over the whole fluid domain S. This kind of scalar product is called the Dirichlet scalar product. The reason it was chosen from among other possible definitions of the scalar product will be discussed shortly.

Here it is important to note that the two subspaces π and Ω are orthogonal to one another in terms of the Dirichlet scalar product. The scalar product of arbitrary vectors lying in the linear subspaces π and Ω, that is, the scalar product of arbitrary vectors I_i and J_k of the homogeneous π^* and Ω^* spaces respectively, is

$$(I_i, J_k) = \iint_S (p_{i1}^* q_{k1}^* + p_{i2}^* q_{k2}^*) dS = \iint_S \left(p_{i1}^* \frac{\partial \phi_k^*}{\partial y} + p_{i2}^* \frac{\partial \phi_k^*}{\partial z} \right) dS \qquad (4.21a)$$

Assuming that both $p_{i1}^* \phi_k^*$ and $p_{i2}^* \phi_k^*$ are continuously differentiable at all points of the fluid domain S, we can transform the surface integral into the line integral along the whole boundary of the fluid domain plus another kind of surface integral as follows:

$$(I_i, J_k) = -\iint_S \left(\frac{\partial p_{i1}^*}{\partial y} + \frac{\partial p_{i2}^*}{\partial z} \right) \phi_k^* \, dS - \int_{\Gamma_1 + \Gamma_2} \left(p_{i1}^* \frac{\partial y}{\partial n} + p_{i2}^* \frac{\partial z}{\partial n} \right) \phi_k^* \, ds = 0$$

$$(4.21b)$$

where n is the unit inner normal to the boundary. According to the definition of the homogeneous spaces $\pi*$ and $\Omega*$, it is obvious that both integrals appearing in the scalar product (U, V) vanish identically. In other words, every vector lying in π-space is always orthogonal to every vector lying in Ω-space in terms of a zero scalar product. Consequently, the two linear subspaces π and Ω are orthogonal to one another.**

**From the definitions of the π- and Ω-spaces, it will be demonstrated that if any two points or vectors $P_A = (p_{A1}, p_{A2})$ and $P_B = (p_{B1}, p_{B2})$ are given in π-space, the straight line joining these two points lies entirely in π-space. This means that π-space is a linear subspace.

Any point on the straight line joining two points P_A and P_B is described by $\alpha P_A + \beta P_B = (\alpha p_{A1} + \beta p_{B2}, \alpha p_{A2} + \beta p_{B2})$, where real numbers α and β are arbitrary except for the restriction $\alpha + \beta = 1$. Then

$$\frac{\partial(\alpha p_{A1} + \beta p_{B1})}{\partial y} + \frac{\partial(\alpha p_{A2} + \alpha p_{B2})}{\partial z} = \alpha\left(\frac{\partial p_{A1}}{\partial y} + \frac{\partial p_{A2}}{\partial z}\right) + \beta\left(\frac{\partial p_{B1}}{\partial y} + \frac{\partial p_{B2}}{\partial z}\right) = 0$$

$$(\alpha p_{A1} + \beta p_{B1})\frac{\partial y}{\partial n} + (\alpha p_{A2} + \beta p_{B2})\frac{\partial z}{\partial n} = \partial\left(p_{A1}\frac{\partial y}{\partial n} + p_{A2}\frac{\partial z}{\partial n}\right) + \beta\left(p_{B1}\frac{\partial y}{\partial n} + \right.$$

$$\left. p_{B2}\frac{\partial z}{\partial n}\right) = (\alpha + \beta)\ g(s) = g(s) \qquad .$$

Therefore, the vector $\alpha P_A + \beta P_B$ is a vector of π-space. Furthermore, if $Q_A = (q_{A1}, q_{A2})$ and $Q_B = (q_{B1}, q_{B2})$ are two arbitrary points (vectors) in Ω-space, or

$$q_{A1} = \frac{\partial \phi A}{\partial y} \quad , \quad q_{A2} = \frac{\partial \phi A}{\partial z} \qquad \text{where } \phi_A = f(s) \quad \text{on } \Gamma_2$$

$$q_{B1} = \frac{\partial \phi B}{\partial y} \quad , \quad q_{B2} = \frac{\partial \Phi B}{\partial z} \qquad \text{where } \phi_B = f(s) \quad \text{on } \Gamma_2 \qquad ,$$

Based on the fact that two orthogonal linear subspaces cannot intersect in more than one point [30], we can obtain important inequalities. Let R_π and R_Ω be arbitrary points or arbitrary vectors in π- and Ω-space respectively. Then,

$$(R_\pi - R_\Omega)^2 = (R_\pi - R)^2 + (R - R_\Omega)^2 \quad , \tag{4.22}$$

since the scalar product $(R_\pi-R, R-R_\Omega)$ is zero because of the orthogonality of the π and Ω spaces. Therefore we obtain the following inequalities:

$$(R_\pi - R_\Omega)^2 \geqq (R_\pi - R)^2 \tag{4.23}$$

$$(R_\pi - R_\Omega) \geqq (R_\Omega - R) \quad . \tag{4.24}$$

What these inequalities say is [30]

(a) For R_Ω arbitrary in Ω-space and R_π fixed in π-space, the squared distance $(R_\pi-R_\Omega)^2$ is minimized by $R_\Omega=R$.

(b) For R_π arbitrary in π-space and R_Ω fixed in Ω-space, $(R_\pi-R_\Omega)^2$ is minimized by $R_\pi=R$.

(c) For R_π and R_Ω arbitrary in π- and Ω-space respectively, $(R_\pi-R_\Omega)^2$ is minimized by $R_\pi=R_\Omega=R$.

**(continued) then any point on the straight line joining Q_A and Q_B, i.e., $\alpha Q_A + \beta Q_B = (\alpha q_{A1} + \beta q_{B1}, \alpha q_{A2} + \beta q_{B2})$ satisfies

$$\alpha q_{A1} + \beta q_{B1} = \alpha \frac{\partial \phi_A}{\partial y} + \beta \frac{\partial \phi_B}{\partial y} = \frac{\partial (\alpha \phi_A + \beta \phi_B)}{\partial y} \text{ where } \alpha \phi_A + \beta \phi_B =$$

$$(\alpha + \beta) f(s) = f(s) \text{ on } \Gamma_2$$

$$\alpha q_{A2} + \beta q_{B2} = \alpha \frac{\partial \phi_A}{\partial z} + \beta \frac{\partial \phi_B}{\partial z} = \frac{\partial (\alpha \phi_A + \beta \phi_B)}{\partial z} \text{ where } \alpha \phi_A + \beta \phi_B = f(s) \text{ on } \Gamma_2.$$

Therefore, the vector $\alpha Q_A + \beta Q_B$ also is a vector of Ω-space. Consequently, both spaces, π and Ω, are linear subspaces.

From these minimum principles, it is clear that if we want to get close to the exact solution of our problem, we have to minimize the squared distance $(R_\pi - R_\Omega)^2$. The p- and q-vectors that were defined by equations (4.18) and (4.19) are obviously the vectors in π- and Ω- space respectively, in which the variable parameters a_i and b_k are not yet fixed. From the minimum principles stated above, it is obvious that minimizing the squared distance $(p-q)^2$ affords us a useful approximate solution of the current problem.

From the equations (4.18) and (4.19), we have

$$(p-q)^2 = (\overline{p}-\overline{q})^2 + \left(\sum_{i=1}^{N} a_i I_i - \sum_{k=1}^{M} b_k J_k\right)^2 + 2\left(\overline{p}-\overline{q}, \sum_{i=1}^{N} a_i I_i - \sum_{k=1}^{M} b_k J_k\right)$$

$$= \left(\overline{p}-\overline{q} + \sum_{i=1}^{N} a_i I_i\right)^2 + \left(\overline{p}-\overline{q} - \sum_{k=1}^{M} b_k J_k\right)^2 - (\overline{p}-\overline{q})^2 \quad . \tag{4.25}$$

Since the last term of the right-hand side is fixed, it is sufficient to minimize the first and the second terms in order to minimize $(p-q)^2$.

Taking the partial derivatives of the first and the second terms with respect to the unknown parameters a_i and b_k respectively, and equating them to zero, the conditions necessary to minimize these terms are described as

$$\left(\overline{p}-\overline{q} + \sum_{i=1}^{N} a_i I_i \, , \, I_j\right) = 0 \qquad (j = 1,2,3, \ldots, N) \tag{4.26}$$

$$\left(-\overline{p}+\overline{q} + \sum_{k=1}^{M} b_k J_k, \, J_\ell\right) = 0 \qquad (\ell = 1,2,3, \ldots, M) \tag{4.27}$$

It can be seen from equations (4.26) and (4.27) that we can determine the variable parameters a_i and b_k independently of one another. From now on, p- and q-vectors are assumed to have the

parameters a_i and b_k determined by minimizing $(p-q)^2$. Then,

$$(R-\bar{p})^2 = (R-p + p-\bar{p})^2$$

$$= (R-p)^2 + (p-\bar{p})^2 + 2(R-p, p-\bar{p}) \qquad . \qquad (4.28)$$

On the other hand,

$$0 = (R-q, I_i) = (R-p + p-q, I_i) = (R-p, I_i) + (p-q, I_i)$$

$$= (R-p, I_i) \qquad , \qquad (4.29)$$

since the scalar product $(p-q, I_i)$ vanishes because of equation (4.26), and so the last term of equation (4.28) vanishes. Hence,

$$(R-\bar{p})^2 = (R-p)^2 + (p-\bar{p})^2 \qquad . \qquad (4.30)$$

From the inequality (4.23), $(R-p)^2 \leqq (p-q)^2$. Finally, we obtain

$$(\bar{p}-p)^2 \leqq (R-\bar{p})^2 \leqq (\bar{p}-p)^2 + (p-q)^2 \qquad ; \qquad (4.31)$$

similarly,

$$(q-\bar{q})^2 \leqq (R-\bar{q})^2 \leqq (q-\bar{q})^2 + (p-q)^2 \qquad . \qquad (4.32)$$

Furthermore, if we can select the zero-vector to be the $\bar{p}$-vector, the inequality (4.31) may become simpler. In this case, the right-hand side of (4.31) reduces to

$$p^2 + (q-p)^2 = (p + q - p)^2 - 2(p, q-p)$$

$$= (p + q - p)^2$$

$$+ q^2 \qquad (4.33)$$

by the same reasoning used to obtain equation (4.29). Consequently, we obtain a simple relationship between the squared vectors R^2, p^2, and q^2:

$$p^2 \leqq R^2 \leqq q^2 \qquad . \qquad (4.34)$$

On the other hand, if we can select the zero-vector to be the $\bar{q}$-vector, the inequality (4.32) reduces to

$$q^2 \leqq R^2 \leqq p^2 \quad . \tag{4.35}$$

Notice that the squared exact solution R^2 of the current problem is exactly the same as the right-hand side of equation (4.8) if the density of fluid ρ is assumed to be unity. Consequently, equations (4.34) and (4.35) can be used to determine the upper and lower bounds of the added mass of a two-dimensional body.

From now on, as stated at the beginning of this section, we shall restrict our consideration to the case where the cross-sectional shape of the body, as well as that of the canal, is rectangular.

Returning to Figure 10, we shall consider a case where a rectangular two-dimensional cylinder translates with unit velocity in the y-direction at the center of a rectangular canal. In Figure 10 is shown the right half of the whole region to be considered. The rectangle AGCO is the right half of the rectangular body, and the rectangle BEDO is the right half of the rectangular canal. The boundary Γ_1 stands for the free surface, to be treated as a rigid wall.

The problem of determining the velocity potential ϕ in this case can be formulated thus:

$$\frac{\partial^2 \phi}{\partial y^2} + \frac{\partial^2 \phi}{\partial z^2} = 0 \qquad \text{in the fluid domain } S \qquad (4.36)$$

$$\frac{\partial \phi}{\partial n} = \begin{cases} 0 \\ 1 \end{cases} \qquad \begin{array}{l} \text{on the boundaries } \Gamma_1, \ \Gamma_3, \ \Gamma_5, \ \Gamma_6 (4.37) \\ \text{on the boundary } \Gamma_2 \qquad\qquad (4.38) \end{array}$$

$$\phi = 0 \qquad\qquad \text{on the boundary } \Gamma_4 \qquad . \qquad (4.39)$$
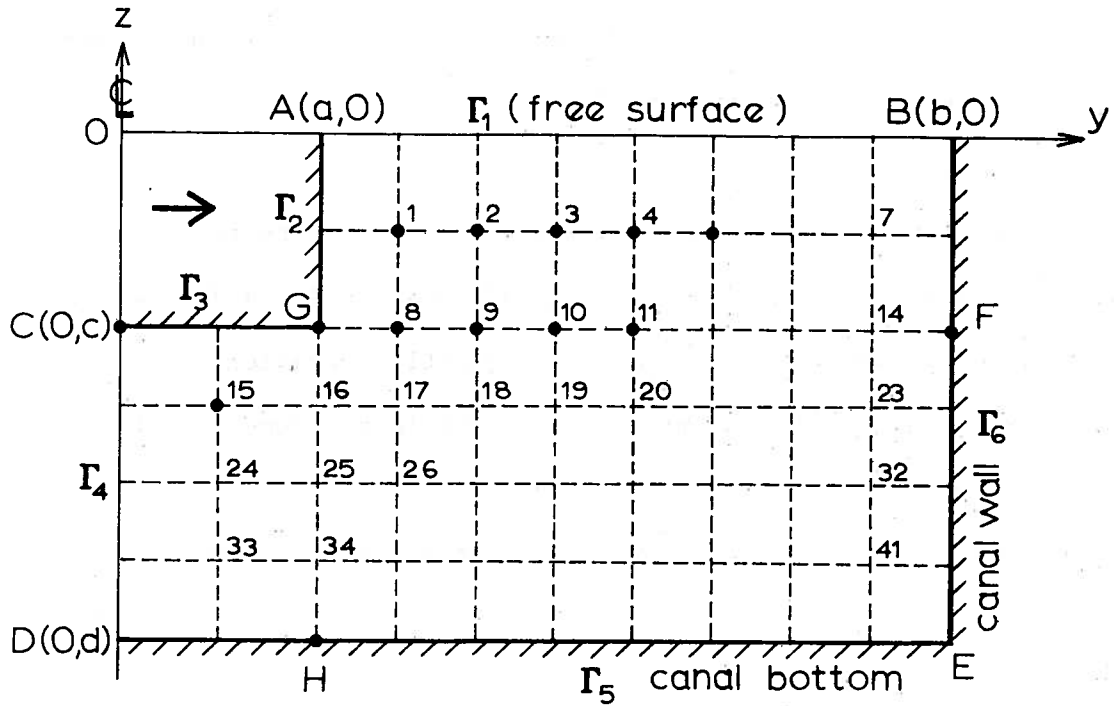
Figure 10. Division of fluid domain bounded by a rectangular body into a net of rectangular meshes (only the right-half of the whole domain is shown).
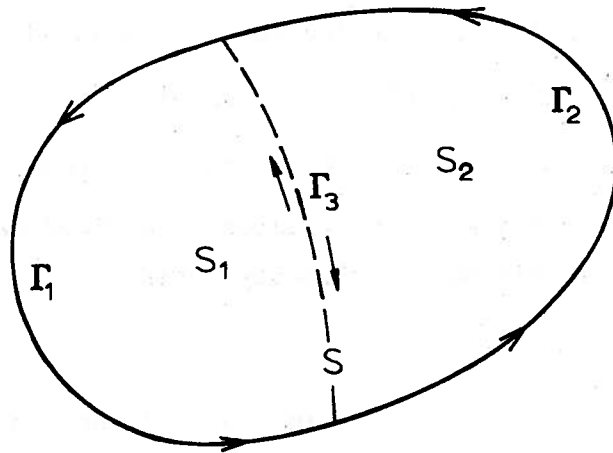

Figure 11. Division of the whole domain S into two subdomains S_1 and S_2 by drawing a curve Γ_3 across which some kinds of discontinuities of ϕ^* or I_i-vector are permissible.

Corresponding to this formulation, we can define the linear subspaces π and Ω immediately:

(I) π-space : $p = (p_1, p_2)$

$$\frac{\partial p_1}{\partial y} + \frac{\partial p_2}{\partial z} = 0 \qquad \text{in the domain } S \qquad (4.40)$$

$$p_1 \frac{\partial y}{\partial n} + p_2 \frac{\partial z}{\partial n} = \begin{cases} 0 & \text{on the boundaries } \Gamma_1 \ \Gamma_3 \ \Gamma_5 \ \Gamma_6 \\ 1 & \text{on the boundary } \Gamma_2 \qquad (4.42) \end{cases}$$

(4.41)

(II) Ω-space : $q_1 = (q_1, q_2)$

$$q_1 = \frac{\partial \phi}{\partial y} , \qquad q_2 = \frac{\partial \phi}{\partial z} \qquad , \qquad (4.43)$$

where ϕ is arbitrary except for the restriciton that ϕ must satisfy $\phi = 0$ on the boundary Γ_4.

The homogeneous spaces π^* and Ω^* are defined by substituting the homogeneous boundary conditions for the nonhomogeneous boundary conditions:

(III) π^*-space : $I_i = (p_{i1}^*, p_{i2}^*)$ $i = 1, 2, \dots.$

$$\frac{\partial p_{i1}^*}{\partial y} + \frac{\partial p_{i2}^*}{\partial z} = 0 \qquad \text{in the domain } S \qquad (4.44)$$

$$p_{i1}^* \frac{\partial y}{\partial n} + p_{i2}^* \frac{\partial z}{\partial n} = 0 \text{ on the boundaries } \Gamma_1, \Gamma_2, \Gamma_3, \Gamma_5, \Gamma_6.$$

(4.45)

(IV) *-space : $J_k = (q_{k1}^*, q_{k2}^*)$ $k = 1, 2, \dots.$

$$q_{k1}^* = \frac{\partial \phi_k^*}{\partial y} , \qquad q_{k2}^* = \frac{\partial \phi_k^*}{\partial z} \qquad , \qquad (4.46)$$

where ϕ_k^* is arbitrary except for the restriction that it must be zero on the boundary Γ_4.

From the above definition, it is evident that we can choose the zero vector, i.e., $0 = (0, 0)$ as an arbitrary $\bar{q}$-vector of Ω-space. Therefore, the added mass of the two-dimensional rectangular body can be evaluated by equation (4.35), and the squared q-vector gives a lower bound of the added mass while the squared p-vector gives an upper bound. Remember that, as stated earlier, it is possible to calculate the lower and upper bounds independently of one another. First, let us consider the upper bound p^2.

   (i)   Evaluation of the Upper Bound of the Added Mass

In order to obtain the upper bound, it is necessary to determine the I_i-vectors of the homogeneous π^*-space, but before we do that, we shall consider the possibility of violating the continuous differentiability condition of the functions p^* and ϕ^*, which were used to verify the orthogonal character of the linear subspaces π and Ω [30]. If we could loosen the continuity restriction throughout the whole region, it would be easier to determine the I_i-vector concretely. The orthogonal character of the two linear subspaces π and Ω is all that we have needed to apply the method so far.

Let us divide the whole fluid domain S into two subdomains S_1 and S_2 by cutting S with a curve Γ_3, and let us assume that in each subdomain, the necessary continuity of the functions p^* and ϕ^* is satisfied, while on the boundary Γ_3 there exists discontinuity. (see Figure 11) The scalar

product of I_i- and J_k-vectors is described as follows:

$$(I_i, J_k) = - \iint\limits_{S_1+S_2} (\frac{\partial p_{i1}^*}{\partial y} + \frac{\partial p_{i2}^*}{\partial z})\, \phi_k^* dS - \int\limits_{\Gamma_1+\Gamma_2} (p_{i1}^* \frac{\partial y}{\partial n} + p_{i2}^* \frac{\partial z}{\partial n})\phi_k^* ds$$

$$- \int\limits_{\Gamma_3} (p_{i1}^* \frac{\partial y}{\partial n} + p_{i2}^* \frac{\partial z}{\partial n})\, \phi_k^* ds \quad . \quad\quad (4.47)$$

The first and second integrals of the right-hand side vanish because of equations (4.44), (4.45), and (4.46), and the third integral should be a sum of two integrals taken over both sides of the boundary Γ_3. Therefore, the orthogonality of π and Ω subspaces is assured if the last integral vanishes. As a result, the following discontinuities are permissible:

(a) If ϕ_k^* is continuous in the whole domain, there may exist a discontinuity in the normal derivative $\partial\phi_k^*/\partial n$ across any curve drawn in the domain S, and

(b) If $p_{i1}^* \frac{\partial y}{\partial n} + p_{i2}^* \frac{\partial z}{\partial n}$, i.e., the normal component of I_i-vector, is continuous across any curve drawn in the domain S, there may exist a discontinuity in the tangential component of I_i-vector.

Now we shall determine the I_i-vectors concretely. To begin with, we divide the whole fluid domain S into a lot of rectangular meshes as shown in Figure 10, and then consider any four meshes that possess a grid-point in common as a basic

unit (see Figure 12). Then we define the I_i-vector
($=(p_{i1}^*, p_{i2}^*)$) as follows: the subscript i stands for the
i-th grid-point and the I_i-vector vanishes outside the i-th
basic unit consisting of the four rectangles possessing the
i-th grid-point in common. In other words, the I_i-vector is
nonzero only inside the i-th basic unit.

In order to solve a system of algebraic equations, for
instance, equations (4.26), we need to know the values of the
scalar products $(\bar{p}, I_j)$ and (I_i, I_j) beforehand. Therefore,
it is better to define the I_i-vector in so simple a form that
we can calculate the above scalar products with ease. For
this purpose we adopt the following linear representation
of the I_i-vector:

$$p_{i1}^* = \alpha_{i1} \, y + \alpha_{i2} \, z + \alpha_{i0} \qquad\qquad (4.48)$$

$$p_{i2}^* = \beta_{i1} \, y + \beta_{i2} \, z + \beta_{i0} \qquad , \qquad (4.49)$$

where α's and β's are constants but are not yet known.
Taking account of the permissible discontinuity (b), these
constants are determined uniquely to within an arbitrary
multiplicative constant [28]. Equation (4.50) to (4.53) are
obtained by normalizing equations (4.48) and (4.49) by
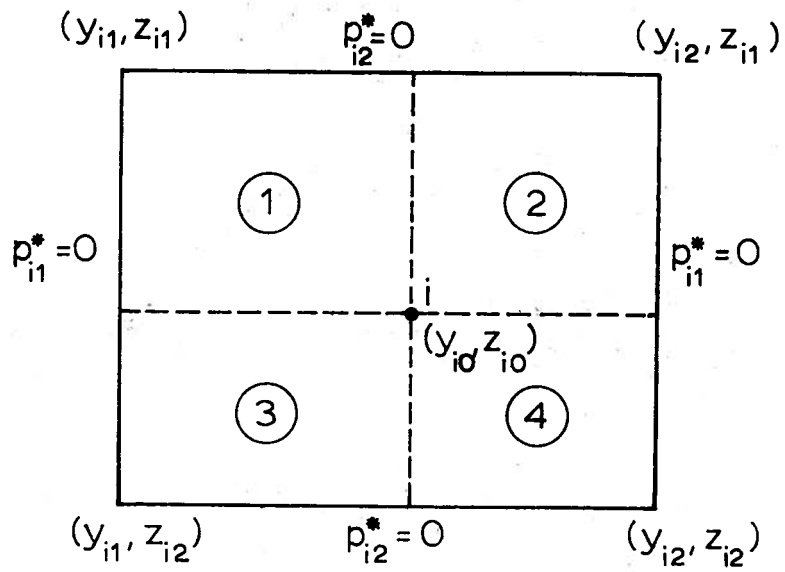dividing them by $(y_{i1} - y_{i0})$ (see Figure 12).

Figure 12. Basic unit consisting of four rectangular meshes
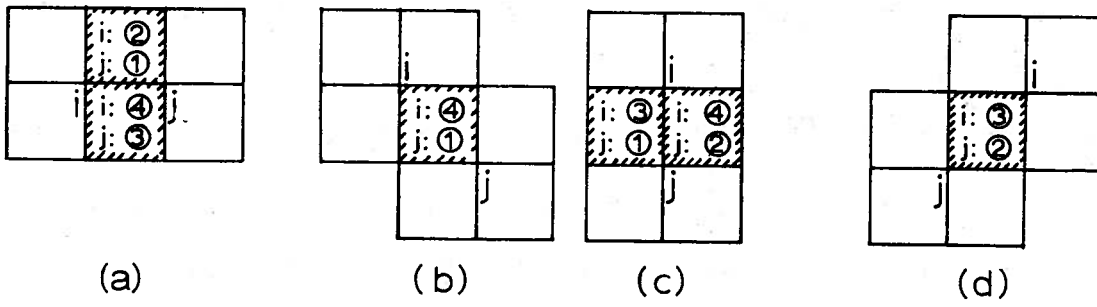possessing a grid-point in common.

(a) (b) (c) (d)

Figure 13. Canonical configurations of two basic units that
produce non-zero scalar products.

(a)   Mesh① $P_{i1}^* = \dfrac{y - y_{i1}}{y_{i0} - y_{i1}}$, $P_{i2}^* = \dfrac{-(z - z_{i1})}{y_{i0} - y_{i1}}$ 　　　　　　　(4.50)

(b)   Mesh② $P_{i1}^* = \dfrac{-(y - y_{i2})}{y_{i2} - y_{i0}}$, $P_{i2}^* = \dfrac{z - z_{i1}}{y_{i2} - y_{i0}}$ 　　　　　　(4.51)

(4.52)

(c)   Mesh③ $P_{i1}^* = \dfrac{(z_{i0} - z_{i1})(y - y_{i1})}{(y_{i0} - y_{i1})(z_{i0} - z_{i2})}$, $P_{i2}^* = \dfrac{-(z_{i0} - z_{i1})(z - z_{i2})}{(y_{i0} - y_{i1})(z_{i0} - z_{i2})}$

(4.53)

(d)   Mesh④ $P_{i1}^* = \dfrac{(z_{i0} - z_{i1})(y - y_{i2})}{(y_{i0} - y_{i2})(z_{i0} - z_{i2})}$. $P_{i2}^* = \dfrac{-(z_{i0} - z_{i1})(z - z_{i2})}{(y_{i0} - y_{i2})(z_{i0} - z_{i2})}$,

where Y_{i0}, Y_{i1}, Y_{i2}, Z_{i0}, Z_{i1}, Z_{i2} are the coordinates of the

four corners and the grid-point of the i-th basic unit.

When we define an arbitrary fixed vector $\bar{p}$ of π-space,

the same discontinuity as that of the I_i-vector is permissible.

So the $\bar{p}$-vector is defined as follows (see Figure 10):

(a) Domain AGFB : $\bar{P}_1 = \dfrac{b-y}{b-a}$, $\bar{P}_2 = \dfrac{z}{b-a}$ 　　　　(4.54)

(b) Domain GHEF : $\bar{P}_1 = \dfrac{c(b-y)}{(b-a)(c-d)}$, $\bar{P}_2 = \dfrac{c(z-d)}{(b-a)(c-d)}$ 　(4.55)

(c) Domain CDHG : $\bar{P}_1 = \dfrac{c}{c-d}$, $\bar{P}_2 = 0$,   (4.56)

where a, b, c, and d are the ordinates or abscissas of the

points A, B, C, and D, and stand for the half-beam of the

body, the half-width of the canal, the draft of the body, and

the depth of the canal respectively.

From the definition of the I_i-vectors, it is easily understood that most of the scalar products (I_i, I_j) $(i, j = 1, 2, \ldots, N)$ in other words, most of the coefficients of the unknown parameters a_i in equation (4.26) vanish. For example, for the basic unit with the subscript $i = 10$ in Figure 10, the scalar products are zero except for (I_2, I_{10}), (I_3, I_{10}), (I_4, I_{10}), (I_9, I_{10}), (I_{10}, I_{10}), (I_{10}, I_{11}), (I_{10}, I_{18}), (I_{10}, I_{19}) and (I_{10}, I_{20}). The non-zero values of the other scalar products can be calculated by either of the following formulas (see Figure 13):

(a) In the case where meshes ②and④ of the i-th basic unit overlap meshes ①and③ of the j=th basic unit:

$$(I_i, I_j) = \tag{4.57}$$

$$\frac{(z_{11}-z_{10})(z_{11}-z_{12})}{6(z_{10}-z_{12})(y_{12}-y_{10})}\left[(y_{12}-y_{10})^2-2(z_{11}-z_{10})(z_{10}-z_{12})\right] \ .$$

(b) In the case where mesh ④ of the i=th basic unit overlaps mesh ① of the j-th basic unit:

$$(I_i, I_j) = \frac{z_{10}-z_{11}}{6(y_{10}-y_{12})}\left[(y_{12}-y_{10})^2 + (z_{10}-z_{12})^2\right] \ . \tag{4.58}$$

(c) In the case where meshes ③and④ of the i-th basic unit overlap meshes ①and② of the j-th basic unit:

$$(I_i, I_j) = \tag{4.59}$$

$$\frac{(z_{11}-z_{10})(y_{12}-y_{11})}{6(y_{10}-y_{11})(y_{12}-y_{10})}\left[(z_{10}-z_{12})^2- 2(y_{10}-y_{11})(y_{12}-y_{10})\right] \ .$$

(d) In the case where mesh ③ of the i-th basic unit overlaps

mesh ② of the j-th basic unit:

$$(I_i, I_j) = \frac{z_{i0} - z_{i1}}{6(y_{i0} - y_{i1})} \left[(y_{i0} - y_{i1})^2 + (z_{i0} - z_{i2})^2 \right] \quad (4.60)$$

(e) The scalar product of the i-th basic unit:

$$(I_i, I_i) = \quad\quad\quad\quad\quad\quad\quad\quad\quad\quad\quad\quad\quad\quad\quad\quad (4.61)$$

$$\frac{(z_{i1} - z_{i0})(z_{i1} - z_{i2})(y_{i2} - y_{i1})}{3(z_{i0} - z_{i2})(y_{i0} - y_{i1})(y_{i2} - y_{i0})} \left[(y_{i0} - y_{i1})(y_{i2} - y_{i0}) + (z_{i1} - z_{i0})(z_{i0} - z_{i2}) \right]$$

T h en, the scalar product $(\bar{p}, I_i)$ is obtained as follows: If

the i-th basic unit is included entirely inside the domain

AGFB or the domain GHEF or the domain CDHG, the scalar product

$(\bar{p}, I_i)$ vanishes as proved immediately after some manipulation

of integration. For instance, the scalar products $(\bar{p}, I_1)$,

$(\bar{p}, I_{15})$, and $(\bar{p}, I_{17})$ in Figure 10 are zero. The non-zero

value of the scalar product $(\bar{p}, I_i)$ occurs in the case where

the grid-point is located just on the boundary line GF or GH.

In the case of Figure 10, for example, the scalar product

$(\bar{p}, I_i)$ has non-zero value for i = 8, 9, 10, . . . , 14, 16,

25, and 34.

(a) In the case where the grid-point is located on the

boundary GF:

$$(\bar{p}, I_i) = \frac{d(z_{i1} - z_{i0})(y_{i2} - y_{i1})(y_{i0} + y_{i1} + y_{i2} - 3b)}{6(b-a)(c-d)} . \quad (4.62)$$

(b) In the case where the grid-point of the i-th basic

unit is located on the boundary GH:

$$(\bar{p}, I_i) = \frac{-c(z_{i1}-z_{i0})(z_{i1}-z_{i2})(z_{i0} + z_{i1} + z_{i2}-3d)}{6(b-a)(c-d)} \qquad (4.63)$$

From the formulas (4.57) to (4.63), we can obtain

immediately the coefficients of the unknown parameters

a_i included in the set of simultaneous linear algebraic

equations (4.26), if only the geometrical size of the

rectangular body as well as that of the rectangular

canal is given. Once the simultaneous equations (4.26)

are solved, the upper bound of the added mass p^2 can be

obtained immediately.

(ii) Evaluation of the Lower Bound of the Added Mass

When we determined the concrete form of the I_i-

vector, we used the permissible discontinuity (b).

Hence, the function $\phi_k^* = 0$ on Γ_4 should be continuous

in the whole domain. Except for this necessary

continuity, the function ϕ_k^* is arbitrary. Here, we

define ϕ_k^* as follows:

$$\phi_k^* = 2b \sin \frac{(2n + 1)\pi y}{2b} \cos \frac{m\pi z}{d} \qquad n,m = 0,1,2, \ldots \quad (4.64)$$

where the subscript k is defined by

$$k = \frac{n(n + 1)}{2} + n\,m + \frac{m(m + 3)}{2} + 1 \quad , \qquad (4.65)$$

so that the k-value increases one by one if the integers n and m are varied as shown in Table 6. Consequently, the J_k-vector of Ω^*-space is defined as follows:

$$q^*_{k1} = (2n + 1)\pi \cos \frac{(2n + 1)\pi y}{2b} \cos \frac{m\pi z}{d} \qquad (4.66)$$

$$q^*_{k2} = - \frac{2bm\pi}{d} \sin \frac{(2n + 1)\pi y}{2b} \sin \frac{m\pi z}{d} \qquad . \qquad (4.67)$$

In order to determine the parameters b_k by solving a set of simultaneous linear equations (4.27), we have to know the values of the scalar products (J_k, J_ℓ) and $(\bar{p}, J_\ell)$ for k, ℓ = 1, 2, . . . , M. By changing the subscript k and the integers n, m to the subscript ℓ and the integers n', m' respectively, the J_ℓ-vector is defined as follows:

$$q^*_{\ell 1} = (2n' + 1)\pi \cos \frac{(2n' + 1)\pi y}{2b} \cos \frac{m'\pi z}{d} \qquad (4.68)$$

$$q^*_{\ell 2} = \frac{-2bm'\pi}{d} \sin \frac{(2n' + 1)\pi y}{2b} \sin \frac{m'\pi z}{d} \qquad (4.69)$$

where the subscript ℓ is defined by ℓ = n'(n'+1)/2 +n'm' + m'(m'+3)/2 +1. After executing the integration, we obtain the analytical formulas of the scalar product (J_k, J_ℓ) as follows:

Table 6. Variation of the subscripts i and j of I_i- and I_j-vectors by the systematic changing of integers n (n') and m (m')

m \ n	0	1	2	3	4	5
0	1	2	4	7	11	16
1	3	5	8	12	17	
2	6	9	13			
3	10	14				
4	15					

Table 7. Upper and lower bounds of the sway added mass of rectangular cylinders translating in the center of rectangular canals with various sectional-forms [28]

a	b	c	d	upper bound p^2	lower bound q^2	by finite element method
2.0	2.1	−2.0	−2.1	109.1	106.7	
2.0	2.2	−2.0	−2.2	55.80	54.55	54.96 (87*)
2.0	2.4	−2.0	−2.4	29.16	28.81	
2.0	2.6	−2.0	−2.6	20.34	19.68	
2.0	3.0	−2.0	−3.0	13.37	13.01	12.90 (60)
2.0	3.6	−2.0	−3.6	9.588	9.211	
2.0	5.0	−2.0	−5.0	6.876	6.258	
2.0	7.0	−2.0	−7.0	5.890	5.177	*Total number
2.0	10.0	−2.0	−10.0	5.610	4.607	of nodal points.
2.0	2.1	−2.0	−3.0	40.38	38.32	
2.0	2.2	−2.0	−3.0	25.48	24.30	
2.0	2.4	−2.0	−3.0	17.76	16.99	
2.0	2.6	−2.0	−3.0	15.22	14.70	
2.0	3.0	−2.0	−3.0	13.37	13.01	
2.0	3.6	−2.0	−3.0	12.64	12.24	
2.0	5.0	−2.0	−3.0	12.42	11.89	11.92 (74)
2.0	7.0	−2.0	−3.0	12.45	11.74	
2.0	10.0	−2.0	−3.0	12.55	11.58	11.91 (95)
2.0	2.2	−2.0	−2.1	96.18	93.85	
2.0	2.2	−2.0	−2.2	55.80	54.55	
2.0	2.2	−2.0	−2.4	36.12	35.38	
2.0	2.2	−2.0	−2.6	29.95	28.93	
2.0	2.2	−2.0	−3.0	25.49	24.31	
2.0	2.2	−2.0	−3.6	23.48	21.64	
2.0	2.2	−2.0	−5.0	22.76	20.76	
2.0	2.2	−2.0	−7.0	23.39	19.59	
2.0	2.2	−2.0	−10.0	25.14	19.52	

(a) $n \neq n'$, $m \neq m'$ (4.70)

$$(J_k, J_\ell) = (2n+1)(2n'+1)bd\left[\frac{1}{2(n-n')}\sin\frac{(n-n')\pi a}{b} + \frac{1}{2(n+n'+1)}\sin\frac{(n+n'+1)\pi a}{b}\right]$$

$$\times\left[\frac{1}{2(m-m')}\sin\frac{(m-m')\pi c}{d} + \frac{1}{2(m+m')}\sin\frac{(m+m')\pi c}{d}\right]$$

$$+ \frac{mm'b^3}{d}\left[\frac{1}{n-n'}\sin\frac{(n-n')\pi a}{b} - \frac{1}{n+n'+1}\sin\frac{(n+n'+1)\pi a}{b}\right]$$

$$\times\left[\frac{1}{m-m'}\sin\frac{(m-m')\pi c}{d} - \frac{1}{m+m'}\sin\frac{(m+m')\pi c}{d}\right]$$

(b) $n \neq n'$, $m = m' \neq 0$ (4.71)

$$(J_k, J_\ell) = (2n+1)(2n'+1)b\left[\frac{1}{2(n-n')}\sin\frac{(n-n')\pi a}{b} + \frac{1}{2(n+n'+1)}\sin\frac{(n+n'+1)\pi a}{b}\right]$$

$$\times\left[\frac{c\pi}{2} + \frac{d}{4m}\sin\frac{2m\pi c}{d}\right]$$

$$+ \frac{m^2 b^3}{d}\left[\frac{1}{n-n'}\sin\frac{(n-n')\pi a}{b} - \frac{1}{n+n'+1}\sin\frac{(n+n'+1)\pi a}{b}\right]$$

$$\times\left[\frac{c\pi}{d} - \frac{1}{2m}\sin\frac{2m\pi c}{d}\right]$$

(c) $n \neq n'$, $m = m' = 0$ (4.72)

$$(J_k, J_\ell) = (2n+1)(2n'+1)bc\pi\left[\frac{1}{2(n-n')}\sin\frac{(n-n'\pi a}{b} + \frac{1}{2(n+n'+1)}\sin\frac{(n+n'+1)\pi a}{b}\right]$$

(d) $n = n'$, $m \neq m'$ (4.73)

$$(J_k, J_\ell) = (2n+1)^2 bd\left[\frac{a\pi}{2b} + \frac{1}{2(2n+1)}\sin\frac{(2n+1)\pi a}{b}\right]$$

$$\times\left[\frac{1}{2(m-m')}\sin\frac{(m-m')\pi c}{d} + \frac{1}{2(m+m')}\sin\frac{(m+m')\pi c}{d}\right]$$

$$+ \frac{mm'b^3}{d}\left[\frac{a\pi}{b} - \frac{1}{2n+1}\sin\frac{(2n+1)\pi a}{b}\right]$$

$$\times\left[\frac{1}{m-m'}\sin\frac{(m-m')\pi c}{d} - \frac{1}{m+m'}\sin\frac{(m+m')\pi c}{d}\right]$$

(e) $n = n'$, $m = m' \neq 0$ (4.74)

$$(J_k, J_\ell) = -\frac{(2n+1)^2\pi^2 bd}{4} + (2n+1)^2 bd \left[\frac{a\pi}{2b} + \frac{1}{2(2n+1)} \sin\frac{(2n+1)\pi a}{b}\right]$$

$$\times \left[\frac{c\pi}{2d} + \frac{1}{4m}\sin\frac{2m\pi c}{d} - \frac{m^2\pi^2 b^3}{d}\right]$$

$$+ \frac{m^2 b^3}{d}\left[\frac{a\pi}{b} - \frac{1}{2n+1}\sin\frac{(2n+1)\pi a}{b}\right]\left[\frac{c\pi}{d} - \frac{1}{2m}\sin\frac{2m\pi c}{d}\right]$$

(f) $n = n'$, $m = m' = 0$ (4.75)

$$(J_k, J_\ell) = -\frac{(2n+1)^2\pi^2 bd}{2} + (2n+1)^2\pi bc\left[\frac{a\pi}{2b} + \frac{1}{2(2n+1)}\sin\frac{(2n+1)\pi a}{b}\right]$$

Furthermore, the scalar product $(\overline{p}, J_\ell)$ is calculated from the following formulas:

(a) $m' \neq 0$ (4.76)

$$(\overline{p}, J_\ell) = \frac{bd^2}{(b-a)(c-d)m'\pi}\sin\frac{m'\pi c}{d}\left[-2(b-a)\sin\frac{(2n'+1)\pi a}{2b} + \frac{4b}{(2n'+1)\pi}\cos\frac{(2n'+1)\pi a}{2b}\right]$$

$$+ \frac{2bcd}{m'\pi(c-d)}\sin\frac{(2n'+1)\pi a}{2b}\sin\frac{m'\pi c}{d} - \frac{4b^2 d^2}{(2n'+1)m'\pi^2(b-a)(c-d)}\cos\frac{(2n'+1)\pi a}{2b}\sin\frac{m'\pi c}{d}$$

(b) $m' = 0$ (4.77)

$$(\overline{p}, J_\ell) = 2bc \sin\frac{(2n'+1)\pi a}{2b}$$

From equations (4.70) to (4.77), all the scalar products necessary to solve a set of simultaneous algebraic equations (4.27) can be calculated, if the geometrical configuration of the body in the canal is given. Once the parameters k_i are determined, the lower bound q^2 of the added mass can be calculated immediately.

-85-

(iii) Some Numerical Examples of the Sway Added Mass of
Rectangular Cylinders

In Table 7 are shown some numerical values of the

upper and lower bounds of the sway added mass of a

rectangular cylinder, for which the beam/draft ratio is

equal to 2, translating in the center of various forms of

rectangular canals. The upper bounds shown in this table

were obtained by dividing the whole fluid domain in a

simple way by dividing the section between the water

surface and the bottom of the body into m_1 equal pieces,

the section between the center of the body and the side

of the body into m_2 equal pieces, and the section between

the side of the body and the wall of the canal into n_1

equal pieces.** The total number of grid-points was

about 190.***

On the other hand, the lower bounds were obtained as

follows: By changing the integers $n(n')$ and $m(m')$ in a

systematic way as shown in Table 6, the variable parameter

$k(\ell)$ was increased one by one. At the same time, the

lower bound q^2 was calculated for each value of the

variable parameter k. When the difference between the

**In Figure 10, $M_1=2$, $M_2=4$, $N_1=2$, and $N_2=8$.

***Where the fluid domain is narrow, we can considerably reduce the
total number of grid-points. For instance, when $a=2.0$, $b=2.2$, $c=-2.0$
and $d=-2.2$, the upper bound obtained by using only 18 grid-points was
55.96, while it is 55.80 in Table 7.

-86-

k-th lower bound and the (k+1)-th lower bound got small enough, the process of increasing the parameter k was interrupted, and the (k+1)-th lower bound was adopted as the expected lower bound. For the calculation whose results are shown in Table 7, the final value of the parameter k was at most 80 to 100.

From this table, it is obvious that the accuracy of the upper bounds is not very good, especially in cases where the fluid domain is large. The accuracy of the lower bounds also gets worse when the fluid domain is extremely large, although it is not too bad compared with the accuracy of the upper bounds.

In the same table are shown a few examples of the sway added mass obtained by the finite element method, which are very close to the lower bounds obtained by the hypercircle method. This can be inferred from the tendency of the finite element method to give an approximate value lower than the exact value, though this statement is not always true [31].

Furthermore, it is seen from the second and the third groups of numerical results shown in Table 7 that if the canal width and the water depth are about five times as large as the beam of the moving body and its draft respectively, the effect of the restricted water on

the sway added mass gets so small as to be negligible
from the practical point of view. With respect to the
added mass of two-dimensional cylinders vibrating on the
free surface, a similar conclusion has been derived by
Matsuura and Kawakami, who examined the propriety of
replacing an infinite fluid with a finite fluid domain
bounded by artificial boundaries when calculating the
added mass of a vibrating cylinder by the finite element
method [32].

For the foregoing reasons, we can consider the lower
bound $q^2=4.607$ listed in the last line of the first group
in Table 7 as an approximate value of the sway added mass
of the rectangular cylinder in infinite water.

Lewis [33] and Wendel [34] calculated the vertical
added mass of a rectangular cylinder oscillating with
infinite frequency in the perpendicular direction on the
free surface of an infinite fluid. This kind of added
mass can be considered as the sway added mass of the
cylinder translating horizontally on the free surface of
an infinite fluid, if the roles of the side wall and the
bottom of the rectangular cylinder are interchanged.

According to Lewis and Wendel, the sway added mass
coefficient of a rectangular cylinder with the beam/draft
ratio being equal to 2 is 1.186, under the assumption

that the density of the cylinder is the same as that of the surrounding fluid, while the lower bound q^2 equal to 4.607 gives 1.152 as the sway added mass coefficient. Therefore, we can consider the lower bound obtained by the aforesaid method as a good approximate value of the added mass. Henceforth, we shall obtain only the lower bounds, and then use them to discuss the restricted water effect on the added mass.

Figure 14 shows the sway added mass coefficient of a rectangular cylinder that translates horizontally at the center of the various rectangular canals. The dotted lines drawn in the same figure represent Newman's formula

$$\frac{m+m_y}{(m+m_y)_H} = 1 + \left[3 \sum_{n=-\infty}^{\infty} \text{cosech}^2 \frac{\pi}{H}(\eta_0 + \frac{W}{2} + nW) - 6 \sum_{n=1}^{\infty} \text{cosech}^2 \frac{n\pi W}{H} \right]$$

$$\times \left[1 - \frac{(m+m_y)_\infty}{(m+m_y)_H} \right] \quad , \quad (4.78)$$

where the subscripts H and ∞ stand for a finite water depth H and infinite water depth respectively, and η_0 and W stand for the distance between the center of the canal and the center of the moving body, and the canal width respectively [35].

When we estimate the wall effect on the added mass from Newman's formula, we have to know the virtual mass
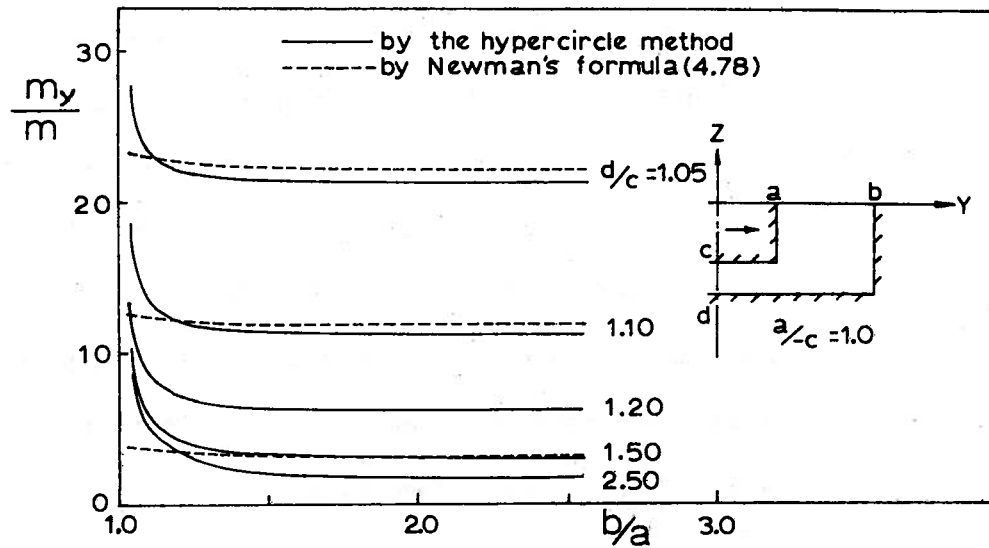
Figure 14. Sway added mass coefficient of a rectangular cylinder
(beam/draft = 2.0) translating horizontally at the center of
rectangular canals (m = mass of the cylinder whose density is
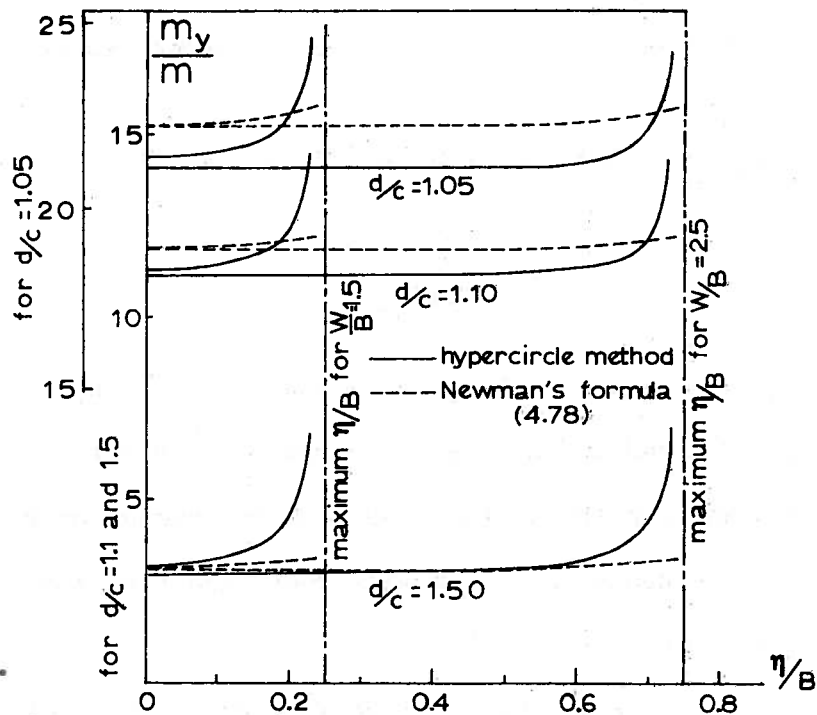assumed to be same as that of the surrounding fluid) [29]).

Figure 15. Finite-width effects on the sway added mass of a rectangular
cylinder (beam/draft = 2) translating at various off-center positions
of a canal.
(m: mass of the cylinder whose density is assumed to be same as that
of the surrounding fluid, and
η: off-center distance from the center of a canal) [29].

in the relevant water depth H.** The dotted lines of
Figure 14 were obtained by making use of the numerical
values of the sway added mass in shallow water,
calculated by Flagg and Newman [36]. Following Gurevich's
analysis [37], involving the conformal mapping of the
fluid domain bounded by a rectangular cylinder and the
channel bottom onto a semi-infinite half-plane, they
derived an approximate formula yielding the sway added
mass coefficients in extremely shallow water. For a
sufficiently small ε as defined by the equation

$$\epsilon = 1 - \frac{T}{H} \quad , \qquad\qquad (4.79)$$

the sway added mass of a rectangular cylinder, whose
breadth is B, is given as follows [36]:

$$\frac{m_y}{4\rho H^2} = \frac{1}{\epsilon}\frac{B}{2H} - \frac{2}{\pi}\log 4\epsilon + \frac{2}{\pi} - \frac{B}{H} + \epsilon\frac{B}{2H} + \frac{2}{3\pi}\epsilon^2 + 0(\epsilon^3) \ . \quad (4.80)$$

In addition, their paper [36] contains a detailed
numerical table of the sway added mass coefficient.

Returning to Figure 14, we shall compare the results
obtained by the hypercircle method with those obtained by

** On the other hand, Newman obtained another formula from which
the added mass in a canal can be directly calculated. However, as he
stated in [35], the formula underestimates the restricted water effect
on the added mass. Therefore, he recommends the use of formula (4.78)
in order to estimate the finite-width effect or the wall effect on the
added mass.

formula (4.78). The hypercircle method gives a larger estimate of the wall effect or the finite-width effect on the sway added mass, compared with formula (4.78). In particular, the difference between the wall effect obtained by both methods is serious in relatively deeper water. For example, when the water-depth/draft ratio and the canal-width/body-beam ratio are 1.50 and 1.05 respectively, the sway added mass coefficient obtained by the hypercircle method is 9.43, while that calculated from (4.78) is only 3.66. On the other hand, in a relatively wider canal, the hypercircle method gives a smaller value than does formula (4.78).

At any rate, it can be concluded from this figure that the finite-width effect on the added mass is quite small except for the case where the side of the moving cylinder is extremely close to the bank of a canal. Therefore, it can be anticipated that the wall effect on the added mass of a rectangular cylinder translating at an off-center position of a canal is also small except for the case of an extreme deviation of the body from the center of a canal.

Incidentally, the previous formulation of the hypercircle method is not applicable for the off-center translation of the body. In this case, we need to take

the whole fluid domain into consideration. Instead of
equations (4.36) to (4.39), the following equations must
be satisfied by the velocity potential function (see
Figure 15):

$$\frac{\partial^2 \phi}{\partial y^2} + \frac{\partial^2 \phi}{\partial z^2} + 0 \qquad \text{in the whole fluid domain S} \qquad (4.81)$$

$$\frac{\partial \phi}{\partial n} = \begin{cases} 0 & \text{on the boundaries } \Gamma_1, \ \Gamma_3, \ \Gamma_5, \ \Gamma_6, \ \Gamma_7, \ \Gamma_8 \quad (4.82) \\ 1 & \text{on the boundary } \Gamma_2 \qquad\qquad\qquad\qquad (4.83) \\ -1 & \text{on the boundary } \Gamma_4 \qquad\qquad\qquad\quad (4.84) \end{cases}$$

This is the so-called Neumann boundary-value problem. In
this case it is convenient to convert this problem into
an equivalent Dirichlet problem, in order to apply the
hypercircle method to the problem. Such a conversion can
be easily executed if the stream function $\psi(y,z)$ is used
to describe the problem instead of the velocity potential
function $\psi(y,z)$. The equivalent Dirichlet problem is
described as follows:

$$\frac{\partial^2 \psi}{\partial y^2} + \frac{\partial^2 \psi}{\partial z^2} = 0 \qquad \text{in the whole fluid domain S} \qquad (4.85)$$

$$\psi = \begin{cases} 0 & \text{on the boundaries } \Gamma_1, \ \Gamma_5, \ \Gamma_6, \ \Gamma_7, \ \Gamma_8 \quad (4.86) \\ z & \text{on the boundaries } \Gamma_2 \text{ and } \Gamma_4 \qquad\qquad (4.87) \\ c & \text{on the boundary } \Gamma_3 \qquad\qquad\qquad\quad (4.88) \end{cases}$$

Since the kinetic energy of the fluid can still be
expressed by equation (4.8), in which the velocity
potential ϕ should be replaced by the stream function ψ,

the inequalities (4.31), (4.32), (4.34), and (4.35)

provide the upper and the lower bounds of the added mass.

The detailed procedure for solving this problem will

be omitted. (See reference [29]). Here, only one

illustration indicating the finite-width effect on the

sway added mass of a rectangular cylinder which translates

at various off-center positions in a canal is shown in

Figure 15. Numerical calculations were executed for two

cases of the canal width. The canal-width/body-beam

ratios were 1.5 and 2.5. In the latter case, the

transverse deviation of the cylinder from the center of

the canal doesn't affect the sway added mass much, as

long as the deviation is not too large.

From Figure 15 as well as Figure 14, it is concluded

that the finite-width effect on the sway added mass is

relatively more important in deeper water than in

shallower water.

According to the two-dimensional theory, the finite-

width effect on the sway added mass proves to be

negligibly small if the canal width is more than about

five times as large as the beam of the moving body. This

conclusion is sustained by the experimental results shown

in Table 3. However, the experimental results obtained

in narrow canals, whose sectional forms don't exactly

coincide with that used in the theoretical calculation,
reveal a more notable finite-width effect on the sway
added mass, compared with the theoretical prediction. In
addition, the experimental finite-width effect on the yaw
added mass moment of inertia is conspicuous. For example,
in a canal where the width is 3 times as wide as the
model's breadth and the depth is 1.20 times as deep as
the model's draft, the yaw added mass moment of inertia
of the oil-tanker model was about 2.4 times as large as
that in otherwise unrestricted shallow water of the same
depth.

In order to explain this marked increase of the yaw
added mass moment of inertia due to restriction of the
water surface, it is necessary either (1) to try to
calculate the three-dimensional yaw added mass moment of
inertia in a canal or (2) to try to calculate the two-
dimensional yaw added mass moment of inertia of a
vertical cylinder placed at the center of two parallel
walls, whose sectional form in the horizontal plane
parallel to the water surface is the same as the water-
plane form of a ship. The latter two-dimensional
approximation may afford a reasonable value of the yaw
added mass moment of inertia in cases where there is no
clearance beneath the ship.

4.1.2. *Sway Added Mass and Yaw Added Mass Moment of Inertia in Shallow Water*

Again, it is possible to make use of the hypercircle method or the finite element method when calculating the sway added mass of two-dimensional bodies in shallow water. The finite element method is especially useful for calculating the added mass of an arbitrary two-dimensional cylinder translating in a waterway of arbitrary shape, and in addition, it can easily be extended to the three-dimensional case if enough computer capacity is available.

Another method was derived by Hess and Smith to represent the flow field around an arbitrary three-dimensional body in terms of a singularity distribution on the body surface [38]. By extending their method, Kan tried to calculate the sway added mass of a ship moving in restricted waters [39], but it is quite tedious to obtain the three-dimensional added mass of many ships in restricted waters by means of either the finite element method or the surface distribution of singularities. Therefore, as stated at the beginning of part 4, we shall adopt the strip theory synthesis (4.7) to obtain the sway added mass and the yaw added mass moment of inertia. For this synthesis, the two-dimensional sway added mass must be known.

Kan and Hanaoka clarified the shallow water effect on the two-dimensional sway added mass of the flat plate and the circular cylinder [40]. In their analysis, the sway added mass of a vertical flat plate with uniform draft T, translating in the direction normal to the

surface of the plate, in other words, in a direction parallel to the free surface, in shallow water of uniform depth H, was obtained as follows: The two-dimensional fluid motion around the plate can be denoted with the velocity potential function that describes the fluid motion around a cascade array of infinite images of the plate with respect to the bottom of the waterway as well as the free surface.

Assuming that the flat plate moves in the starboard direction with unit velocity, and taking account of the identity $\phi_{2r}=-\phi_{2\ell}$, the sway added mass of the plate of width 2T is

$$m_y = - \rho \iint_{S_B} \phi_2 \frac{\partial \phi_2}{\partial n} dS = - \rho \int_{-L/2}^{L/2} \int_{-T}^{T} (\phi_{2r}-\phi_{2\ell}) dxdz = - 2\rho \int_{-\frac{L}{2}}^{\frac{L}{2}} \int_{-T}^{T} \phi_{2r} dxdz \ , \quad (4.89)$$

where the subscripts r and ℓ stand for the velocity potential function on the starboard surface and on the port surface of the plate respectively. According to reference [41], which gives the velocity potential function for the cascade array,

$$\phi_{2r} = - \frac{2H}{\pi} \cosh^{-1} \frac{\cos (\pi z/2H)}{\cos (\pi T/2H)} \ . \quad (4.90)$$

Consequently,

$$m_y = \frac{4\rho HL}{\pi} \int_{-T}^{T} \cosh^{-1} \frac{\cos(\pi z/2H)}{\cos(\pi T/2H)} dz = \frac{4\rho HLT}{\pi} \int_{-1}^{1} \cosh^{-1} \frac{\cos(\pi T\zeta/2H)}{\cos(\pi T/2H)} d\zeta \ . \quad (4.91)$$

In the deep water case, under the two-dimensional approximation, the sway added mass of a flat plate with length and width L and 2T respectively, translating in the transverse direction in infinite fluid, is $\rho\pi T^2 L$. Let us describe the shallow water effect on the sway

added mass of the flat plate in terms of the coefficient k_F defined as the ratio of the sway added mass in restricted water to that in deep water:

$$k_F = \frac{4H}{\pi^2 T} \int_{-1}^{1} \cosh^{-1} \frac{\cos(\pi T \zeta / 2H)}{\cos(\pi T / 2H)} d\zeta \quad . \tag{4.92}$$

Newman derived a similar formula which affords the shallow water effect on the sway added mass, the yaw added mass moment of inertia, the lateral force, and the yaw moment of a rectangular flat plate [42]. He took account of the three-dimensionality of the flat plate, while equation (4.92) was obtained on the basis of the two-dimensional approximation of a three-dimensional flat plate.

According to Newman's matrix notation, the shallow water effects are described as follows:

$$k_i(A) = \frac{F_i(A,H)}{F_i(A,\infty)} = \left[A \frac{T}{H} \beta_i^{-1} - \frac{\pi^2 (\frac{T}{H})^2}{8 \log(\cos\frac{\pi T}{2H})} \right]^{-1} \tag{4.93a}$$

where A stands for the aspect ratio of a rectangular plate defined by 2T/L and the characters with the subscript i stand for

$$F_i = \{m_y, J_{zz}, Y, N\}$$
$$\beta_i = \{1, 3/8, 4, 2\} \quad . \tag{4.93b}$$

The second term in the right-hand brackets of equation (4.93a) represents the shallow water effect at the limit of zero aspect-ratio, which gives a numerical value almost equal to the k_F-value defined by equation (4.92). The first term represents the three-dimensional component of the shallow water effect.

Since a smaller β_i amounts to a bigger three-dimensional effect, it is understood from formula (4.93) that the yaw added mass moment of inertia is most affected by the three-dimensionality of the flow around the plate, while the lateral force is least affected.

In Figure 16 are shown the shallow water effects on the sway added mass of a flat plate, a semi-immersed circular cylinder, and a rectangular cylinder with a beam/draft ratio equal to 2. In the same figure, some experimental data are plotted for the purpose of comparison. Roughly speaking, the shallow water effect on the sway added mass of a three-dimensional ship can be estimated by that of either the semi-immersed circular cylinder or the rectangular cylinder. In extremely shallow water, however, any two-dimensional calculation tends to overestimate the added mass, since the added mass obtained by the two-dimensional theory goes to infinity sooner or later as the water depth decreases, while the added mass of a three-dimensional ship remains finite. The fluid surrounding a real ship moves around both ends of the ship in horizontal planes parallel to the water surface rather than in transverse vertical planes, when the ship translates in the transverse direction in extremely shallow water. Therefore, if we calculate the sway added mass and the yaw added mass moment of inertia according to the strip theory synthesis (4.7), the values obtained thus will be too large compared with the true values, and it is necessary to correct for this discrepancy.
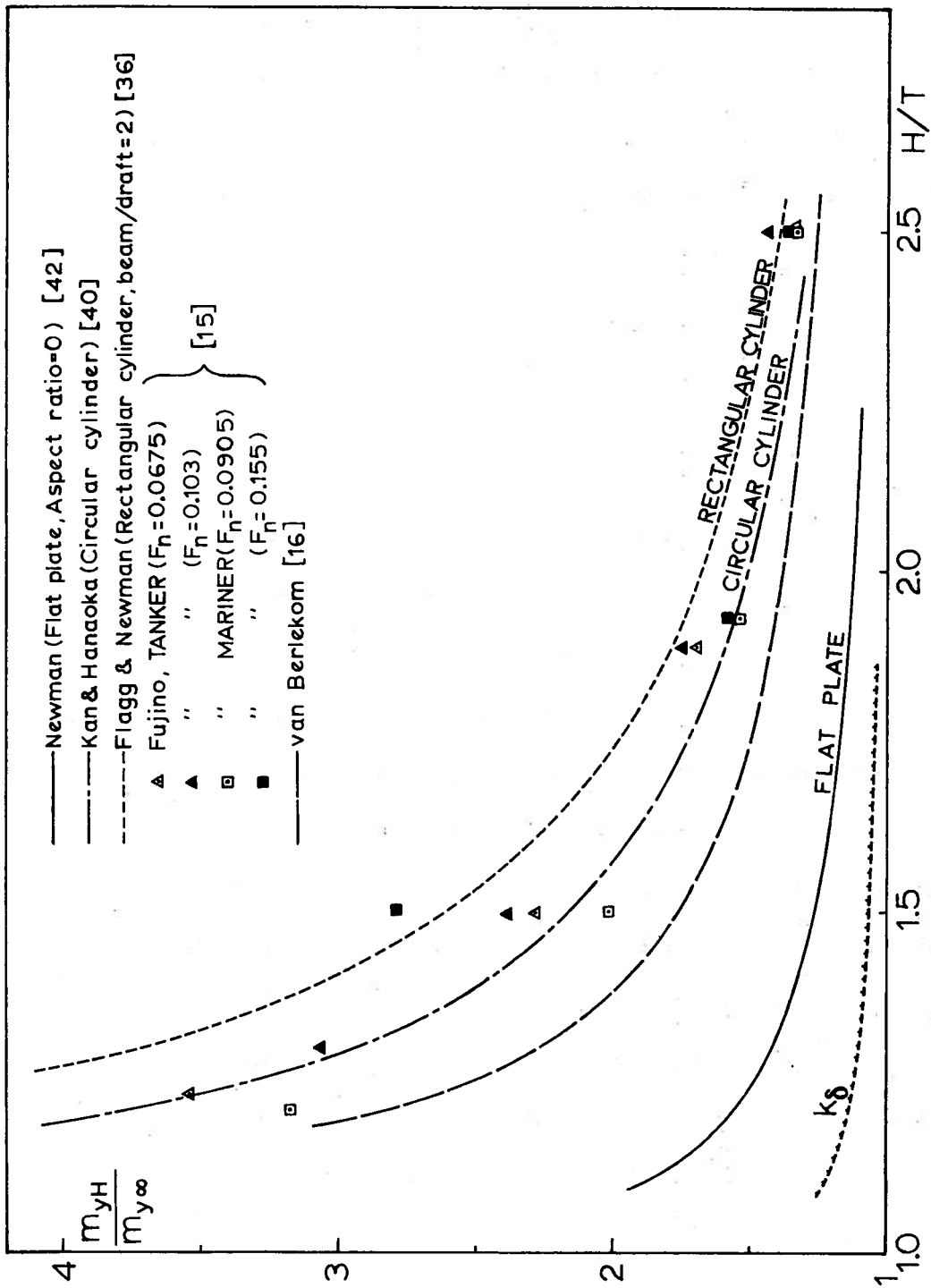
Figure 16. Comparison of the shallow water effects on the sway added mass obtained by two-dimensional calculation and by experiments.

We shall introduce the three-dimensional correction factors of the sway added mass and the yaw added mass moment of inertia, which will be denoted by C_y and C_{zz} defined as follows:

$$C_y = \frac{\text{three-dimensional sway added mass}}{\int_L m_y^*(x)\,dx} \qquad (4.94)$$

$$C_{zz} = \frac{\text{three-dimensional yaw added mass moment of inertia}}{\int_L m_y^*(x)\,x^2 dx} \qquad (4.95)$$

As an example, the correction factors C_y and C_{zz} are shown in Figure 17 for the Mariner-type ship and the oil-tanker, whose three-dimensional added mass and added mass moment of inertia are already known from P.M.M. tests. The two-dimensional sway added mass $m_y^*(x)$ in this illustration was calculated by the finite element method. The three-dimensional value of the sway added mass and the yaw added mass moment of inertia were obtained by the finite element method as well.

The circles and the triangles of Figure 17 represent the three-dimensional correction factors which are obtained by using the experimental values of the sway added mass and the yaw added mass moment of inertia as the three-dimensional values in equations (4.94) and (4.95), while the solid lines and the dotted lines in the same figure were obtained by using the sway added mass and the yaw added mass moment of inertia obtained by the three- dimensional finite element method.

According to this figure, it is clear that the effect of the three-dimensionality of the ship's shape is more pronounced on the yaw added mass moment of inertia than on the sway added mass, and increases monotonically as the water depth decreases. This conclusion coincides with Newman's formula (4.93) as well as with our intuition that the yaw added mass moment of inertia is much affected by the three-dimensionality of the ship's shape, because the end parts of a ship make more contribution to the yaw added mass moment of inertia than to the sway added mass.

As stated above, the formula (4.93) provides the three-dimensional correction factors C_y and C_{zz}. If we use the subscripts H and ∞ to denote a finite water depth H and infinite water depth respectively, we obtain

$$\frac{C_{yH}}{C_{y\infty}} = \frac{F_1(A,H)}{F_1(0,H)} \cdot \frac{F_1(0,\infty)}{F_1(A,\infty)} = \frac{k_1(A)}{k_1(0)} \quad , \quad (4.96)$$

and similarly, we obtain

$$\frac{C_{zzH}}{C_{zz\infty}} = \frac{k_2(A)}{k_2(0)} \quad . \quad (4.97)$$

In Figure 18 are drawn the formulas (4.96) and (4.97) together with the numerical values of the ratios, $C_{yH}/C_{y\infty}$ and $C_{zzH}/C_{zz\infty}$, obtained from the three-dimensional correction factors shown in Figure 17.
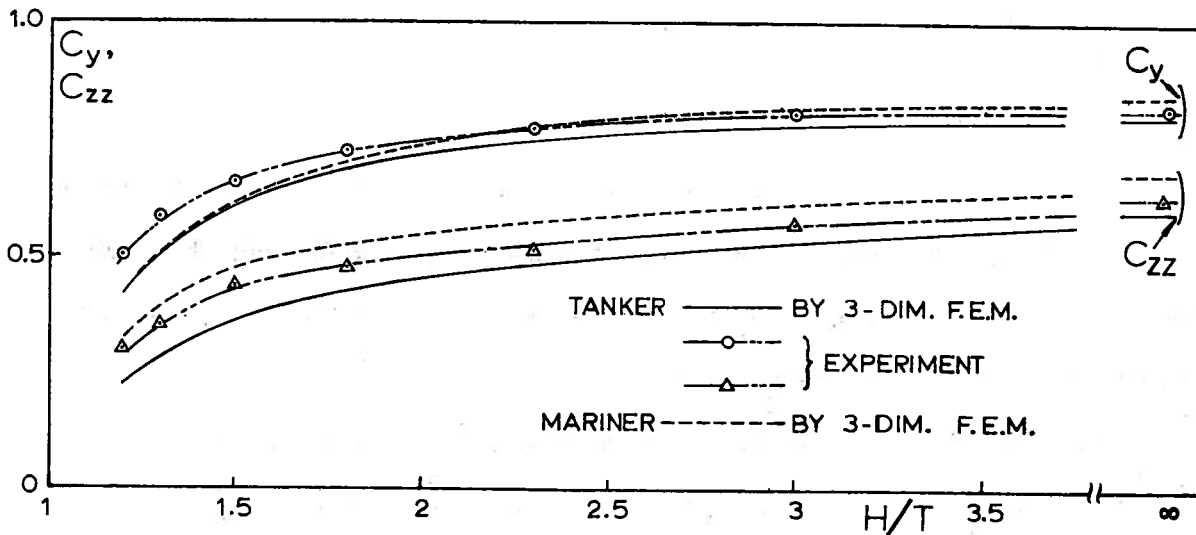
Figure 17. Three-dimensional correction factors, C_y and C_{zz}, of the sway added mass and the yaw added mass moment of inertia. [43]. (Remarks in this figure designate how the three-dimensional added mass and added mass moment of inertia were obtained).
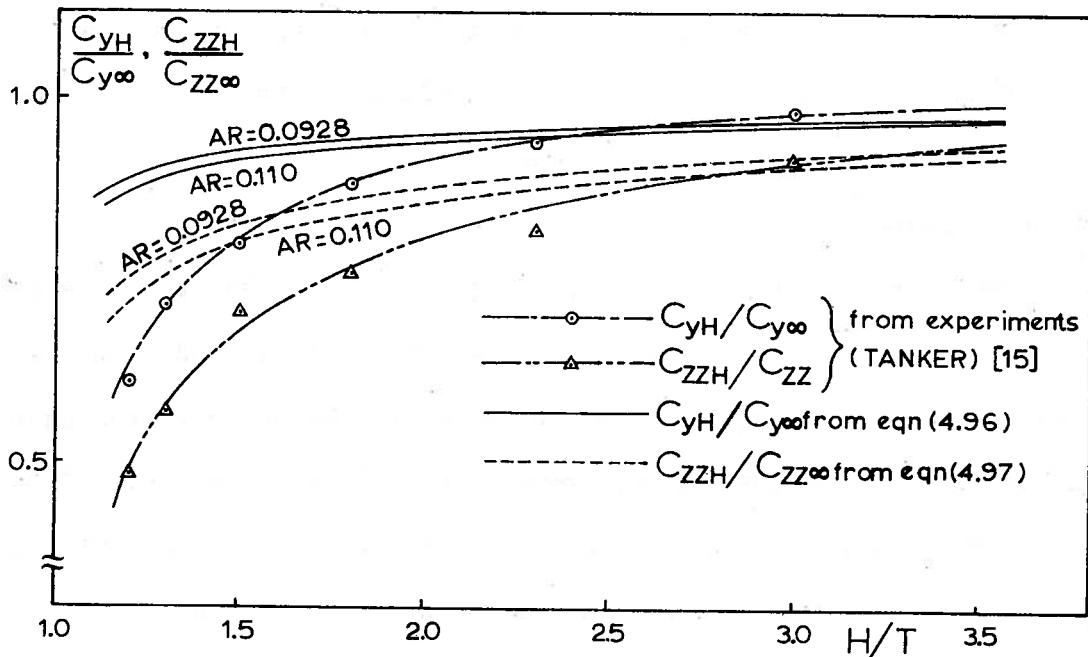

Figure 18. $C_{yH}/C_{y\infty}$ and $C_{zzH}/C_{zz\infty}$ versus water depth.

4.2. *Damping Derivatives*

Four linear derivatives, namely, Y_β, N_β, Y_r, and N_r, are the linear coefficients of the damping force and the damping moment, and they are important aids in judging the course stability of a ship, not only in deep water but also in shallow water.

Inoue and Murayama applied Kármán-Bollay's low aspect-ratio wing theory to evaluate the shallow water effect on the linear damping derivatives of a rectangular flat plate [44]. In their analysis, the free surface is considered a rigid wall, so that the rectangular plate with draft T is exchanged for a rectangular plate fully immersed in the fluid and equal to 2T in span-length. Further, the effect of the bottom of the waterway is represented by taking infinite images of the plate with span 2T with respect to the bottom. This substitution is the same as that used to analyze the shallow water effect on the sway added mass of the flat plate.

Following Bollay's assumption [45], they assumed that the strength of the bound vortex $\gamma(x)$ is constant across the span 2T, and that the downwash is constant along the span and equal to the value at the center of the span. Furthermore, it was assumed that the angle at which each bound vortex leaves the edge of the span, i.e., the edge of the plate, is equal to half of the geometrical attack angle of the plate.

With these assumptions, they derived an integral equation from Biot-Savart's law, which determined the vortex strength $\gamma(x)$:

$$U \sin \beta + \frac{L}{2} rx = \frac{A}{4\pi} \int_{-1}^{1} \frac{\gamma(\xi)}{x-\xi} K(x, \xi) d\xi \qquad , \qquad (4.98)$$

where U, L, and A are the advance speed, the length, and the aspect ratio of the rectangular plate respectively. It must be noted that the longitudinal coordinate x(or ξ) is a dimensionless coordinate introduced by dividing the longitudinal distance by the half-length of the plate. The detailed description of the kernel function $K(x,\xi)$ is omitted, as well as the method for solving the integral equation (4.98).

Once the vortex strength $\gamma(\xi)$ is determined, the lateral or sway force Y and the turning or yaw moment about the mid-section are calculated as follows:

$$Y = \rho TL \int_{-1}^{1} U \cos \beta \ \gamma(\xi) d\xi \qquad (4.99)$$

$$N = \rho TL^2 \int_{-1}^{1} U \cos \beta \ \gamma(\xi) \xi d\xi \qquad (4.100)$$

According to this method, the shallow water effect on the linear derivatives Y_β, N_β, Y_r, and N_r of rectangular flat plates was investigated for various aspect ratios. Some numerical results are shown in Figure 19, where the ordinate stands for the ratio of the derivative at a finite water depth H to that in infinite fluid. For the sake of comparison, the experimental data are also plotted.
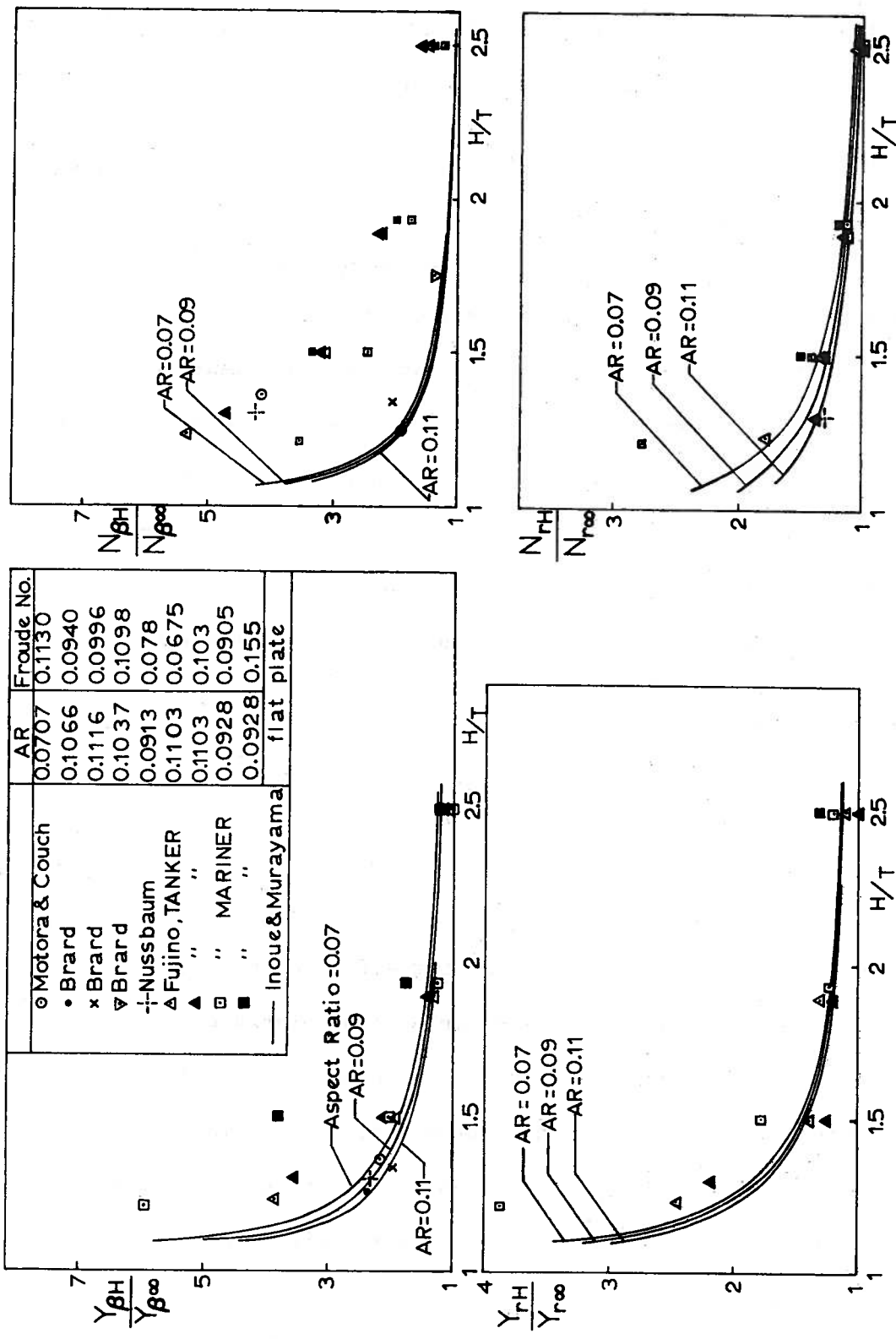
Figure 19. Shallow water effect on the linear damping derivatives (the aspect ratio is defined by 2T/L).

The shallow water effects predicted by the low aspect-ratio wing theory mentioned above agree relatively well with the experimental results except for the derivative N_β. The theory notably underestimates the shallow water effect on the derivative N_β.

As has been pointed out by some persons (see, for example, [46]), the hydrodynamic moment acting on a slender non-lifting body that translates in a direction inclined to the longitudinal axis can be evaluated quantitatively by the hydrodynamic instability moment which is related to the discrepancy between the transverse added mass and the longitudinal added mass of the body.**

This fact indicates that the great portion of the hydrodynamic turning moment acting on a ship translating obliquely is due to the instability moment or Munk moment rather than to the vortex contribution. Actually, the experimental curve of the $N_{\beta H}/N_{\beta\infty}$ ratio shown in Figure 19 is closer to the experimental curve of the $m_{yH}/m_{y\infty}$ ratio shown in Figure 16 than to the theoretical values of the $N_{\beta H}/N_{\beta\infty}$ ratio obtained by the low aspect-ratio wing theory. Inoue and Murayama's theory doesn't,however, include the moment corresponding to the hydrodynamic instability moment. This is the main reason why the low aspect-ratio wing theory cannot predict the shallow water effect on

_____

**Based on this fact, Inoue derived a formula by which the hydrodynamic turning moment acting on a ship translating obliquely in infinite fluid can be approximately predicted [47].

the derivative N_β.**

Kan and Hanaoka showed that the shallow water effects on the lateral or sway force and the turning or yaw moment acting on a flat plate traveling obliquely in a straight line or turning at a small yaw-rate can be expressed by the coefficient k_F defined by equation (4.92) [40]. Of course, it is impossible to explain the relatively large shallow water effect on the derivative N_β.

The shallow water experiments referred to in part 3 revealed that an oil-tanker was unstable on course in a certain range of shallow water, and that this instability was mainly due to the convex character of the N_β/Y_β curve versus the water depth.

This convex character cannot be explained by any existing theory: Kan and Hanaoka's theory, Inoue and Murayama's theory, or Newmans's theory.*** According to Kan and Hanaoka's theory, the N_β/Y_β ratio is always constant and independent of water depth. This inconsistent conclusion is deduced by Newman's theory as well, in cases where the aspect ratio is assumed to be zero. Furthermore, both Inoue and Murayama's theory and Newman's theory for a finite aspect ratio say that the $N_{\beta H}/N_{\beta\infty}$ ratio diminishes monotonically as the water depth decreases.

**Newman also gave the same explanation with respect to the discrepancy between his theoretical prediction of the turning moment acting on a ship translating obliquely in shallow water and the experimental value of the moment [42].

***However, one must remember that Newman pointed out the importance of taking account of the hydrodynamic instability moment or Munk moment.

As stated before, the derivative N_β consists of two parts: one due to the bound vortex on the ship's hull and the other due to the hydrodynamic instability moment. In general, the latter part is significantly greater than the former. Therefore, it is not surprising that the low aspect-ratio wing theory fails to explain properly the convex character of the ratio N_β/Y_β. The experimental results indicate that the quantitative nature of the increase of the derivative N_β due to the finiteness of the water depth is very close to that of the sway added mass.

In relatively shallow water, the shallow water effect on the sway added mass is greater than that on the lateral or sway force, while in extremely shallow water, the latter is bigger than the former. Consequently, if the hydrodynamic instability moment were taken into consideration, the convex character of the N_β/Y_β ratio could be explained.

Inoue and Kijima extended Inoue and Murayama's method in order to estimate the finite-width effects on the stability derivatives Y_β and N_β. In addition to the images of a rectangular flat plate with respect to the bottom of a canal, the images with respect to the side walls of the canal were taken into consideration. In their paper [48], the finite-width effect is expressed in terms of the ratios $Y_{\beta WH}/Y_{\beta \infty H}$ and $N_{\beta WH}/N_{\beta \infty H}$ which stand for the ratios of the derivatives Y_β and N_β obtained at a finite water depth H and at a finite canal width W to those obtained in shallow water with depth H but without lateral

restriction of the water surface. Some of their results are shown in Figure 20, where the experimental results obtained by Eda [19] are plotted for the purpose of comparison.** Obviously, from this figure, the theoretical and experimental values do not agree well.

4.3. *Asymmetrical Hydrodynamic Force and Bank Suction*

Newman derived a formula from which the asymmetrical hydrodynamic force can be calculated for an arbitrary three-dimensional slender body, improving his two-dimensional theory [49]. Starting with the fact that in an unbounded fluid, the velocity potential function to describe the fluid motion around a body of revolution traveling in a straight line can be represented by an axial source-distribution as follows:

$$\phi(x,\ y,\ z) = \frac{U}{4\pi} \int_{-\frac{L}{2}}^{\frac{L}{2}} \frac{dS(\xi)}{d\xi} \left[(x-\xi)^2 + y^2 + z^2 \right]^{-(1/2)} d\xi \ , \qquad (4.101)$$

where $S(\xi)$ stands for the sectional area of the body at $x=\xi$; he obtained the following expression of the asymmetrical hydrodynamic force by taking account of two kinds of images of the body: those with respect to the side walls and those with respect to the bottom of the waterway [35]:

**Eda did not do any experiments in shallow water. Hence, the circular points denoting Eda's experiments are obtained by considering the derivatives in a canal with W/L equal to 9.88 as equal to those in an infinitely wide canal.
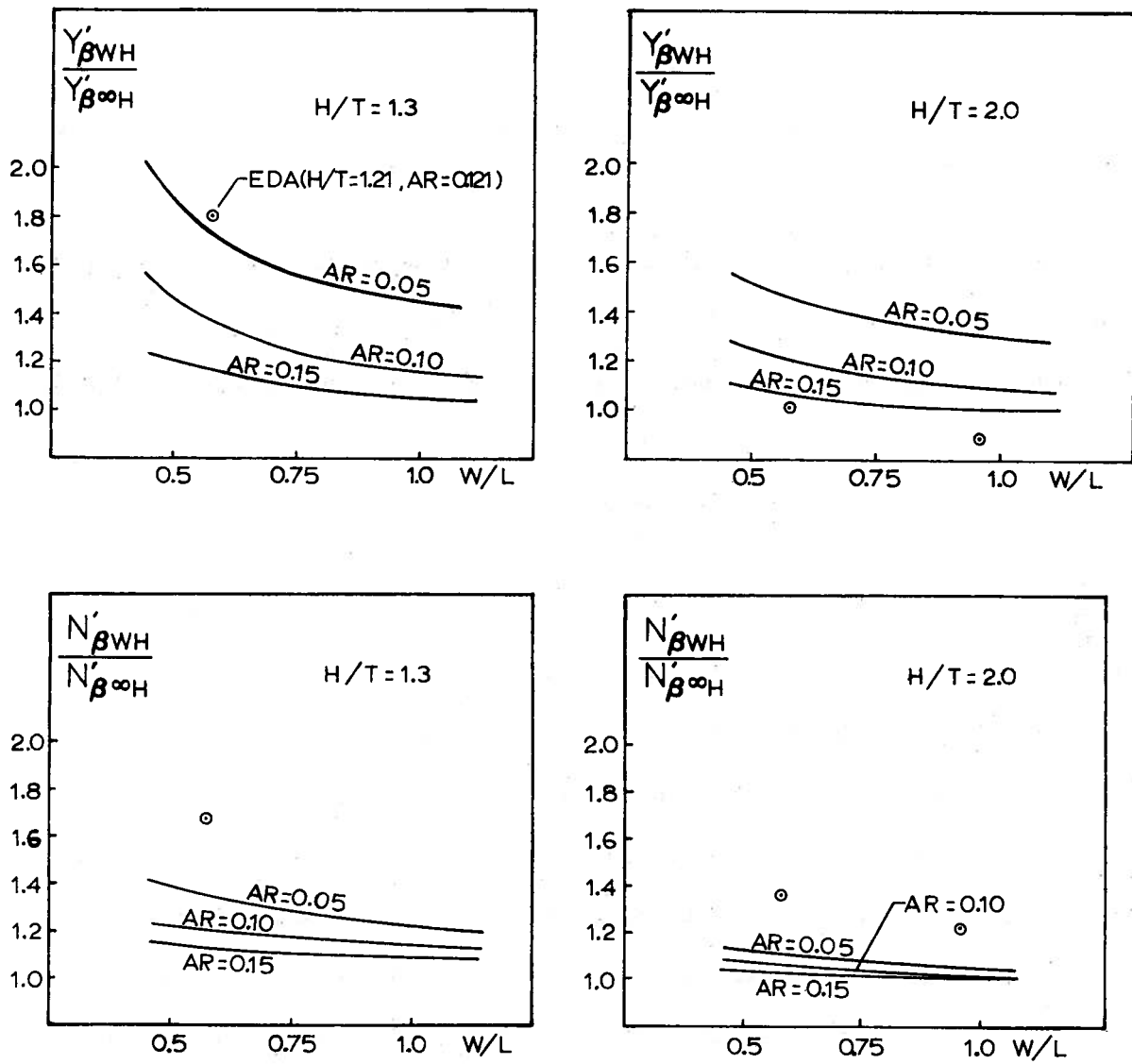
Figure 20. Finite-width effects on the derivatives Y_β and N_β [48].

$$Y = \rho \ \frac{U^2}{4\pi} \int_{-\frac{L}{2}}^{\frac{L}{2}} S'(x) \ dx \int_{-\frac{L}{2}}^{\frac{L}{2}} S'(\xi) \ K(x-\xi) \ d\xi \qquad . \qquad (4.102)$$

The kernel function $K(x-\xi)$ in the above formula is given for some simple configurations of the moving body and the canal. For instance, the kernel function for a rectangular canal with width and depth W and H is

$$K(x-\xi) = -\sum_{m=-\infty}^{\infty} \sum_{\substack{n=-\infty \\ n:odd}}^{\infty} \frac{2\eta + nW}{[(x-\xi)^2 + (2\eta+nW)^2 + 4m^2H^2]^{3/2}} \qquad , \qquad (4.103)$$

where η stands for the distance from the center of the moving body to the centerline of the canal.

He showed some numerical examples of asymmetrical hydrodynamic force and bank suction for a spheroid. As a result, it is clear that the symmetrical hydrodynamic force increases monotonically as the body is increasingly far away from the centerline of a canal. When a body moves parallel to a single wall, the bank suction acting on the body is inversely proportional to the distance from the wall (see Figure 21).

On the other hand, Norrbin tried to calculate the asymmetrical hydrodynamic force by means of a purely numerical calculation of three-dimensional fluid motion around a ship traveling in the vicinity of a single wall [20]. Following Hess and Smith [38], he represented the moving body with a surface distribution of sources so that the normal velocity at some discrete points on the body surface might vanish.

Then the bank suction was obtained by integrating the hydrodynamic pressure due to the perturbation velocity over the hull surface.

In Figure 22 is shown only one example of the calculated bank suction, which agrees very well with the experimental data. This illustration is obtained for a single vertical wall located at the port side of a tanker-type ship. With $^{H}/L = 0.203$ and $^{n}P/B=1.0$, the calculated value of the dimensionless bank suction force Y' is -0.003158, while the experimental value is -0.002933. It should be pointed out, however, that the pressure distribution is discontinuous at the stern; that is, the Kutta condition is not satisfied.**

Tuck and Newman dealt with the hydrodynamic interaction problem between two ships in very shallow water [50]. They extended the classical thin wing theory to solve the problem, since the flow around the body in very shallow water seems to be two-dimensional in a horizontal plane parallel to the bottom of the waterway. In their analysis, the flow field around the ships is represented by a source distribution to express the thickness effect of the bodies and by a vortex distribution to express the interaction of the bodies with the induced lateral flow. Furthermore, in order to obtain a unique solution of the integral equation denoting the vortex strength, the Kutta condition is imposed at the sterns of both ships. This is an important difference in their analysis compared with Norrbin's analysis.

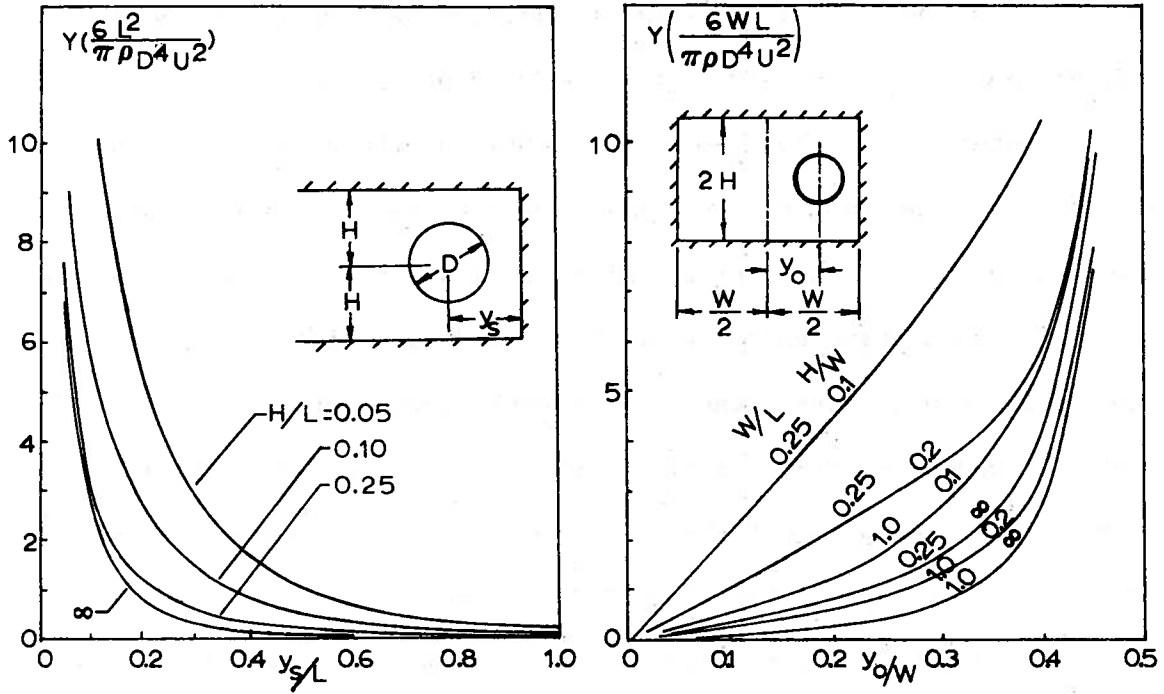**See Figure 15 in the original paper [20].

Figure 21. Asymmetrical force and bank suction for a spheroid [35].
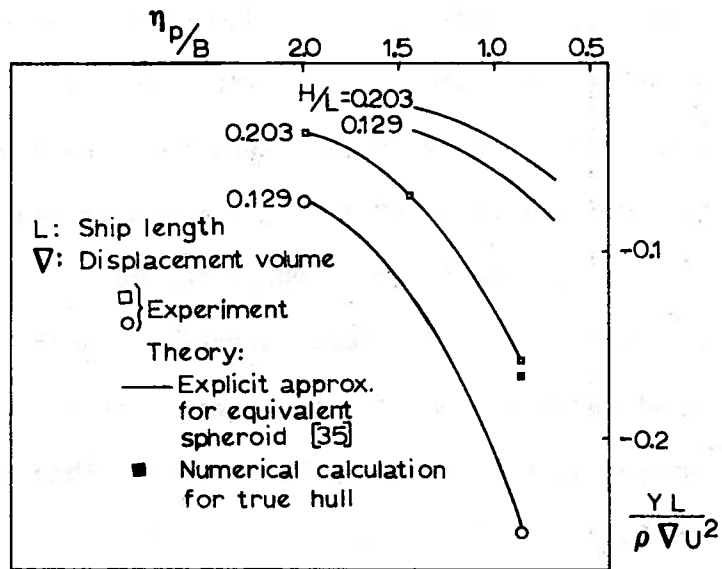(L: body length)

Figure 22. Bank suction: comparison of numerical calculation and
experimental results [20].

They compared their numerical results with those obtained by
Collatz, who did not take account of the circulation around the hulls,
or, what amounts to the same thing, did not impose the Kutta condition
at the sterns. As a result of the comparison, it was shown that imposing
the Kutta condition improved the theoretical estimate of the
hydrodynamic interaction force, but did not improve the prediction of
the interactive turning moment very much (see Figure 23). In
particular, in case of zero-stagger which is equivalent to the sit-
uation where a single ship moves in proximity to a vertical wall and
parallel to it, neither the Tuck/Newman theory nor the Collatz theory
gives a turning moment. This conclusion disagrees with the actual
situation that any ship experiences a bow-out turning moment from the
bank.

Recently, Beck tried to calculate the asymmetrical hydrodynamic
force acting on a slender ship traveling with a constant velocity
parallel to the centerline of a rectangular canal by adopting the
method of matched asymptotic expansions [51]. The basic assumption in
his analysis is that the canal depth is of the same order as the ship's
draft and the ship is far enough from the both canal walls. Under this
assumption, the flow field is represented by source and vortex
distributions along the ship's length, the strengths determined by
matching the outer solution with the inner solution and imposing the
Kutta condition at the stern. The lateral force and the turning moment
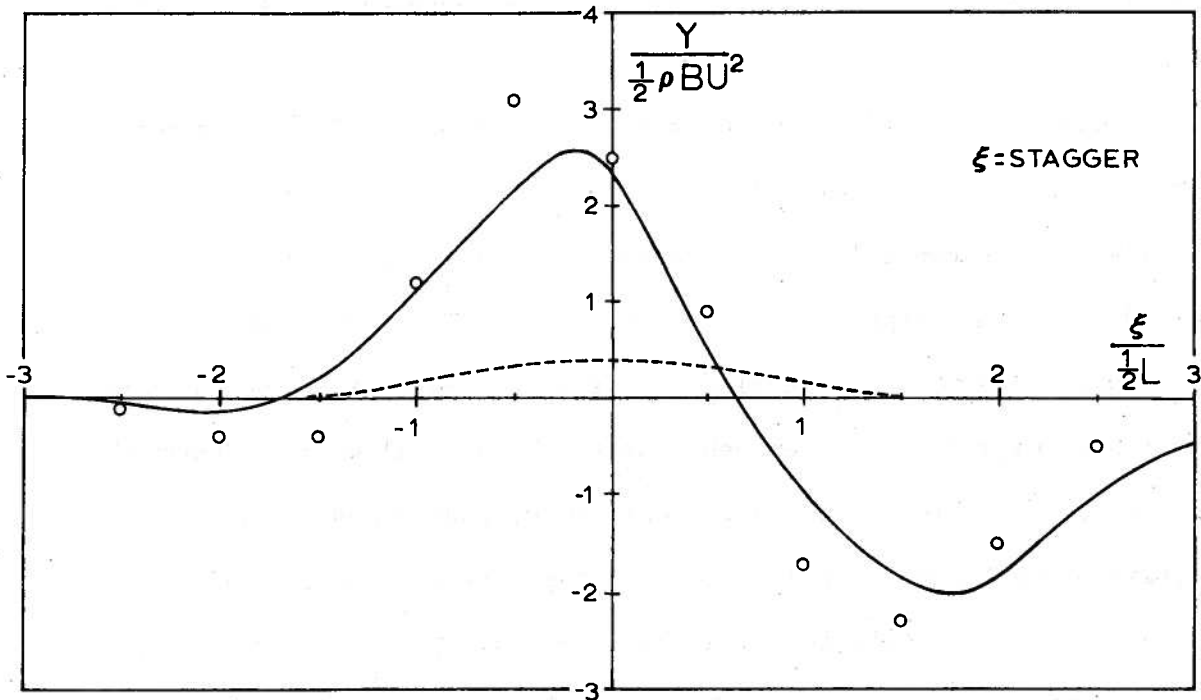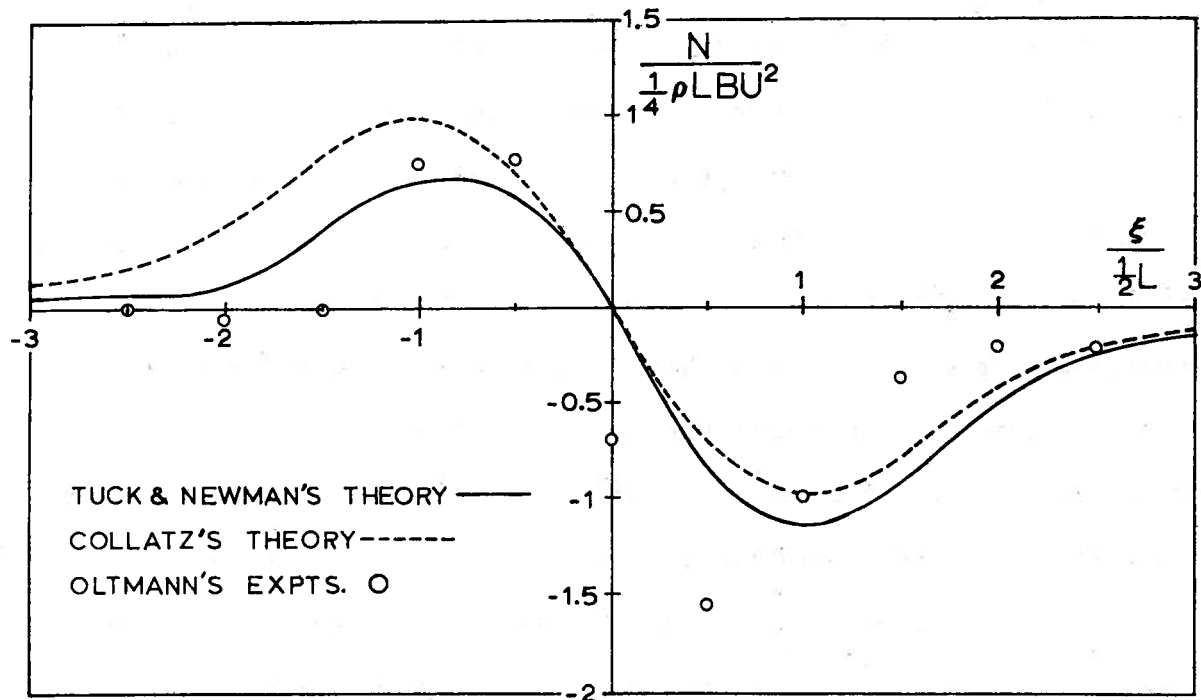acting on the ship are obtained by integrating the hydrodynamic pressure

Figure 23. Hydrodynamic interaction force and moment acting on each of two identical two-dimensional bodies in steady motion, at a separation distance of 0.3125L [50].

over the whole surface of the ship's hull. Numerical calculations show that his method can give good qualitative predictions of both lateral force and turning moment, but that it needs improvement in order to give good quantitative predictions.

Besides the restricted water effects on the stability derivatives which have already been discussed, we have to consider the restricted water effect on the rudder effectiveness, because the rudder is the sole control device in most ships. The effectiveness of a rudder placed at the stern is affected by not only the characteristic of the rudder itself but also by other factors: wake behind the ship, slip stream behind the screw, ship's motion, interaction between the rudder and the hull at the stern, and so on. It is difficult to evaluate properly the restricted water effect on the rudder effectiveness unless the restricted water effect on each of these factors is first understood.

The flow around a ship's hull in shallow water is more two-dimensional or confined to the horizontal planes than that in deep water. The curvature of the flow becomes greater so that the flow around the stern in shallow water tends to separate. Accordingly, there occurs the "dead-water" region at the stern, diminishing the effectiveness of the rudder.

On the other hand, a conspicuous increase in the total resistance due to the restriction of the waterway reduces the ship's speed, so that the slip stream behind the screw gets stronger. The increase of the screw's slip brings an increase of the effectiveness of a rudder behind

the screw, which, roughly speaking, compensates for or exceeds the decrease due to the wake. This reasoning is verified by some model experiments [15, 19], except that the effect of the slip stream behind the screw is exaggerated in the model experiment, compared with that of the full-size ship.

The shallow water effect on a detached rudder, meaning that only the rudder is placed in the water, is estimated by Kan and Hanaoka [40], who applied Kármán and Burgers' method to estimate the side-wall effect on the lift of a wing measured in the wind tunnel [52], for the purpose of estimating the bottom effect on the rudder effectiveness. In Figure 16 is plotted the ratio of the rudder force at a finite water depth H to that in infinite water, obtained on the assumption that the aspect ratio of the rudder is equal to H and is denoted by k_δ. This illustration shows that the shallow water effect on the rudder force is remarkably small, compared with the shallow water effect on the other stability derivatives.

On the other hand, using a model with twin screws and a single rudder, Bottomley measured the initial turning moment of the rudder acting on a ship [53]. According to Bottomley's results, the restricted water effect on the rudder effectiveness proved to be quite changeable, depending on the rudder configuration behind the ship's stern: The unbalanced rudder, which means a large gap between the leading edge of the rudder and the stern-post, generates a larger initial turning moment than the balanced rudder does, in which the leading edge is

located just behind the stern-post. The initial turning moment of the unbalanced rudder in a canal was about twice as large as that in deep water, while the initial turning moment of the balanced rudder in a canal was about 1.5 times as large as that in deep water. Comparing these results with other experimental results [15, 19], the restricted water effect on the rudder effectiveness obtained by Bottomley seems to be too large.

At any rate, as stated a few paragraphs ago, the rudder effectiveness is strongly dependent on many factors not related to the characteristics of the naked rudder. In order to clarify the restricted water effect on the rudder effectiveness, the restricted water effects on those factors must be investigated.

5. *SIMPLIFIED NONLINEAR MATHEMATICAL MODELS TO DESCRIBE MANEUVERING MOTION*

In order to discuss the course stability of a ship in restricted waters, we derived the linear maneuvering equations of motion in part 2 on the assumption that the perturbations from a straight motion with a constant speed are small. This assumption brought a great advantage: it is sufficient to consider the sway and yaw motions because the longitudinal motion or the surge motion doesn't couple with the sway and yaw motions.

The usefulness of the linear equations is, however, limited to the course-keeping maneuver; in other cases, the linear predictions are inaccurate. In particular, in the case of an unstable ship, the linear prediction is unworkable because the response of an unstable ship to any small disturbance diverges to infinity unless the motion is controlled by adequately deflecting a control surface. Therefore, nonlinear maneuvering equations of motion are essential for predicting any kind of maneuvering response for an unstable ship. Furthermore, even in cases of stable ships, the accuracy of the linear prediction accompanied by a significant perturbation is very poor. One of the important defects of the linear prediction, i.e., equations (2.8) to (2.10), is that the decrease of the longitudinal velocity due to the sway and yaw motions cannot be predicted by the linear maneuvering equations of motion. Hence, in this chapter, we shall discuss some

nonlinear mathematical models, without confining our consideration to the maneuvering motion in restricted waters. The purpose of the following investigation, however, is not to examine the nonlinear response but to discuss the feasibility of some different nonlinear mathematical models.

One of the methods used to construct nonlinear models is to expand the hydrodynamic force and moment functions, i.e., $X(u, v, r, \delta, \dot{u}, \dot{v}, \dot{r}, \dot{\delta}, \eta, \psi)$, $Y(u, v, \ldots, \psi)$ and $N(u, v, \ldots, \psi)$ of the equation (2.2) with the variables $u, v, \ldots, \eta,$ and ψ. When we derived the linear equations of motion (2.8) to (2.10), we retained only the linear terms. But now we shall retain some nonlinear terms as well.

One way to introduce the nonlinear terms is to use Taylor's expansion in terms of the variables. For instance, when we expand the hydrodynamic sway force in terms of the variable v only, the expansion is described as follows:

$$Y = Y_0 + Y_v v + Y_{vv} v^2 + Y_{vvv} v^3 + \ldots \ldots \qquad . \qquad (5.1)^{**}$$

On the other hand, considering the hydrodynamic point of view that the main nonlinear characteristic of the hydrodynamic force is dependent on the squared velocity, another type of nonlinear term is used frequently:

$$Y = Y_0 + Y_v v + Y_{vv} v^2 \frac{|v|}{v} + \cdots = Y_0 + Y_v v + Y_{v|v|} v|v| + \ldots \qquad . \qquad (5.2)$$

**Of course, the final expansion of the right-hand side functions of equation (2.1), namely X, Y, and N, includes not only nonlinear terms of a single variable but also such coupled nonlinear terms as $v^2 r$, vr^2 and so on.

Among the nonlinear models belonging to the first category, i.e., Taylor's expansion, there exist some different models which are proposed by Eda and Crane [54], Strøm-Tejsen and Chislett [55], Ogawa [56], Eda [19], and so on, while Inoue [57], Norrbin [23] etc., use models of the second category, i.e., the nonlinear models of the type (5.2). The usefulness of those nonlinear models has been investigated in enough detail and has been recognized.

Consequently, in cases where we want an accurate prediction of the maneuvering motion, which is required by the simulators used to train ship's operators, nonlinear mathematical models with a lot of nonlinear terms should be built up so as to give predictions as accurately as possible. However, one of the main drawbacks of those models is that they have too many unknown coefficients to be determined. Incidentally, the system-identification technique mentioned in part 3 in principle is available for determining the unknown derivatives included in the nonlinear mathematical model, but is not very reliable at present. Accordingly, we can only rely on the captive model tests in order to determine such unknowns, if we want accurate derivatives.

We often need to grasp quickly the maneuverability of a ship already on a voyage. A ship has a variable maneuverability according to its loading condition, i.e., the draft, the trim, etc., but it seems impractical to examine beforehand the maneuverability of every ship, to obtain in advance the stability derivatives of every ship in all possible cases of its loading condition by means of the captive model test.

Unfortunately, the amount of information on the maneuvering motion that we can obtain from a real ship is not great. The instantaneous values of ship's speed, rudder angle, directional angle, and yaw angular velocity are all that we can get unless special instruments are installed in the ship.

Therefore, if we want to assess the maneuverability of a ship from the limited amount and the limited kinds of information on the maneuvering motion, we must use a simplified mathematical model, instead of a detailed one. If an adequate, simplified model were used properly, the prediction obtained would be useful enough. From this point of view, we shall introduce some simplified nonlinear models and describe the practical methods to determine the unknown coefficients included in those models.

Model 1: The so-called first-order maneuvering equation of motion which was proposed by Nomoto [58] has been used to describe the relationship of the rudder angle versus turning rate.

$$T \frac{dr}{dt} + r = K\delta \tag{5.3}$$

The unknown coefficients, namely T and K, are determined by analyzing Kempf's zigzag maneuver. The index T represents the extent of the course stability of a ship or the quickness of ship's response, and the index K represents the extent of the turning ability.

The origin of this model is equation (2.45); on the assumption that the maneuvering motion depends on the response-characteristic in the low frequency range, the first-order equation (5.3) was derived

from the second-order equation (2.45), in which the index T was defined as $T_1+T_2-T_3$.

Subsequent investigation has unfortunately revealed that this first-order model will not always satisfactorily describe even a small-perturbation motion such as Kempf's zigzag maneuver; that, indeed, the indices T and K of this model are dependent on the kind of zigzag maneuver: a different zigzag maneuver produces a different set of T and K values. This is a fatal defect, but, as if this weren't enough, the model (5.3) proved unable to describe adequately the yaw motion of either a less stable or an unstable ship, partly because it is a first-order equation and partly because it lacks the nonlinearity essential for prediction of the motion of an unstable ship.

Therefore, instead of the first-order linear model, some second-order models with nonlinear terms are proposed, but the validity of these new models is still being examined. For example, these nonlinear models are proposed as substitutes for the model (5.3) [59,60]:

$$T_1T_2 \, \dddot{\psi} + (T_1+T_2)\ddot{\psi} + \dot{\psi} + \alpha\dot{\psi}^3 \quad = K\delta + KT_3\dot{\delta} \tag{5.4}$$

$$T_1T_2 \, \dddot{\psi} + (T_1+T_2)\ddot{\psi} + H(\dot{\psi}) \quad = K\delta + KT_3\dot{\delta} \tag{5.5}$$

Comparing these models with the second-order equation (2.45), it is clear that these new models are constructed by replacing the linear stationary turning characteristic $\dot{\psi} = K\delta$ with the nonlinear stationary turning characteristics $K\delta = \dot{\psi} + \alpha\dot{\psi}^3$ or $K\delta = H(\dot{\psi})$. Then, we shall consider how the unknown coefficients and function T_1, T_2, T_3, α, K, and $H(\dot{\psi})$ can be determined from the free-sailing trials of a ship.

One of the practical methods is the phase-plane analysis of the zigzag maneuver, which was proposed by Bech and Smitt [61]. The outline of the phase-plane analysis proposed by them is as follows: To begin with, the stationary turning characteristic $\delta = (\dot{\psi} + \alpha \dot{\psi}^3)/K$ or $\delta = H(\dot{\psi})/K$ is assumed to be known from the spiral or the reversed spiral tests. Then the trajectory of the zigzag maneuver is plotted on the $\dot{\psi}$ versus $\ddot{\psi}$ phase-plane (see Figure 24).** From this trajectory, we know the value of $\dddot{\psi}$ at a certain instant $t = t_i$ as follows:

$$\dddot{\psi}(t_i) = \left[\ddot{\psi} \frac{\partial \dot{\psi}}{\partial \ddot{\psi}} \right]_{t=t_i} \tag{5.6}$$

On the other hand, we already know the values of $\dot{\psi}(t_i)$, $\ddot{\psi}(t_i)$, $\delta(t_i)$, and $\dot{\delta}(t_i)$ from the time-histories of the rudder angle and the yaw rate. Therefore, we can consider equation (5.4) or (5.5) as an algebraic equation with respect to the unknowns T_1, T_2, and T_3. If we have enough equations like (5.4) or (5.5) to determine the unknowns, three equations at least, we can determine T_1, T_2, and T_3.

The most important defect of this method is inaccuracy of the derivative $\dddot{\psi}$. It is impossible to obtain an accurate value of the time-derivative $\dddot{\psi}$ from equation (5.6), because the yaw acceleration $\ddot{\psi}$ obtained through the numerical differentiation of the yaw rate $\dot{\psi}$ is badly blemished by even small-amplitude noise involved in the measured values of the yaw rate $\dot{\psi}$.

**The instrument used to pick up the ship's yaw rate is the rate gyroscope, but the instrument used to record the yaw acceleration directly is not so well-known, so the yaw acceleration is usually obtained from numerical differentiation of the yaw rate.
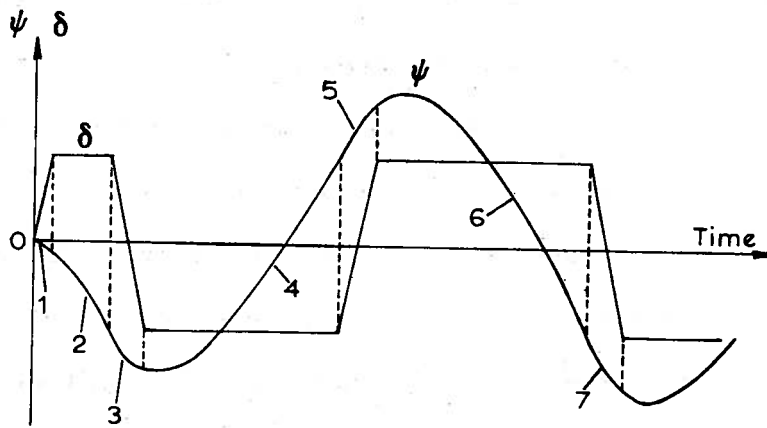
(a) Typical time-history of zig-zag maneuver
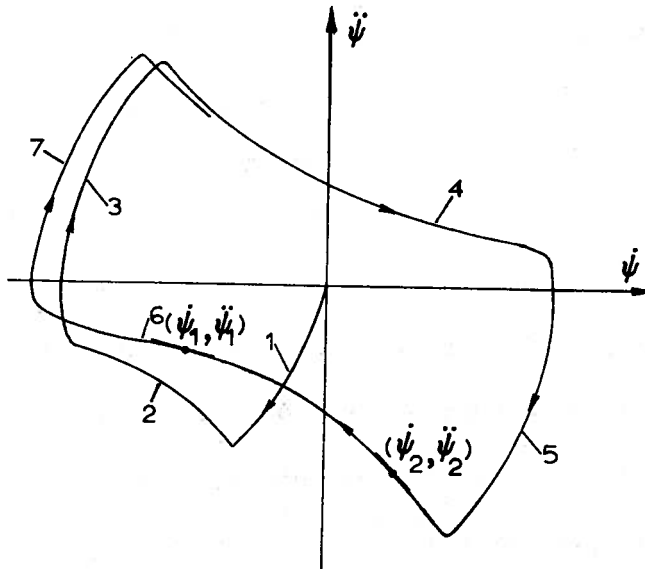
(b) Phase-plane trajectory on $\dot{\psi} \sim \ddot{\psi}$ plane

Figure 24.   Outline of the principle of phase-plane analysis.

If we make use of the trajectory drawn on the phase-plane, it is expected that we can determine the unknowns T_1, T_2, and T_3 more accurately. From this point of view, some attempts have been made. One idea is to use the limit cycle of the trajectory drawn on the phase-plane. In the case of a stable ship, the trajectory of the zigzag maneuver always converges to a limit cycle; even for an unstable ship, it is possible to make the trajectory converge to a limit cycle if we conduct adequate modified zigzag maneuvers [62]. As for methods to determine the unknowns T_1, T_2, and T_3 using the limit cycle, two have been tried so far. One of them is to use the areas enclosed by the limit cycles drawn on the various phase-planes [63, 64].

Let both sides of equation (5.5) be multiplied by a variable $\dot{\psi}$, and then let them be integrated with respect to time over the interval (t_0, t_1), where the two instants t_0 and t_1 correspond to a single point on the limit cycle and the difference, namely t_1-t_0, is equal to the time interval necessary to go completely around the limit cycle. In other words, the following relationships hold good for the two instants t_0 and t_1; $\psi(t_0)=\psi(t_1)$, $\dot{\psi}(t_0)=\dot{\psi}(t_1)$, $\ddot{\psi}(t_0)=\ddot{\psi}(t_1)$, etc.

As a consequence of integration, we obtain

$$\frac{T_1 T_2}{K} \oint \dot{\psi} d\dddot{\psi} + \frac{T_1+T_2}{K} \oint \dot{\psi} d\ddot{\psi} + \oint \frac{H(\dot{\psi})}{K} d\psi = \oint \delta d\psi + T_3 \oint \dot{\psi} d\delta \qquad (5.7)$$

The first integral of the left-hand side is

$$\oint \dot{\psi} d\ddot{\psi} = -D_2 \qquad , \qquad (5.8)$$

where D_2 is the area enclosed by the limit cycle drawn on the $\dot{\psi}$-$\ddot{\psi}$

phase-plane. Similarly, the integrals $\oint \delta d\psi$ and $\oint \dot{\psi} d\delta$ are defined as the areas D_3 and D_4 of the limit cycles on the ψ-δ and $\dot{\psi}$-δ phase-plane respectively:

$$\oint \delta d\psi = D_3 \qquad\qquad (5.9)$$

$$\oint \dot{\psi} d\delta = -D_4 \quad , \qquad\qquad (5.10)$$

while the integral $\oint \dot{\psi} d\psi$ vanishes. Finally, let us consider the integral $\oint (H(\dot{\psi})/K) d\psi$; we assume that the stationary turning characteristic of a ship, $\delta = H(\dot{\psi})/K$, is known, and in order to calculate the integral, we have to know the trajectory of the limit cycle on the $H(\dot{\psi})/K$-versus-ψ phase-plane. For this purpose, we plot the stationary turning characteristic $\delta = H(\dot{\psi})/K$ on the ψ-$\dot{\psi}$ phase-plane. Then the desired trajectory ψ-$H(\dot{\psi})/K$ is obtained as follows (see Figure 25):

(a) First, let us draw a straight line through a certain point on the ψ-$\dot{\psi}$ limit cycle, for instance, point A, and parallel to the abscissa or ψ-axis, and let it intersect the $\dot{\psi}$-axis and $\delta = H(\dot{\psi})/K$ curve, which are denoted by B and C respectively.

(b) Next, let us draw another straight line through point A so that it crosses the ψ axis at a right angle, and let D denote this cross-point. Then, let us define point E on this perpendicular so that the distance $\overline{ED}$ may be equal to $\overline{BC}$. By drawing a curve through the points E obtained

successively in this manner, we get the desired

trajectory $\psi - H(\dot\psi)/K$.

In Figure 25(a), the $\psi - H(\dot\psi)/K$ trajectory obtained thus is shown

with a dotted line. Let D_5 denote the area of the limit cycle on the

$\psi - H(\dot\psi)/K$ phase-plane; that is to say,

$$\oint \frac{H(\dot\psi)}{K} d\psi = -D_5 \qquad . \qquad\qquad (5.11)$$

For an unstable ship also, the same procedure to get the $\psi - H(\dot\psi)/K$

trajectory is entirely applicable. It should be noted that the

movement on the limit cycle is in the counter-clockwise direction for

part of the limit cycle (Figure 25(b)) or on the whole limit cycle

(Figure 25(c)), while in the case of a stable ship, the travel on the

limit cycle is in the clockwise direction.

The area enclosed by a closed curve on which a point travels

counter-clockwise has to be reckoned as a negative value. For instance,

in case of Figure 25(b), the entire limit cycle consists of three parts

whose areas are denoted by D_5, D_5 and D_5 . In this case, equation

(5.11) must be replaced by equation (5.12).

$$\oint \frac{H(\dot\psi)}{K} d\psi = -D'_5 + D''_5 + D'''_5 \qquad . \qquad\qquad (5.12)$$

Summarizing, we obtain the following from equation (5.7):

$$-\frac{T_1 T_2}{K} D_2 + T_3 D_4 = D_3 + D_5$$

$$= D_3 + D'_5 - D''_5 - D'''_5 \qquad . \qquad\qquad (5.13)$$

(a) Stable ship

(b) Unstable ship (Case 1)

(c) Unstable ship (Case 2)
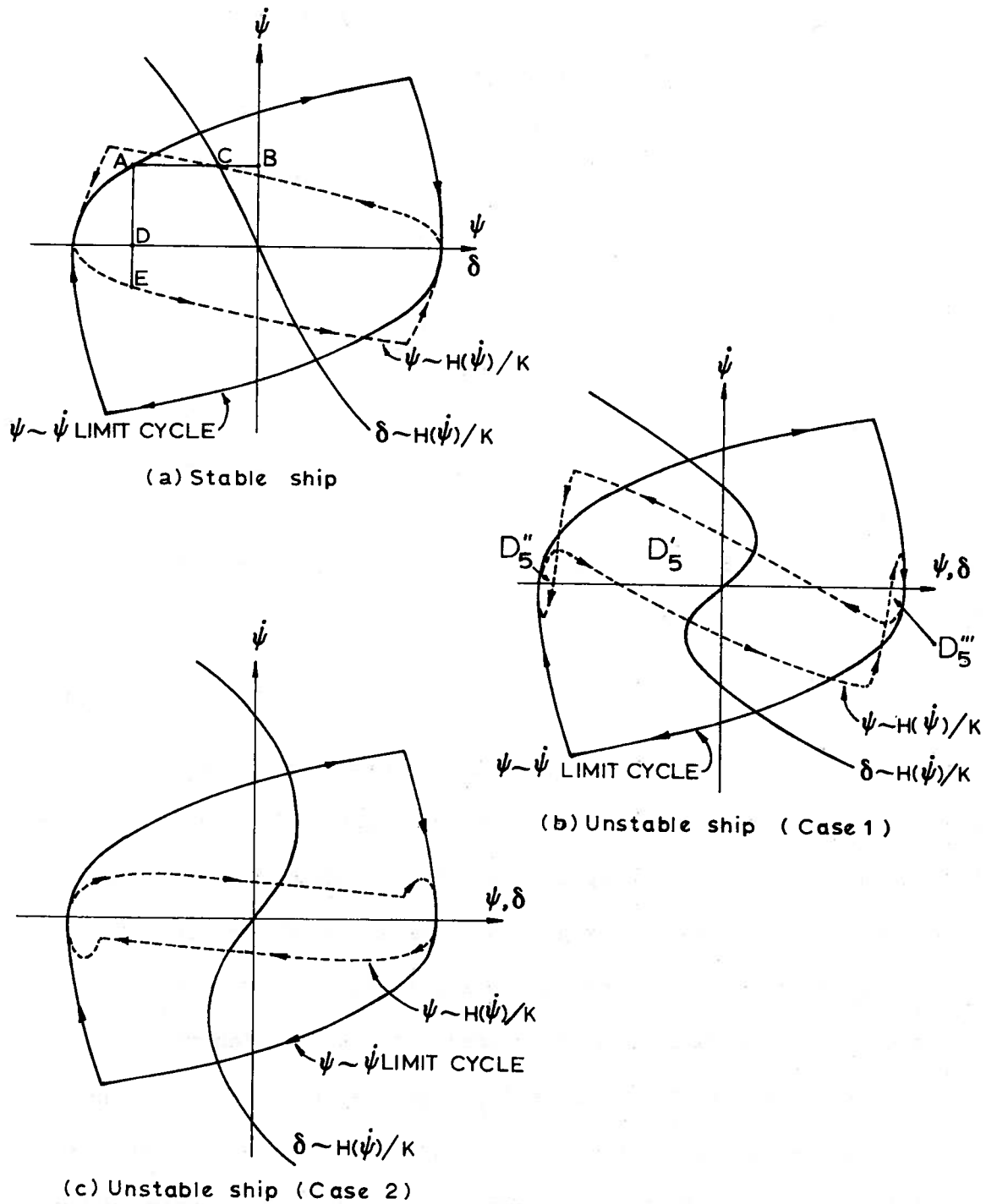
Figure 25.   Schematic method to obtain ψ~$H(\psi)$/K trajectory.

Then, let us multiply both sides of equation (5.5) by the variable and integrate over the time interval (t_0, t_1):

$$\frac{T_1 T_2}{K} \oint \ddot{\psi} d\ddot{\psi} + \frac{T_1 + T_2}{K} \oint \ddot{\psi} d\dot{\psi} + \oint \frac{H(\psi)}{K} d\dot{\psi} \quad \oint \delta d\dot{\psi} + T_3 \oint \dot{\delta} d\dot{\psi} \quad (5.14)$$

Because

$$\left. \begin{array}{rcl} \oint \ddot{\psi} d\ddot{\psi} &=& 0 \\[2ex] \oint \ddot{\psi} d\dot{\psi} &=& -\oint \dot{\psi} d\ddot{\psi} = D_2 \\[2ex] \oint \delta d\dot{\psi} &=& -\oint \dot{\psi} d\delta = D_4 \\[2ex] \oint \dot{\delta} d\dot{\psi} &=& D_6 \\[2ex] \oint \frac{H(\psi)}{K} d\dot{\psi} &=& 0 \quad , \end{array} \right\} \quad (5.15)$$

where D_6 denotes the area enclosed by the limit cycle on the $\delta - \dot{\psi}$ phase-plane, we obtain

$$\frac{T_1 + T_2}{K} D_2 - T_3 D_6 = D_4 \quad . \quad (5.16)$$

From equations (5.13) and (5.16), we can determine the unknowns $T_1 T_2 / K$, $(T_1 + T_2)/K$ and T_3, if we have equations enough to solve for the three unknowns. For this purpose, we have to execute at least two different zigzag or modified zigzag maneuvers. On the other hand, if we replace the integrals along the entire limit cycle with the integrals over an arbitrary time interval (t_0, t_1), which means that the conditions $\psi(t_0) = \psi(t_1)$, $\dot{\psi}(t_0) = \dot{\psi}(t_1)$, $\ddot{\psi}(t_0) = \ddot{\psi}(t_1)$, etc., are not always satisfied along arbitrary trajectories on the phase-planes, we need not execute different zigzag maneuvers in order to determine three unknowns [64].

There is another method used to determine the unknown indices T_1, T_2, and T_3 from the limit cycle drawn on the phase-plane [65]. The outline of this method is as follows: To begin with, the mathematical model described by equation (5.5) is constructed on the analog-simulator, where the unknown coefficients are set on the variable potentiometers. Then, the zigzag maneuvers that had been executed on a real-scale ship or on a model are repeated on the analog simulator. The variable potentiometers are adjusted so that the limit cycle drawn on the simulator best fits the limit cycle produced by the experiments. The final values of the potentiometers are the desired values of the unknown indices T_1, T_2, and T_3.

Model 2: The reasoning through which the nonlinear term was introduced into equations (5.4) and (5.5) wasn't really mathematically rigorous.

To remedy this, Clarke tried to derive a more reasonable nonlinear mathematical model analogous to equation (5.4) or (5.5). He assumed that the hydrodynamic force and moment acting on a ship were described as follows:

$$Y' = Y'_0 + Y'_v v' + Y'_{\dot{v}} \dot{v}' + Y'_r r' + Y'_{\dot{r}} \dot{r}' + Y'_\delta \delta' + Y'_{vv} v'^2 + Y'_{vr} v'r' + Y'_{rr} r'^2$$
$$+ Y'_{vvv} v'^3 + Y'_{vvr} v'^2 r' + Y'_{vrr} v'r'^2 + Y'_{rrr} r'^3 + Y'_{\delta\delta\delta} \delta'^3 \quad (5.17)$$

$$N' = N'_0 + N'_v v + N'_{\dot{v}} \dot{v}' + N'_r r' + N'_{\dot{r}} \dot{r}' + N'_\delta \delta' + N'_{vv} v'^2 + N'_{vr} v'r' + N'_{rr} r'^2$$
$$+ N'_{vvv} v'^3 + N'_{vvr} v'^2 r' + N'_{vrr} v'r'^2 + N'_{rrr} r'^3 + N'_{\delta\delta\delta} \delta'^3 \quad . \quad (5.18)$$

If one could eliminate the variable v from the latter two equations of (2.1), whose right-hand sides are replaced by equations (5.17) and

(5.18), the desired nonlinear yaw equation would appear immediately. But it is impossible to eliminate the variable v through formal manipulation only because of the presence of nonlinear terms.

In order to remove this difficulty, Clarke assumed that there existed a definite relationship between the instantaneous values of two dependent variables v and r. That the variables $v(t)$ and $r(t)$ are strongly connected to one another would be illustrated if we should plot a lot of pairs of the variables on the v-r phase-plane; most of the points would concentrate in a certain narrow region.

The relationship which Clarke assumed is as follows:

$$v' = \ell_0 + \ell_1 r' + \ell_2 r'^2 + \ell_3 r'^3 \qquad , \qquad (5.19)$$

where the coefficients ℓ_i are constants.

Eliminating the variable v on this assumption, we obtain the following nonlinear yaw equation:

$$A_0 \ddot{r}' + (A_1 + A_2 r' + A_3 r'^2) \dot{r}' + (A_4 + A_5 r' + A_6 r'^2) r'$$
$$+ (A_7 + A_8 \delta'^2) \dot{\delta}' + (A_9 + A_{10} \delta'^2) \delta' + A_{11} = 0 \qquad (5.20)$$

where the coefficients A_i are constants and can be expressed in terms of the hydrodynamic coefficients. Comparing this equation with equations (5.4) and (5.5), it is seen that the simplified models (5.4) and (5.5) are special cases of equation (5.20). Since there are twelve unknown coefficients A_i (i=0, 1, ..., 11) in the model (5.20), it seems to be necessary to reduce the number of unknown coefficients by introducing other reasonable assumptions, because it is difficult to determine so many unknowns from the results of either real-scale

maneuvering trials or free-sailing model tests.

Model 3: The above examples give the nonlinear yaw equations of motion only, but when the nonlinearity becomes important it will be necessary to take the change of longitudinal velocity of a ship due to its motion into consideration. If we want to predict the speed change accurately, we have to take account of all factors governing it. Here, out of several simplified models that take account of the speed variation macroscopically or in a simple way, we shall introduce a mathematical model proposed by van Leeuwen [67]. He pointed out that it was important to use dimensionless variables v' and r' that were defined by dividing the variables v and r by the instantaneous advance speed U. In order to describe the nonlinear stationary turning characteristic, he adopted the following equation which is analogous to that used in equation (5.4):

$$\alpha_0' + r' + \alpha_2' r'^2 + \alpha_3' r'^3 = K'\delta' , \tag{5.21}$$

where α_0', α_2', and α_3' are constants, but are different from those defined by equation (2.37). Then, a term $T' \dot{r}'$ is added to the left-hand side in order to take account of the transient motion. Therefore, the yaw equation is

$$T'\dot{r}' + r' + \alpha_0' + \alpha_2' r'^2 + \alpha_3' r'^3 = K'\delta' . \tag{5.22}$$

The unknown coefficients α_0', α_2', α_3', and K' of the equation (5.22) can be determined from spiral or reversed spiral tests, and the time constant T' can be determined by analyzing the transient response in the spiral tests.

As for the sway equation, a simple relationship analogous to equation (5.19) is proposed:

$$v' + \alpha_4'r' + \alpha_5'r'^3 = 0 \qquad (5.23)$$

The unknown constants α_4' and α_5' can be determined if we know the drifting velocity of the ship or model in the spiral tests. Assuming that the speed drop due to turning motion is proportional to the squared yaw rate, r'^2, van Leeuwen described the surge motion as follows:

$$T_u' \, \dot{u}' + u' = K_u' \, r'^2 \qquad , \qquad (5.24)$$

where u' stands for the perturbation of the surge velocity. The time-constant T_u' and the coefficient K_u' are determined by analyzing the time-history of the surge velocity recorded in the spiral tests.

Equations (5.22), (5.23), and (5.24) are the nonlinear models proposed by van Leeuwen, who verified the usefulness of his models in reference [67].

Here, it must be pointed out again that the validity of the above-stated simple mathematical models is very limited compared with the detailed mathematical models. Further, these models are applicable for describing the maneuvering motion in shallow water, but are not applicable in canals. In the latter case, some modifications or refinements will be necessary.

REFERENCES

1. Tuck, E.O.: "Shallow-Water Flows past Slender Bodies", <u>J. Fluid Mechanics</u>, Vol.26, part 1, 1966.

2. Davidson, K.S.M. and Schiff, L.I.: "Turning and Course Keeping Qualities of Ships", <u>Trans. S.N.A.M.E.</u>, Vol.52, 1946.

3. Motora, S.: "On the Course Stability of Ships", <u>Journal Society of Naval Architects, Japan</u>, Vol.77, 1955 (read in 1946).

4. Brard, B.: "A Vortex Theory for the Maneuvering Ship", <u>5th Symposium on Naval Hydrodynamics</u>, 1964.

5. Cummins, W.E.: "The Impulse Response Function and Ship Motions", D.T.M.B. Report No. 1661, 1962.

6. Fujino, M.: "The Effect of Frequency Dependence of the Stability Derivatives on Maneuvering Motion", (to be published).

7. Mandel, P.: "Ship Maneuvering and Control", Chapter VIII of <u>Principles of Naval Architecture,</u> S.N.A.M.E., 1967.

8. Kaplan, W.: <u>Operational Methods for Linear Systems</u> , Addison-Wesley, 1962.

9. Holbrook, J.G.: <u>Laplace Transforms for Electronic Engineers</u> , Pergamon Press, 1966.

10. Nonaka, K.: "Determination of Hydrodynamic Coefficients from a Free-Sailing Model Tests", <u>20th Seminar in Ship Research Institute</u>, 1970 (in Japanese).

11. Kaplan, P. and others: "The Application of System Identification to Dynamics of Naval Craft", <u>9th Symposium on Naval Hydrodynamics,</u> 1972.

12. Brard, R.: "Maneuvering of Ships in Deep Water, in Shallow Water, and in Canals", <u>Trans. S.N.A.M.E.</u>, Vol.59, 1951.

13. Motora, S. and Couch, R.B.: "Manoeuvrability of Full Bodied Ships in Restricted Waters", University of Michigan, 1961.

14. Nussbaum, M.: "Längskräften am Modell eines Grosstankers", <u>VBD Berichten</u> Nr. 396 I - II and 406, 1966 (or see [23]).

15. Fujino, M.: "Experimental Studies on Ship Manoeuvrability in Restricted Waters--Part I", <u>International Shipbuilding Progress,</u> Vol. 15, No. 168, 1968.

16. van Berlekom, W.B. and Goddard, T.A.: "Maneuvering of Large Tankers", <u>Trans. S.N.A.M.E.</u>, Vol.80, 1972.

References (continued)

17. Schoenherr, K.E.: "Data for Estimating Bank Suction Effects in Restricted Water on Merchant Ship Hulls", 1st Symposium on Ship Maneuverability, D.T.M.B. Report No. 1461, 1960.

18. Moody, C.G.: "The Handling of Ships through a Widened and Asymmetrically Deepened Section of Gaillard Cut in the Panama Canal", D.T.M.B. Report No. 1705, 1964.

19. Eda, H.: "Directional Stability and Control of Ships in Restricted Channels", Trans. S.N.A.M.E., Vol. 79, 1971.

20. Norrbin, N.H.: "Bank Effects on a Ship Moving through a Short Dredged Channel", 10th Symposium on Naval Hydrodynamics, 1974.

21. Fujino, M.: "New Experimental Results of Forced Yaw Tests in Shallow Water", Report of Dept. of Naval Architecture, University of Tokyo, No. 5001, 1972.

22. Fujino, M.: "Experimental Studies on Ship Manoeuvrability in Restricted Waters -- Part II", International Shipbuilding Progress, Vol.17, No. 186, 1970.

23. Norrbin, N.H.: "Theory and Observations on the Use of a Mathematical Model for Ship Manoeuvring in Deep and Confined Waters", Swedish State Shipbuilding Experimental Tank, Report No. 68, 1971.

24. Koseki, N., Yamanouchi, Y., Matsuoka, S. and Yamazaki, Y.: "Some Model Experiments on Shallow Water Effects upon Turning Ability", Journal Society Naval Architects, Japan, Vol.117, 1965 (in Japanese).

25. The Shipbuilding Research Association of Japan: "Experimental Studies on Maneuverability of Large-sized Ships", Report No.SR-98, 1968 (in Japanese).

26. Lamb, H.: Hydrodynamics , 6th edition, Dover, 1932.

27. Motora, S.: "Maneuverability, State of the Art", Proc. of International Jubilee Meeting at N.S.M.B., 1973.

28. Fujino, M.: "Application of the Hypercircle Method to Estimating the Transverse Added Mass of Two-Dimensional Bodies in Restricted Waters", Journal Society Naval Architects, Japan, Vol.134, 1973 (in Japanese).

29. Fujino, M.: "On the Added Mass of a Rectangular Cylinder Moving in a Rectangular Channel", International Shipbuilding Progress, Vol.22, No. 248, 1975.

References (continued)

30. Synge, J.L.:   The Hypercircle in Mathematical Physics , Cambridge University Press, 1957.

31. Zienkiewicz, O.C. and Cheung, Y.K.:   The Finite Element Method in Structural and Continuum Mechanics , McGraw-Hill, 1967.

32. Matsuura, Y. and Kawakami, H.:   "Calculation of Added Virtual Mass and Added Virtual Mass Moment of Inertia of Ship Hull Vibration by the Finite Element Method", Journal Society Naval Architects, Japan, Vol.124, 1968 (in Japanese).

33. Lewis, F.M.:   "The Inertia of the Water Surrounding a Vibrating Ship", Trans. S.N.A.M.E., Vol.37, 1929.

34. Wendel, K.: "Hydrodynamische Massen und Hydrodynamische Massentragheitsmomente", Jahrb. d. STG, Vol.44, 1950.

35. Newman, J.N.:   "Some Theories for Ship Manoeuvring", Journal of Mechanical Engineering Science, Vol.14, No.7, 1972.

36. Flagg, C.N. and Newman, J.N.:   "Sway Added-Mass Coefficient for Rectangular Profiles in Shallow Water", Journal Ship Research Vol.15, 1971.

37. Gurevich, M.I.:   "Added Mass of a Lattice Consisting of Rectangles", Prokl. Mat. i. Mech., Vol.4, No.2, 1940.

38. Hess, J.L. and Smith, A.M.O.:   "Calculation of Non-Lifting Potential Flow about Arbitrary Three-Dimensional Bodies", Journal Ship Research, Vol. 8, 1964.

39. Kan, M.:   "Calculation of Nonlifting Potential Flow about Ship Hulls in Shallow Water", Journal Society Naval Architects, Japan, Vol.129, 1971 (in Japanese).

40. Kan, M. and Hanaoka, T.:   "Analysis for the Effect of Shallow Water upon Turning", Journal Society Naval Architects, Japan, Vol.115, 1964 (in Japanese).

41. Sasaki, T.:   Applications of Conformal Mapping , Fuzan-bo, 1939 (in Japanese).

42. Newman, J.N.:   "Lateral Motion of a Slender Body between Two Parallel Walls", Journal Fluid Mech., Vol.39, 1969.

References (continued)

43. Fujino, M., Takashina, J. and Yamamoto, S.: "On the Three-Dimensional Correction Factors for the Added Mass and the Added Mass Moment of Inertia Related to Manoeuvrability in Shallow Water", Journal Society Naval Architects, Japan, Vol.135, 1974 (in Japanese).

44. Inoue, S. and Murayama, K.: "Calculation of Turning Ship Derivatives in Shallow Water", Trans West-Japan Society Naval Architects, Vol.37, 1969 (in Japanese).

45. Bollay, W.: "Non-Linear Wing Theory and Its Application to Rectangular Wings of Small Aspect Ratio", ZAMM, 1939.

46. Ashley, H. and Landahl, M.: Aerodynamics of Wings and Bodies , Addison-Wesley, 1965, pp40.

47. Inoue, S.: "On the Turning of Ships", Memoirs of the Faculty of Engineering, Kyushu University, Vol.16, 1956.

48. Inoue, S. and Kijima, K.: "Force Calculation of a Rectangular Plate Moving Obliquely in Water Channels", Trans. West-Japan Society Naval Architects, Vol.39, 1970 (in Japanese).

49. Newman, J.N.: "The Force and Moment on a Slender Body of Revolution Moving Near a Wall", D.T.M.B. Report No.2127, 1965.

50. Tuck, E.O. and Newman, J.N.: "Hydrodynamic Interactions between Ships", 10th Symposium on Naval Hydrodynamics 1974.

51. Beck, R.F.: "Forces and Moments on a Ship in a Shallow Canal", (to be published).

52. Durand, W.F.: Aerodynamic Theory , Vol. II (this part is written by Th. von Kármán and J.M.Burgers), 1934.

53. Bottomley, G.H.: Appendix of "Steering of Ships in Shallow Water and Canals" by G.S.Baker, Trans. I.N.A., 1924.

54. Eda, H. and Crane, C.L.: "Steering Characteristics of Ships in Calm Water and Waves", Trans. S.N.A.M.E., Vol.73, 1965.

55. Strøm-Tejsen, J. and Chislett, M.S.: "A Model Testing Technique and Method of Analysis for the Prediction of Steering and Manoeuvring Qualities of Surface Vessels", Hydro-and Aerodynamics Laboratory (Lyngby, Denmark) Report No. Hy-7, 1966.

References (continued)

56. Ogawa, A.: "Calculations on the Steered Motion of a Ship under the Action of External Forces", Part 1 --- Journal Society Naval Architects Japan, Vol.126, 1969; Part 2 --- Vol.134, 1973 (in Japanese).

57. Inoue, S.: "Non-Linear Hydrodynamic Force Acting on a Turning Ship", Trans. West-Japan Society Naval Architects, Vol.32, 1966 (in Japanese).

58. Nomoto, K.: "Analysis of Kempf's Standard Maneuver Test and Proposed Steering Quality Indices", First Symposium on Ship Maneuverability, D.T.M.B. Report No.1461, 1960.

59. Nomoto, K.: "Approximate Non-Linear Analysis on Steering Motion" Proc. of 12th I.T.T.C., 1969.

60. Norrbin, N.H.: "Zig-Zag-Proveto Technik och Analys", Allmän Rapport fran SSPA, 1965.

61. Bech, M. and Smitt, L.W.: "Analogue Simulation of Ship Manoeuvres Based on Full-Scale Trials of Free-Sailing Model Tests", Hydro-and Aerodynamic Laboratory Report No. Hy-14, 1969.

62. Fujino, M. and Motora, S.: "On the Modified Zigzag Maneuver and Its Application", Journal Society Naval Architects,Japan, Vol.128, 1970 (in Japanese).

63. Fujino, M.: "An Analyzing Method of Manoeuvrability with the Phase Portrait", Journal Society Naval Architects,Japan, Vol.132, 1972 (in Japanese).

64. Fujino, M.: "An Analyzing Method of Manoeuvrability with the Phase Portrait" (continued report), Journal Society Naval Architects,Japan, Vol.134, 1973 (in Japanese).

65. Nomoto, K., Kose, K. and Yoshimura, Y.: "A New Procedure of Analysing Zig-zag Test", Journal Society Naval Architects,Japan, Vol. 134, 1973 (in Japanese).

66. Clarke, D.: "A New Non-Linear Equation for Ship Manoeuvring", International Shipbuilding Progress, Vol. 18, No.201, 1971.

67. van Leeuwen, G.: "A Simplified Non-Linear Model of a Manoeuvring Ship", Laboratorium voor Scheepsbouwkunde, Delft. Report No.262, 1970.

ERRATA

page		for	read
9	eq.(2.5), first line	$m(\frac{d\Delta v}{dt} + Ur)$	$m(\frac{d\Delta v}{dt} + U\Delta r)$
12	eq.(2.15)	$Y_{\dot{r}}\dot{r}' + Y_{\dot{\delta}}\dot{\delta}'$	$Y_{\dot{r}}'\dot{r}' + Y_{\dot{\delta}}'\dot{\delta}'$
15	line 8	$I_{zz} + J_{zz}$	$I_{zz}' + J_{zz}'$
21	eq.(2.50)	$\alpha_0 s + \alpha_1 s^2 + \alpha_2 s + \alpha_3$	$\alpha_0 s^3 + \alpha_1 s^2 + \alpha_2 s + \alpha_3$
36	additional remark of Table 3		W is the bottom-width of a canal, so that the surface-width of the canal is equal to W + 2H
39	line 16	(see reference [15].	(see reference [15]).
44	line 13	(3.24) is always	(3.24) is always satisfied because of negative nature of the coefficients a and b;
46	line 6	mathmatically	mathematically
56	line 9	the ratio of turning radius to ships's length	the ratio of ship's length to turning radius
60	eq.(4.3)	$\phi_\gamma \cdot \frac{\partial \phi i}{\partial n}$	$\phi_j \frac{\partial \phi i}{\partial n}$
65	first line	$\pi^*(p^*, p^*)$	$\pi^*(p_1^*, p_2^*)$
	line 7	$I_i = p_{i1}^*, p_{i2}^*)$	$I_i = (p_{i1}^*, p_{i2}^*)$
67	line 3	(U, V)	(I_i, J_k)
	line 13	$\alpha p_{A1} + \beta p_{B2}$	$\alpha p_{A1} + \beta p_{B1}$
	line 17	$\partial (P_{A1} \frac{\partial y}{\partial n} + P_{A2} \frac{\partial z}{\partial n})$	$\alpha (P_{A1} \frac{\partial y}{\partial n} + P_{A2} \frac{\partial z}{\partial n})$

Page		for	read
		for	*read*
70	eq.(4.33), third line	$+ q^2$	$= q^2$
73	line after eq.(4.45)	(IV) $*$-space	(IV) $\Omega*$-space
74	last line	discontinuity. (see Figure 11)	discontinuity (see Figure 11).
78	eq.(4.51)	$P_{i2}^* = \dfrac{z-z_{i1}}{y_{i2}-y_{i0}}$	$P_{i2}^* = \dfrac{z-z_{i1}}{y_{i2}-y_{i0}}$
	line after eqn(4.53)	$Y_{i0}, Y_{i1}, Y_{i2}, Z_{i0}, Z_{i1}, Z_{i2}$	$y_{i0}, y_{i1}, y_{i2}, z_{i0}, z_{i1}, z_{i2}$
79	line 12	j=th	j-th
	line 15	i=th	i-th
	eq.(4.58)	$\dfrac{z_{i0}-z_{i1}}{6(y_{i0}-y_{i2})}$	$\dfrac{z_{i0}-z_{i1}}{6(y_{i2}-y_{i0})}$
	eq.(4.59)	$(y_{i2}-Y_{i0})$	$(y_{i2}-y_{i0})$
83	title of Table 6	i and j of I_i- and I_j-vectors	k and 1 of J_k- and J_1-vectors
84	eq.(4.72)	$\dfrac{1}{2(n-n')} \sin \dfrac{(n-n'\pi a}{b}$	$\dfrac{1}{2(n-n')} \sin \dfrac{(n-n')\pi a}{b}$
85	eq.(4.74), second line	$[\dfrac{c\pi}{2d} + \dfrac{1}{4m} \sin \dfrac{2m\pi c}{d} - \dfrac{m^2 \pi^2 b^3}{d}]$	$[\dfrac{c\pi}{2d} + \dfrac{1}{4m} \sin \dfrac{2m\pi c}{d}] - \dfrac{m^2 \pi^2 b^3}{d}$
	second line from bottom	k_i	b_k
86	between lines 10 and 11		the section between the bottom of the body and the bottom of the canal into m_2 equal pieces,

-2-

| page		for	read
86	line 12	m_2	n_1
	line 13	n_1	n_2
	line 5 from bottom	$M_1=2$, $M_2=4$, $N_1=2$, and $N_2=8$.	
			$m_1=2$, $m_2=4$, $n_1=2$, and $n_2=8$.
93	eq.(4.81)	$+0$	$=0$
	line 15	$\psi(y,z)$	$\phi(y,z)$
97	eq.(4.90)	$\dfrac{\cos(\pi z/2H)}{\cos(\pi T/2H}$	$\dfrac{\cos(\pi z/2H)}{\cos(\pi T/2H)}$
103	remarks in Figure 18	C_{zzH}/C_{zz}	$C_{zzH}/C_{zz\infty}$
108	line 19	$N_{\beta H}/N_{\beta\infty}$	N_β/Y_β
110	eq.(4.101)	$[\ldots\ldots]^{-(1/2)}$	$[\ldots\ldots]^{-1/2}$
112	line 10	symmetrical	asymmetrical
118	line 13	equal to H	equal to 4
126	eq.(5.6)	$\ddot{\psi}\,\dfrac{\alpha\dot{\psi}}{\alpha\psi}$	$\dot{\psi}\,\dfrac{d\dot{\psi}}{d\psi}$
130	line 9	counter-clockwise	clockwise
	line 12	clockwise	counter-clockwise
	line 16	D_5, D_5 and D_5.	D_5', D_5'' and D_5'''
131	title of Figure 25	$H(\psi)/K$	$H(\dot{\psi})/K$
132	first line	the variable	the variable $\ddot{\psi}$
	eq.(5.14)	$\cdots+\oint\dfrac{H(\dot{\psi})}{K}d\dot{\psi}\ \oint\delta d\dot{\psi}$	$\cdots+\oint\dfrac{H(\dot{\psi})}{V}d\dot{\psi}=\oint\delta d\dot{\psi}$

page		for	read
133	eq.(5.18), first line	$\cdots + N_v' v + \cdots$	$\cdots + N_v' v' + \cdots$
	eq.(5.18), second line	$+ N_{vvv}' 3v' + \cdots$	$+ N_{vvv}' v'^3 + \cdots$
134	line eq.(5.19)	ℓ_1	ℓ_i
	eq.(5.20)	$\cdots + A_{10} \delta^{12})$	$\cdots + A_{10} \delta'^2)$

90   additional remark to Figure 15
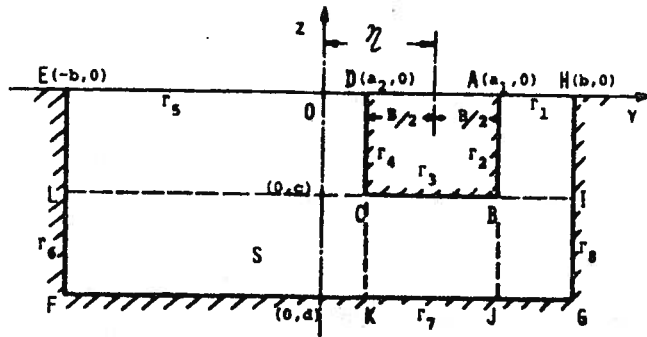
		for	read
35	title of Table 2.B.	$F_n = 0.103$ (12 knots, full-scale ship)	$F_n = 0.116$ (12 knots, full-scale ship)
37	Figure 5	(b) $F_n = 0.103$	(b) $F_n = .116$
100	Remarks of Figure 16, 4 lines from bottom	$(F_n = 0.103)$	$(F_n = 0.116)$
106	Remarks in a graph $Y_{\beta H}/Y_{\beta \infty}$ of Figure 19, right column indicating Froude No., 4 lines from bottom.	0.103	0.116